MAY 1958 VOLUME 2 (1958) No. 4

GREGG M. SINCLAIR LIBRARY
UNIVERSITY OF HAWAII
8-7-63

NUCLEAR INSTRUMENTS

A JOURNAL ON ACCELERATORS, INSTRUMENTATION AND TECHNIQUES IN NUCLEAR PHYSICS

EDITOR: K. SIEGBAHN - UPPSALA

CONTENTS

N. M. KING and W. WALKINSHAW, Spiral ridge cyclotron particle dynamics applied to conversion of the Harwell synchrocyclotron 287
D. MAEDER, Photographic recording methods in nuclear pulse spectrometry 299
H. SLÄTIS, On a set of permanent magnet beta-ray spectrometers 332
M. HUQ, Simple Čerenkov detector for the measurement of the energy of relativistic charged particles 342
E. FRANKLIN and J. B. JAMES, Magnetic-memory scaling-system with magnetic count indication 348
N. SARMA, Thin carbon films for use with electrostatic accelerators (Letter to the Editor) . 361
Author Index 363
Subject Index 365

NORTH-HOLLAND PUBLISHING COMPANY - AMSTERDAM

NUCLEAR INSTRUMENTS

A journal on accelerators, instrumentation and techniques in nuclear physics

EDITOR: K. SIEGBAHN, UPPSALA

EDITORIAL BOARD:

J. B. ADAMS (CERN)
E. AMALDI (Rome)
H. L. ANDERSON (Chicago)
K. T. BAINBRIDGE (Cambridge, Mass.)
C. J. BAKKER (CERN)
P. R. BELL (Oak Ridge)
R. E. BELL (Montreal)
A. BERTHELOT (Saclay)
H. BRINKMAN (Groningen)
S. DE BENEDETTI (Pittsburgh)
M. DE HEMPTINNE (Louvain)
A. DE-SHALIT (Rehovoth)
M. DEUTSCH (Cambridge, Mass.)
S. DU TOIT (Pretoria)
B. S. DŽELEPOV (Leningrad)
W. GENTNER (CERN)
P. C. GUGELOT (Amsterdam)
H. HALBAN (Paris)
O. HAXEL (Heidelberg)
P. HUBER (Basel)
D. J. HUGHES (Brookhaven)
S. KIKUCHI (Tokyo)
J. KOCH (Copenhagen)
M. S. KOZODAEV (Moscow)
S. LIVINGSTON (Cambridge, Mass.)
E. M. MCMILLAN (Berkeley)
M. G. MEŠČERJAKOV (Moscow)
P. B. MOON (Birmingham)
M. L. OLIPHANT (Canberra)
W. PAUL (Bonn)
A. S. RAO (Bombay)
G. SALVINI (Rome)
P. SAVIĆ (Belgrade)
P. SCHERRER (Zürich)
CH. SCHMELZER (CERN)
H. W. B. SKINNER (Liverpool)
R. TANGEN (Blindern)
D. TAYLOR (Harwell)
V. I. VEKSLER (Moscow)
O. WERNHOLM (Stockholm)
G. VON DARDEL (CERN)
R. R. WILSON (Cornell)
S. D. WINTER (Saclay)

Contributions may be sent to the Editor, Professor K. Siegbahn, Institute of Physics, the Uuiversity of Uppsala, either directly or through the intermediary of one of the members of the Editorial Board of the country or region in which the author is working. Contributions may be written in English, French or German, with an abstract in English.

Books for review should be sent to Professor Siegbahn.

Nuclear Instruments is published in bi-monthly issues. The subscription price of a volume of 360 pages is $ 17.00 (130 s), postage free.

Subscriptions should be sent to the publishers, North-Holland Publishing Company, P.O.Box 103, Amsterdam or to any subscription-agent.

No part of this issue may be reproduced in any form, by print, photoprint, microfilm or any other means without written permission from the publisher. Reprints, photoprints or microfilms are obtainable at cost from the publisher.

THE DEKATRON

COLD-CATHODE DECADE SCALING TUBE

"Scaling equipment has also undergone a number of changes in recent years and probably the most significant was the introduction of the decade scaling tubes. In general the introduction of such tubes has simplified circuits and allowed improved reliability, and in some cases it has resulted in a reduction in cost. The Dekatron tube, manufactured by Ericsson Telephones Ltd. is now very popular and deservedly so, and is used in many scaling and timing equipments."

... DENIS TAYLOR, M.SC., PH.D., M.I.E.E., F.INST.P. REVIEW ARTICLE "NUCLEAR POWER YEAR BOOK" 1957-58.

SCALING UNIT Type 1221

As originators and sole manufacturers of the DEKATRON, and having developed most of its associated circuitry, we believe that we know best how to put it to work to meet your requirements. Illustrated is the well-known Ericsson Scaling Unit which was developed in conjunction with the Atomic Energy Research Establishment (Harwell) for reliable general purpose scaling.

OTHER PRODUCTS INCLUDE

Industrial Counting Equipment
Batching Equipment
Survey Meters
Radiation Monitors
Field Ratemeters
Laboratory Ratemeters
Quench Units
E.H.T. Power Units
Custom-built Counting Units
Reactor Instrumentation

Write now for your copy of "ELECTRONIC & NUCLEONIC INSTRUMENTS"

Your complete supply source for

ELECTRONIC AND NUCLEONIC INSTRUMENTS

ERICSSON

INSTRUMENT DIVISION

HIGH CHURCH STREET, NEW BASFORD, NOTTINGHAM. Tel. 75115

ERICSSON TELEPHONES LTD. HEAD OFFICE: 22 LINCOLN'S INN FIELDS, LONDON, W.C.2

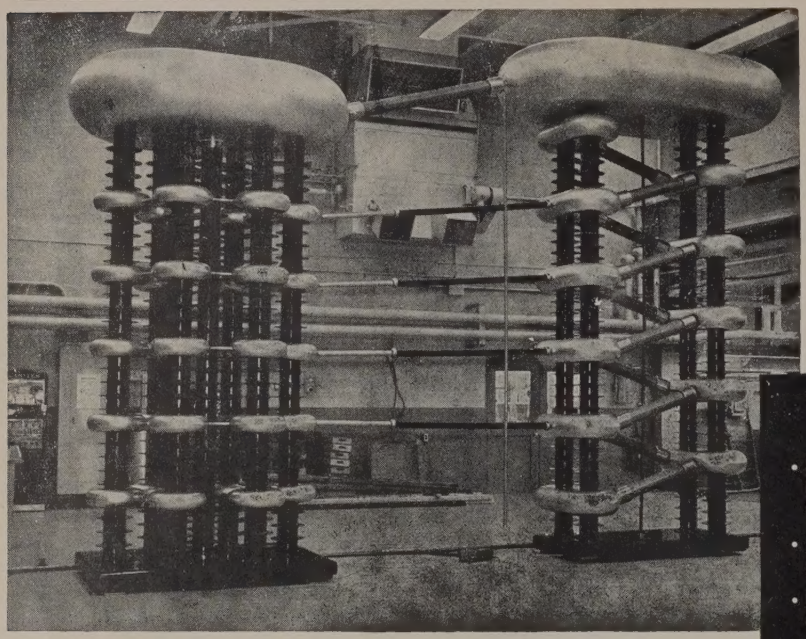

Stabilized
H.V. supply 800 kV/8 mA

(Photo by courtesy of the Brookhaven National Laboratory, Upton L.I., N.Y., U.S.A.)

- Synchro-cyclotrons for various final energies.
- Linear electron accelerators.
- Cockcroft-Walton accelerators.
- Radiation measuring and detection equipment.
- Area monitoring instrumentation.
- Civil defence instruments.
- Reactor control instrumentation.
- Geiger counter tubes.
- Radio-active isotopes.
- Air liquefiers.
- Generators for very high d.c. voltages.

PHILIPS *equipment for Nuclear Physics and Atomic Energy*

This Cockcroft-Walton generator will serve as a pre-injector for the 25 BeV Alternating Gradient Synchrotron under construction at the Brookhaven National Laboratory.
A similar installation is used at the Atomic Energy Research Authority at Harwell, England for injection into a proton linear accelerator.

PHILIPS

PHILIPS

Nuclear Equipment

For further information please apply to one of the following addresses:

N.V. PHILIPS' GLOEILAMPENFABRIEKEN,
Scientific Equipment Department, Eindhoven - Holland
PHILIPS ELECTRICAL LTD.,
Research and Control Instruments Division, Shaftesbury Avenue, London W. C. 2
PHILIPS ELECTRONICS INC.,
Instruments Division, 750, South Fulton Avenue, Mount Vernon N.Y. U.S.A.

A Beta-Ray Spectrometer in commercial production, engineered to highest standards of performance

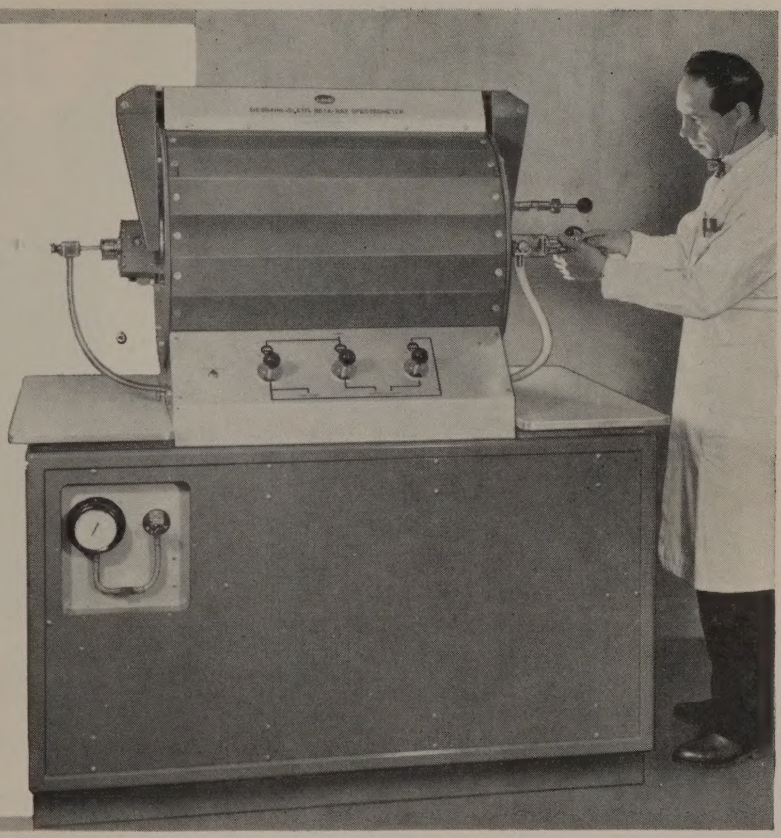

▲ Operator inserting source holder into spectrometer chamber through lock valve. Control console and 50 kW motor-generator set not shown.

The LKB 3024 B Siegbahn-Slätis Intermediate Image Beta-Ray Spectrometer

Features distinguishing the LKB Beta-Ray Spectrometer include:

Energy Range: 1 keV to 8.3 MeV electrons, or, when used as pair spectrometer, up to 17.6 MeV gammas.

Transmission: up to 8% of 4π.

Resolution: 0.7% at 1% transmission or 1.2% at 6% transmission.

Linearity: $B\rho$ proportional to magnet current within ±0.11% between 36 keV and 8.3 MeV.

Shielding: Spectrometer is iron-jacketed, insuring extremely low stray-field level.

Operation: Safe and fast. There are protective devices against all possible kinds of failure. Precision electronic regulator with follow-up servo facilitates current setting.

To be shown at the Geneva "Atoms for Peace" Exhibition, Sept. 1–14, 1958

Other LKB Products for the Nuclear Physicist:
Custom-built Precision-Stabilized and Transient-Free High Current D. C. Power Supplies.
Autovac Vacuum Gauge.

LKB

Write for details and references to:

LKB-PRODUKTER

Fabriksaktiebolag

P.O. Box 12220, Stockholm 12, Sweden

Distributors throughout the world

a Complete Scintillation Service FOR RESEARCH & PROCESS CONTROL

phosphors & counters

PLASTIC, LIQUID, AND CRYSTAL PHOSPHORS

* PLASTIC PHOSPHOR N.E. 102, light output 65% anthracene, available in all sizes and shapes up to one ton, in thin sheet form, in fine tubes for the construction of scintillation flow counters, or as filaments for the construction of scintillation nuclear track chambers. (Bulletin 11).
* BORON POLYESTER PLASTIC PHOSPHOR N.E. 400 and N.E. 401 for neutron detection.
* LOADED LIQUID SCINTILLATORS in bulk or encapsulated, containing Pb for extreme X-ray sensitivity, and Gd, B, Cd, and Sm for neutron detection (Bulletins 9 and 9a).
* SCINTILLATING GELS for efficient internal counting of suspended materials, (Bulletin 9).
* SCINTILLATION CHEMICALS of highest purity P.B.D., POPOP, T.P.B., p-terphenyl, PPO, D.P.H., alpha-N.P.O., D.M.C., B.B.O., B.P.O., vinyltoluene, styrene, xylene, toluene, and methyl borate (Bulletin 10).
* LIGHT PIPES of polyvinyltoluene and polystyrene.
* HARSHAW SODIUM IODIDE CRYSTALS. Exclusive concessionaire for Great Britain. Also LiI (Eu) and CsI (Tl).

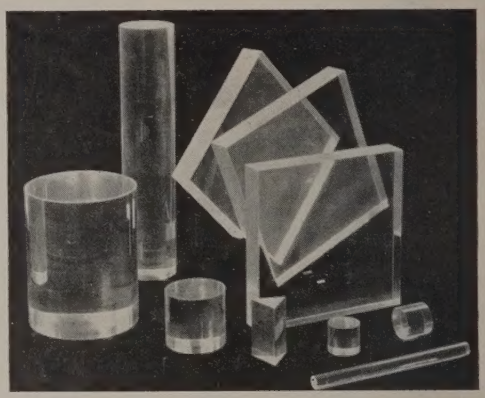

NEW LINE OF PRECISION NUCLEAR INSTRUMENTS

* Non Overloading Linear Pulse Amplifier N.E.5202 of the Fairstein type (Bulletin14).
* Pre-Amplifier and Cathode Follower N.E. 5202 A.
* Single Channel Pulse Height Sorter N.E. 5102.
* Shielded Scintillation Head Unit N.E. 5501.
* Highly Stabilised EHT Supply N.E. 5301.
* Complete assembly for C14 and tritium counting, N.E. 8301.
* Complete Human Body Counter Installation N.E. 8101.
* Multi-Channel Scintillation Spectrometer N.E. 8201 for Industrial Tracer Investigations.
* Scintillometers for Geophysical Exploration, Mark VI and Mark IX.

Nuclear Enterprises (G.B.) Ltd.

Bankhead Medway, Sighthill, Edinburgh - Scotland - Tel.: CRA 4513

Write now for Bulletins 9, 9a, 10, 11, 12, 13, 14 and 1958 PRICE LIST

Associate Company: Nuclear Enterprises Ltd., 1750 Pembina Highway, Winnipeg, Canada (ndk) 10193

general radiological

Manufacturers of complete neutron flux monitoring systems for Reactors.

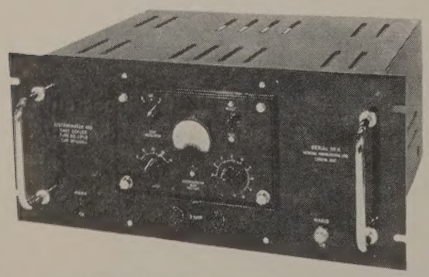

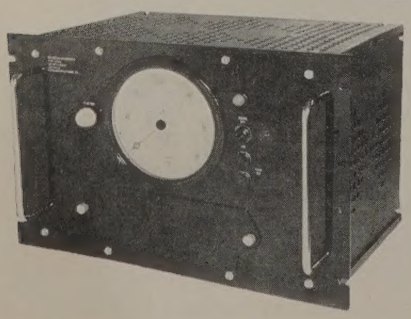

NE. 030 Discriminator and Fast Prescaling Unit for low flux counting channel of Nuclear Reactor Control circuits.

Max. average count rate 7×10^5 c/s. Resolution time $^1/_4$ μ/sec. Built-in test oscillator. Output used to drive:–

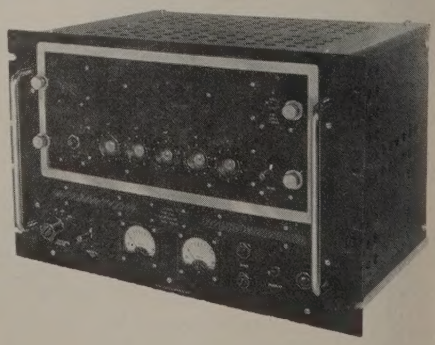

NE. 002 Scaler Unit. Nominal Resolution time 5 μ/sec. Max. displayed count 1×10^7. Outputs $\div 1 \div 10 \div 100$ used to drive:–

NE. 003 Logarithmic Ratemeter. Resolution Time $^1/_4$ μ/sec. Meter display of 1×10^6 counts.

These units are normallly preceded by NE. 041 Pulse Amplifier, and followed by NE. 057 Reactivity Meter

general radiological ltd

15/18 Clipstone Street - London - W.1.

PARTICLE ACCELERATORS

in Nuclear Physics, Chemistry, and Biology

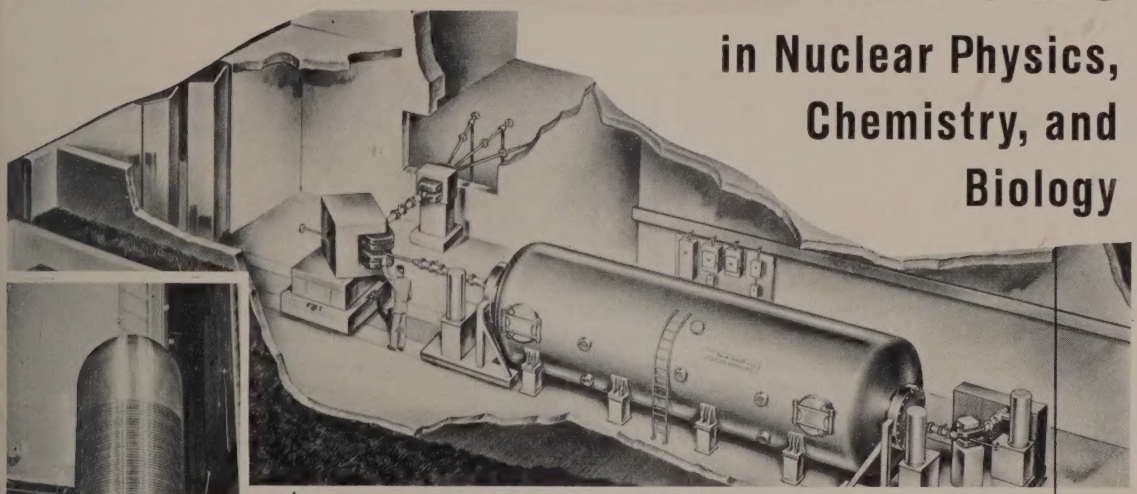

10-Mev Tandem Van de Graaff® Positive-ion Accelerator, Model EN. Designed for nuclear research at the Chalk River establishment of Atomic Energy of Canada Limited, this is the first of three high-energy machines being built by HIGH VOLTAGE for installation in various parts of North America. With this new design, physicists will, for the first time, be able to explore with precision the binding-energy physics of higher atomic numbers.

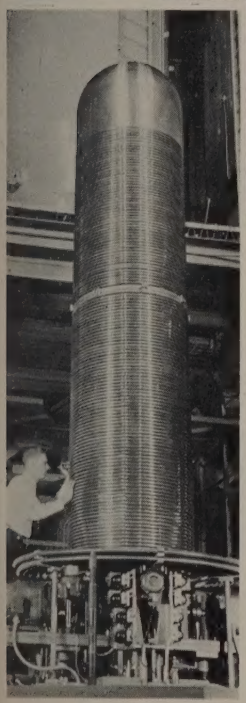

5.5 Mev Van de Graaff Model CN

This machine, widely used for neutron cross-section studies and nuclear-energy-level determinations, will be displayed at the Second International Exhibition of the Peaceful Uses of Atomic Energy, in Geneva, Switzerland.

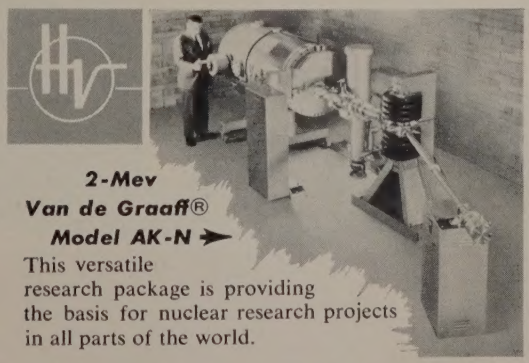

2-Mev Van de Graaff® Model AK-N

This versatile research package is providing the basis for nuclear research projects in all parts of the world.

0.25-Mev Van de Graaff®, Model PN-250

The most recent development in particle accelerators, this new, low-energy machine is designed as a pulsed-neutron source for use with subcritical assemblies in reactor research and teaching.

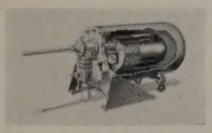

Van de Graaffs®

1 Mev – Model JN
Economical neutron source for reactor research

1 Mev – Model JS
Simplified electron source for transistor and crystal research

2 Mev Model AK-N
Precise, multiple-purpose instrument for general physics research and teaching

2 Mev Model AK-S
Moderate-power electron source for quantitive radiation research

3 Mev – Model KN
Powerful neutron source and effective instrument for binding-energy physics

5.5 Mev - Model CN
Ideal positive-ion accelerator for broad-range nuclear research programs

10 Mev – Model EN
New, precise, high-energy, tandem accelerator for binding-energy investigation of heavy nuclei

Microwave Linear Electron Accelerators – 5 to 50 Mev Linacs
A series of high-energy, high-powered electron accelerators for research and production

Write us for the name of your nearest distributor and for informative reprints in your field of interest

HIGH VOLTAGE ENGINEERING CORPORATION
BURLINGTON MASSACHUSETTS

acf

reactor diversification and reliable design ...

Unlike other builders of nuclear reactors who specialize in specific types — ACF has achieved prominence through diversification. This diversification is a tribute to the range and depth of our scientific, engineering and manufacturing skills. As a result of our field proven designs — today we offer a group of "standard reactors". The ACF Heavy Water Tank Type standard reactor is the direct result of the experience gained with the MIT reactor, the Italian National Committee reactor in Italy and other designs recently completed for government and private organizations. By combining the best features of each of these installations ACF is ready to offer a standard Heavy Water Tank Type research reactor with power levels ranging from 1000 KW to 10,000 KW.

Another standardized reactor is the ACF Light Water Tank Type—based on the best design features of 4 similar units now under construction in the U.S., Holland and Sweden with power outputs ranging from 10,000 KW to 30,000 KW. Used primarily for materials testing and engineering development, these units are further evidence of ACF's established pattern of reliability in reactor design and construction.

Two ACF Power Reactor Designs have recently been completed — one the Boiling Water Reactor Type and the other the Gas Cooled Type. The ACF approach to power reactor construction is based on the use of **proven** engineering and **sound** design to provide the customer with the most economic solution of his problem with **existing** technology.

LIGHT WATER POOL TYPE | HEAVY WATER TANK TYPE | LIGHT WATER TANK TYPE | PROCESS HEAT

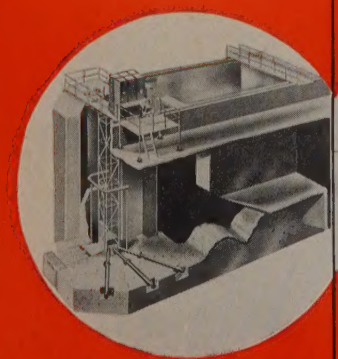

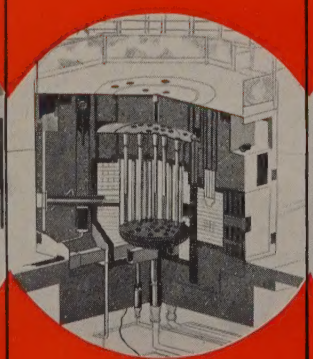

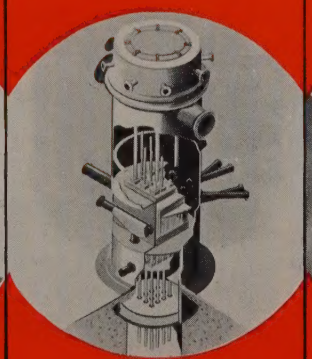

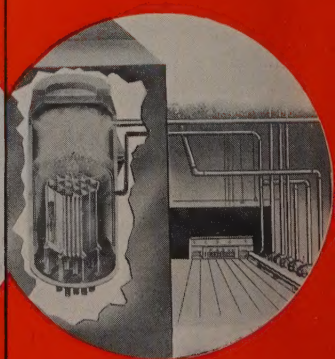

based on experience

Other new design developments at ACF include the Process Heat Reactor and the complete line of Pool Training Reactors as announced recently.
Reactors from a 1 watt trainer to 150,000 TKW power unit have already been designed by ACF. No matter what your requirements are in the area of nuclear reactors, the diversification, experienced personnel and proven designs found at ACF are your best assurance that we have a sound technical and economic approach to your problem. We are free at any time to undertake exploratory discussions.

Write us for further information

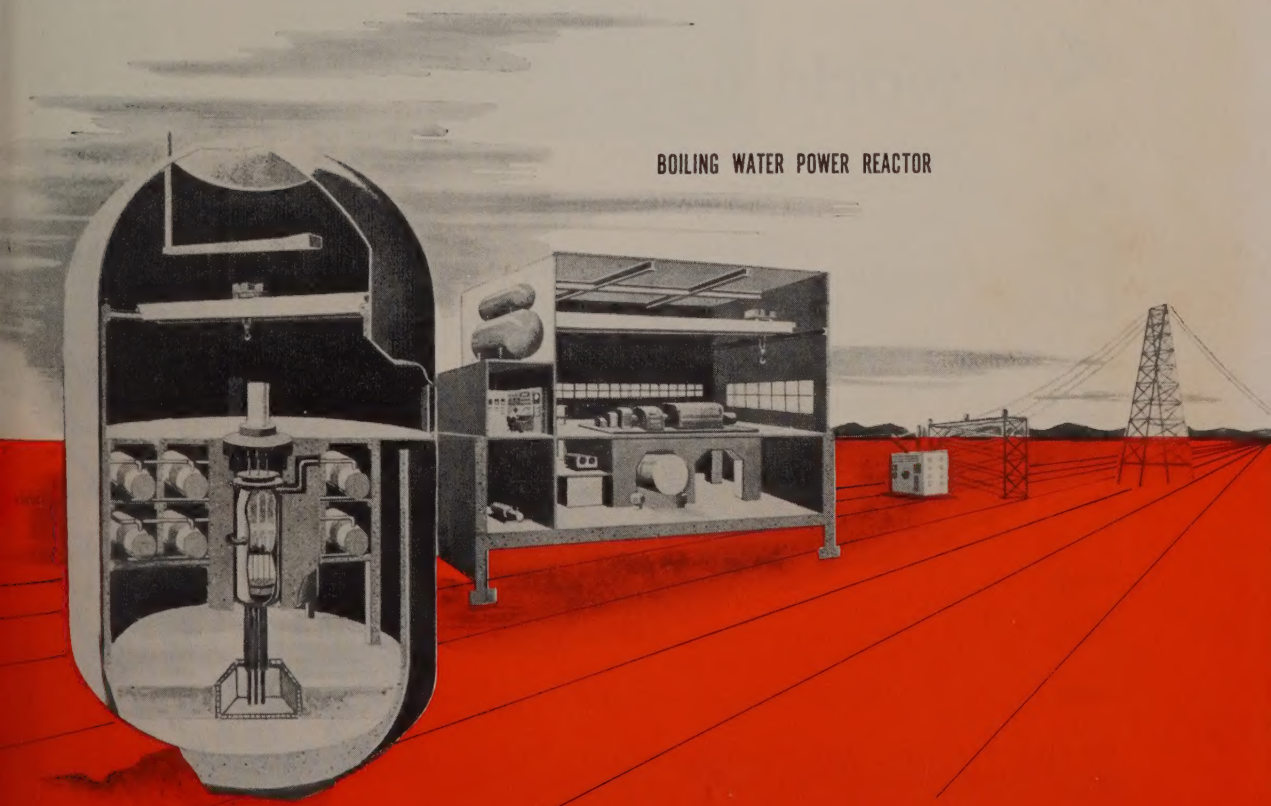

BOILING WATER POWER REACTOR

acf

NUCLEAR PRODUCTS–ERCO

Division of ACF Industries Incorporated

508 Kennedy Street N.W., Washington 11, D.C.

INTERNATIONAL

advertise
YOUR NUCLEAR PRODUCTS IN

sell
YOUR NUCLEAR PRODUCTS

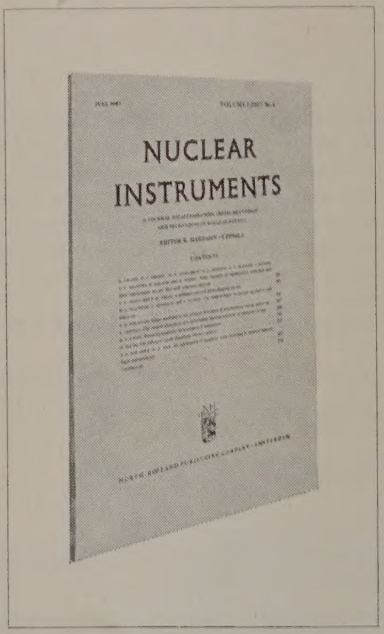

reap
YOUR NUCLEAR SALES
REWARDS

world wide
KEY NUCLEAR MANAGEMENT
NUCLEAR SCIENTISTS
NUCLEAR ENGINEERS
NUCLEAR PRODUCTION
PERSONNEL

SUBSCRIBE TO

you reach
THE WHOLE
NUCLEAR SALES WORLD IN

Entirely international in scope Nuclear Instruments is the one nuclear scientific journal that has an established subscription clientele through-out the whole world-where-ever nuclear men are at work—they want your nuclear products—they need your nuclear products—advertise in Nuclear Instruments and tell them WHAT – HOW – WHERE they can get your nuclear products

GO INTERNATIONAL WITH YOUR SALES PROGRAM TODAY WRITE

WILLIAM F. BAARS - ADVERTISING MANAGER NORTH-HOLLAND PUBLISHING COMPANY

P.O. BOX 103 – AMSTERDAM, HOLLAND

INTERNATIONAL

NEUTRON GENERATOR "J"

150 kV

PORTABLE

SMALL SIZE

LARGE NEUTRON RATE

OTHER PRODUCTS

PARTICLE ACCELERATOR "S" - 600 kV, AND "P" 1,2 MV
ELECTROSTATIC GENERATORS FROM 50 kV TO 1,2 MV
HIGH VOLTAGE POWER SUPPLY WITH HIGH STABILITY FROM 0,1% TO 0,001%
NUCLEAR ELECTRONIC EQUIPMENT

EDIPRESS

SAMES

P. O. BOX 150 GRENOBLE (ISERE) FRANCE
PHONE : 44-77-64 TEL. ADDRESS : ELECTROSTATIC
17, RUE DUPHOT PARIS 1er

Check the many ways ANTON can serve your nuclear needs

☐ **Anton's Electrically Compensated Ion Chambers and BF_3 Counter Tubes**

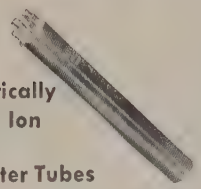

(Enriched, normal or depleted in B^{10}) for detection of either slow or fast neutrons are widely-used in reactor control and monitoring, oil well logging and neutron survey. Available in a wide range of diameters, sensitive lengths and wall thicknesses in 2S aluminum or stainless steel.

☐ **Anton End Mica Window Counters**

Alpha, beta, gamma counters are halogen quenched, stainless steel. Also available with special organic as well as other rare gas fills. Window thicknesses available from 1 mg/cm². Tubes vary from subminiature to standard conventional sizes and are based with standard RMA connectors. JAN types available.

☐ **Anton Thin Wall Counter Tubes**

Stainless steel, halogen quenched counter tubes for beta, gamma studies are extremely sensitive and can meet all JAN-MIL specifications. They are the only commercial metal thin wall tubes available with a stainless steel 30 mg/cm² wall which will not dent or collapse. Instruments using groups of these tubes exceed in sensitivity and stability most scintillation units.

☐ **Anton's Pancake Tubes**

Halogen quenched, sensitive beta-gamma detectors with end mica window. These units are designed for low intensity measurement and are widely used in facilities doing low-count work. Flat pancake design offers advantage of large diameter window without large volume and high background count.

Anton high efficiency tubes are Platinized*. This process provides sensitivity beyond that of standard tubes.

*Reg. pending

☐ **229 Ratemeters**

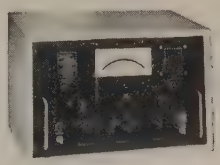

The most precise laboratory ratemeter available, Anton's 229 Series has 7 scales, including a single log scale from 300-50,000 cpm with accuracy of better than ±2% of meter reading above ⅓ scale. It has dual range input sensitivity and provides precise and efficient measurement of radioactivity in industry, research and medicine.

☐ **700 Survey Meter**

Portable laboratory or field survey meter (.5; 5; 50 mr/hr full scale) is built to FCDA specifications — the only CDV-700 type survey meter which can be exposed continuously to high intensity radiation without detector failure. Probe uses Anton halogen quenched, very thin wall, stainless steel counter tube. Accuracy assured from −55°C to +75°C.

☐ **44 Ratemeter**

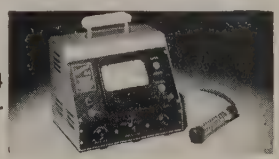

Low-cost, accurate, dual range (0-5000; 0-50,000 cpm) . . . exclusive input design. Supplied with Anton long-lived, stainless steel, halogen quenched, thin wall (30 mg/cm²) counter tube or a wide range of other tubes. Unit features a jack for external meters, terminal board construction and oscilloscope connections.

☐ **6001 Sample Changer**

For quick, accurate measurement of low intensity radiation. Designed for use of one or two Anton pancake type, high beta sensitivity, low background counter tubes. Provides 2″ lead plus 3/16″ aluminum shielding in all directions, lowering the background count by a factor of from two to four. Makes possible counting geometry of nearly 100%.

☐ **High Pressure Reactor Connectors**

Anton's stainless steel, hermetically sealed reactor heater-end connector withstands 2000 PSI at temperatures of 636°F, with terminals capable of carrying a load of 16 amperes with a potential drop of less than 10 milliwatts. A wide variety of conventional and specialized connectors is available.

☐ **Medical Eye, Brain And Ingestion Probes**

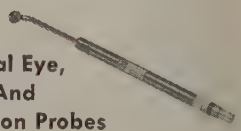

These tubes are rugged, sensitive alpha beta, gamma radiation detectors specifically designed for reliable, low count medical tracer work. They can be cold sterilized and their pulse intensity obviates the need for a preamplifier.

☐ **Air Particle Monitors**

Monitoring systems for aerosol contamination (alpha, beta, gamma) are available in a full range of moving filter paper, fixed filter paper and impact instruments. Rack mounted, cart mounted and portable instruments available.

☐ **Corona Discharge V-R Tubes (300V-30KV)**

Anton is licensed under the basic patent in this field. Valuable data available concerning this low-cost solution to high voltage low current regulation problems.

. . . and many more. SEND FOR FREE DATA CONCERNING YOUR SPECIFIC NUCLEAR INSTRUMENT, TUBE OR COMPONENT NEEDS.

ANTON ELECTRONIC LABORATORIES, INC.

A subsidiary of United States Hoffman Machinery Corporation

1226 FLUSHING AVE., BROOKLYN 37, N. Y.

BROWN BOVERI

The first English

nuclear power stations

Calder Hall and Chapel Cross are equipped with

32 BROWN BOVERI **voltage regulators**

for the automatic precision speed control
of the carbon dioxide circulating blowers

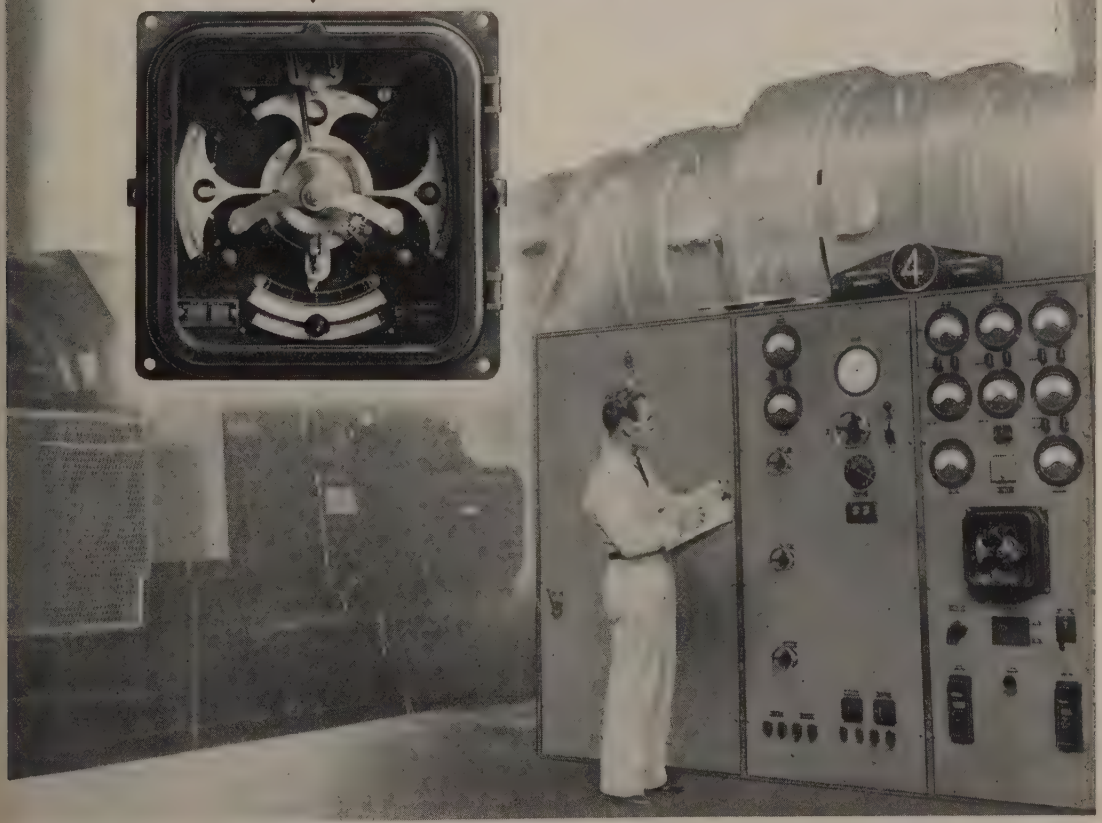

BROWN, BOVERI & CO., LTD., BADEN (SWITZERLAND)

Representatives in most countries

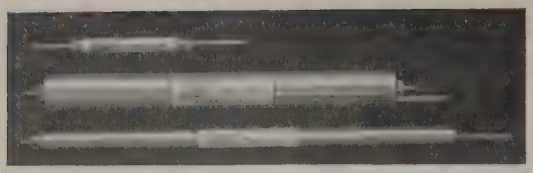

LELAB METAL-WALLED G-M TUBES

for anti-coincidence applications where uniformity counts !

Lelab Counter Tubes are individually constructed, filled, and tested. Each is fabricated almost entirely of metal. All components are confined within the diameter of the tube shell to permit close stacking.

Compare our low prices on these superior tubes!

(Makers of Lelab [Robinson-Selverstone Type] Probe Counters for neurosurgery and where a fine needle-like probe for highly localized measurements is useful.)

Write for complete information

H. W. Leighton Laboratories

York & Sunset Lane - Hatboro, Pa. U.S.A.

MODEL 412 MERCURY RELAY

PRECISION SLIDING PULSER

for Precise Calibration of Single & Multi-Channel Pulse Height Analyzers

Determines Window Widths Using Principle of *Constant Angular Velocity* — **AUTOMATICALLY** 10 × more accurately, 40 × faster than conventional pulsers

Incorporates Both Manual Control and Precision Motor Drive

Simulates Pulses from Scintillation, Proportional or Geiger Counters

RISE TIME—Less than .003 usec.

DECAY TIME CONSTANT—1, 10, 100, 350, usec.

LINEARITY—0.1% 10 turn potentiometer with 5" dial.

CALIBRATION—Self contained standard cell and null balance circuit for precision adjustment.

MERCURY PULSER, Model 401

Featuring Versatility and Precision

Specifically designed for the Nuclear Physics Laboratory

RISE TIME—Less than .003 usec

DECAY TIME CONSTANT—1, 10, 100 usec

Fast rise and exponential decay simulates scintillation, proportional or geiger counter pulses for test and calibration of amplifiers, pulse height analyzers, scalers, etc.

MODEL 412 . . . $450.00 — MODEL 401 . . . $125.00

RADIATION INSTRUMENT CO.

P. O. BOX 733, SILVER SPRING, MARYLAND, U.S.A.

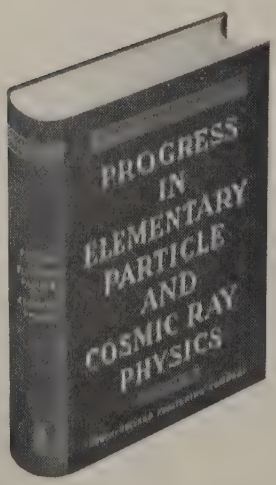

PROGRESS IN ELEMENTARY PARTICLE AND COSMIC RAY PHYSICS VOL. IV

Editors

J. G. WILSON, *Professor of Physics, University of Leeds*

and

S. A. WOUTHUYSEN, *Professor of Physics, University of Amsterdam*

6 × 9″ XII + 482 p. 110 illus. Guilders 45.00 (90 s)

CONTENTS

1. *Some Theoretical Aspects of the Strong Interactions of the New Particles* (B. D'Espagnat and J. Prentki). 2. *The Properties and Production of K-mesons* (W. D. Walker). 3. *The Interaction of μ-Mesons with Matter* (G. N. Fowler and A. W. Wolfendale). 4. *The Primary Cosmic Radiation and its Time Variations* (S. F. Singer). 5. *The Origin of Cosmic Radiation* (V. L. Ginzburg).

Sole Agency for U.S.A.: Interscience Publishers, Inc. — New York

NORTH-HOLLAND PUBLISHING COMPANY - AMSTERDAM

Send your order to your bookseller or directly to us

NUCLEAR INSTRUMENTS 2 (1958) 287–298; NORTH-HOLLAND PUBLISHING CO. – AMSTERDAM

SPIRAL RIDGE CYCLOTRON PARTICLE DYNAMICS APPLIED TO CONVERSION OF THE HARWELL SYNCHROCYCLOTRON

N. M. KING and W. WALKINSHAW

Atomic Energy Research Establishment, Harwell, Didcot, Berks

Received 27 November 1957

A theoretical design study for conversion of the Harwell synchrocyclotron to spiral ridge operation is outlined. Effects due to non-linearities in the dynamics have a major influence on the design. The initiation of large radial betatron oscillations at the centre of the machine could have serious consequences, and experimental model studies are now in progress to examine the problem. Apart from this, the suggested conversion should be feasible with careful design and construction.

1. Introduction

Fixed frequency, (C.W.), operation of conventional cyclotrons is limited by the condition for contemporary radial and vertical stability, $0 < n < 1.0$. In 1938, L. H. Thomas[1]) pointed out that by introducing suitable azimuthal field variation, vertical focusing might be achieved, even though the radially-increasing mean field necessary for C.W. operation, $(n < 0)$, were maintained. The *Thomas cyclotron* would have flat sector-shaped ridges on the polefaces.

More recently, the proposals of the Mid-West group of Universities relating to *Fixed Field. Alternating Gradient*, (FFAG), ring accelerators[2]) have found application in cyclotron design. With some modification, the "Mark V" FFAG principle is the basis of the *Spiral Ridge Cyclotron.* This machine would have spiral ridges on the magnet polefaces as indicated in fig. 1; the spiralling has the effect of increasing the degree of vertical focusing over that obtainable in a Thomas machine.

The non-linear fields resulting from such a poleface configuration lead to great mathematical complexity in the dynamics, the motion being both non-linear and coupled. However, as a starting point, we may disregard coupling terms and linearize the equations. A great deal of useful design information is obtained in this way, and a rough survey indicates the course which more accurate investigation should take.

Non-linear studies may then proceed in two stages. First, the median plane motion may be examined retaining non-linear radial terms in the equation, but neglecting coupling terms. Second, the coupled oscillations may be studied using a simplified pair of non-linear equations.

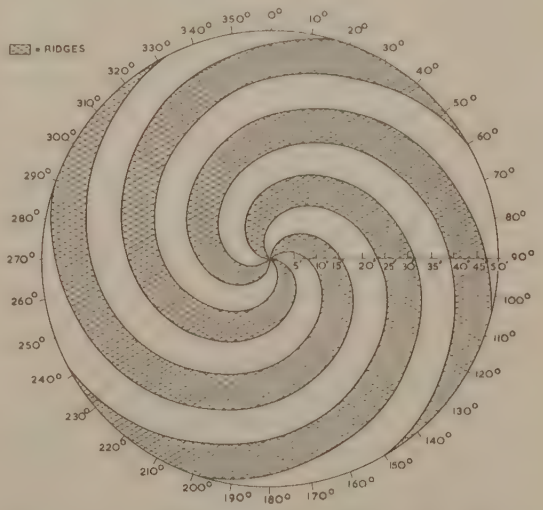

Fig. 1. Schematic Spiral Ridge Poleface with $N = 4$. A "linear spiral" law, $\theta = \alpha r$ has been chosen, with $\alpha = 0.1$ rad/in.

[1]) L. H. Thomas, Phys. Rev. **54** (1938) 580.

[2]) e.g. K. R. Symon *et al.*, Phys. Rev. **103** (1956) 1837.

As in the A.G. synchrotron[3]), the periodic nature of the fields leads to a great number of resonances in the motion, both intrinsic and error-induced. Many of these arise from non-linear terms inherent in the dynamics, and have proved to be extremely serious. Moreover, C.W. operation of a spiral ridge cyclotron differs fundamentally from acceleration in a synchrotron, in that the frequency of radial betatron oscillation is an increasing function of energy and radius in the machine. Hence it is not possible to select a fixed *working point* on a resonance chart[3]); rather must an extended *working path* be chosen. Only by introducing frequency modulation may the working point be "frozen". The working path must pass between, and possibly through, the resonance bands, a precise knowledge of which therefore assumes great significance.

With the advent of the spiral ridge principle, the possibility of converting the 110″ Harwell synchrocyclotron to C.W. operation came under active consideration. A considerable gain in beam intensity was anticipated, and moreover, an increase in proton kinetic energy to 240 MeV was projected. Calculations indicated that this could be achieved by re-distribution and augmentation of the present magnetic flux. Hence, the attractive prospect of obtaining low energy mesons, at greater intensities than any at present available, became apparent.

The theoretical studies outlined here were therefore initiated, analysis and computation progressing concurrently. A considerable understanding of the dynamics has been achieved; the analytic methods developed have proved satisfactory, and should greatly diminish the volume of computation necessary to establish any future design.

The consequences of the fact that the project concerned conversion of an existing machine should be emphasized. First, limitations on choice of parameters, imposed by practical requirements, quickly served to channel the theoretical studies on to a firm design, so that a concentrated and detailed investigation was carried out. On the other hand, this design was perforce more restricted than could have been devised for an entirely new machine. Many of the severe tolerances encountered might be relaxed in a future accelerator. However, the theoretical work indicates that conversion should be feasible given careful design and construction—with one important proviso.

This concerns the initiation of large radial oscillations at the centre of the machine. The effect occurs in conventional cyclotrons, but its consequences could be more serious in a spiral ridge machine. A tolerance of about 0.5″ on the amplitude of these oscillations in the conversion is demanded by the dynamics, and experimental studies are now in progress to decide if this is a realistic requirement.

The experimental programme at Harwell is proceeding along several lines. One group, under the direction of M. Snowden, has carried out extensive magnet measurements on a fifth-scale magnet. This magnet is now being modified for use as a 4 MeV spiral ridge cyclotron model, representing the centre of the converted machine. The particle orbits may then be examined in a region which is difficult to treat theoretically. Further studies will also be made in the present synchrocyclotron, to trace the source of radial oscillations.

Another group under J. D. Lawson is constructing an electron analogue of the conversion, in order to check the present theory and to estimate tolerances in the dynamics. The same group has set up a pendulum analogue[8]) which has already confirmed many aspects of the theory of radial oscillations.

The theoretical work has already been published in detail in a series of recent Harwell reports[4,5,6,7]), and in this paper we can only present a brief outline of the results. Many aspects of the data which do not bear directly

[3]) e.g. J. B. Adams and M. G. N. Hine, CERN-PS/JBA-MGNH/23 (1954).

[4]) W. Walkinshaw and N. M. King, A.E.R.E. GP/R 2050.

[5]) N. M. King and W. Walkinshaw, A.E.R.E. GP/R 2095.

[6]) N. M. King, A. E. R. E. GP/R 2205.

[7]) J. W. Burren, N. M. King and W. Walkinshaw, A.E.R.E. T/R 2342.

[8]) M. Russell, A.E.R.E. GP/R 2252.

on the conversion have been omitted, as has most of the mathematical treatment.

2. Machine Parameters

By choosing a field law which allows the equations of motion to be written independently of particle energy, we obtain *scaled dynamics*. Taking a sinusoidal modulation of field with azimuth†, which spirals in phase with increasing radius, the vertical component of magnetic field may be written,

$$B = B_0 \left(\frac{r}{r_0}\right)^k \left[1 + \delta \sin\left(N\theta - K \log \frac{r}{r_0}\right)\right] \quad (1)$$

with

$$r_0 = -Mv/eB_0 . \quad (1a)$$

Here, δ is the amplitude of modulation, or *flutter*, at a given radius, and N is the number of ridges. If we define the *spiral angle*, σ, to be the angle at which the spirals cut the circle r_0, then the parameter K is given by

$$\tan \sigma = N/K . \quad (1b)$$

It will be observed that the mean field of eq. (1) is power law in character, with *field index* k,

$$k = (r/B)\,(\partial B/\partial r) = -n , \quad (1c)$$

n being the conventional field gradient parameter. In the C.W. cyclotron, the mean field would have the form,

$$B = B_0\,[1 - (r/r_1)^2]^{-\frac{1}{2}}, \quad (2)$$

with

$$k = \gamma^2 - 1 , \quad (2a)$$

where $r_1 = c/\omega$, the radius of a relativistic particle of orbital frequency ω, and $\gamma = E/E_0$, the ratio of total to rest energy. Hence, in applying eq. (1) to the cyclotron, we must fit the C.W. mean field to the power law field at the particular energy under consideration, by proper choice of k. The procedure is accurate provided we are not too near the centre of the machine.

Choice of the other parameters is influenced considerably by practical requirements. In particular, sufficient flutter at the inner radii may only be obtained provided that N is small; in the Harwell conversion, (240 MeV at 50″), this restricts our choice to $N = 3$ or 4. The flutter will fall rapidly to zero at the centre, and, depending on the poleface geometry and the mean field required, may not exceed a certain value at any radius; for the conversion, the maximum attainable value of δ will be in the region of 0.15.

Finally, it is desirable, although not essential, for accuracy and ease of manufacture, to choose an Archimedean or *linear spiral* law, given by

$$\theta = \alpha r \quad (3)$$

so that

$$K = N\alpha r . \quad (3a)$$

In fig. 1 we illustrate the case $N = 4$, $\alpha = 0.1$ radians/inch. For computing proton trajectories at a given energy characterised by the radius r_0, we may take K to be a constant given by $N\alpha r_0$.

3. Linear Dynamics

To a good approximation, the median plane equation of motion for a proton of given energy may be written,

$$R'' - R = -R^2 \left(\frac{B}{B_0}\right)$$
$$= -R^{2+k}\,[1 + \delta \sin (N\theta - K \log R)] \quad (4)$$

where θ is the independent variable, and $R = r/r_0$. Writing $R = 1 + x$, and linearising in x, we obtain

$$x'' + [(1 + k) + (2 + k)\delta \sin N\theta - \delta K \cos N\theta]\, x = -\delta \sin N\theta . \quad (5)$$

Due to the forcing term on the right hand side, a particular solution of this equation is periodic with the ridge periodicity, $N\theta$. This solution is referred to as the *closed orbit*, and the free oscillations, (betatron oscillations), may be regarded as taking place around it. Several methods have been developed giving accurate formulae for the closed orbit, but to good accuracy we may use the simple relation,

$$x \approx -\frac{1}{2}\left(\frac{2 + k}{1 + k}\right)\frac{\delta^2}{N^2 - (1 + k)} + \frac{\delta}{N^2 - (1 + k)} \sin N\theta . \quad (6)$$

† In practice, ridges of rectangular section would be employed, and the resulting field modulation would consist of a series of harmonics. However, those of second and higher order would have small coefficients, and it is found that they would not affect the salient features of the dynamics to any great extent. Allowance must, of course, be made for them in an accurate design.

Denoting the normalised radial displacement from the closed orbit by y, we write $R = 1 + x + y$. Expanding about the closed orbit, we linearize in y, and discarding small terms, obtain the linear equation of radial betatron oscillations,

$$y'' + [\gamma_0 + \gamma_1 \sin N\theta + \gamma_2 \cos N\theta]\, y = 0 , \quad (7)$$

with

$$\left.\begin{aligned} \gamma_0 &\approx (1 + k) - \frac{1}{2}\delta^2 K^2/\{N^2 - (1 + k)\} \\ \gamma_1 &\approx \delta(2 + k)N^2/\{N^2 - (1 + k)\} \\ \gamma_2 &\approx -\delta K . \end{aligned}\right\} \quad (7a)$$

Similarly, the linearized equation of vertical betatron oscillations may be written in the form,

$$Z'' + \left[-R^2 \frac{\partial}{\partial R}\left(\frac{B}{B_0}\right) + \frac{\partial R}{\partial \theta}\frac{\partial}{\partial \theta}\left(\frac{B}{B_0}\right)\right] Z = 0 \quad (8)$$

where Z is the normalised vertical co-ordinate z/r_0. Assuming that the vertical oscillations are taking place about the radial closed orbit, we write $R = 1 + x$, given by eq. (6), and obtain the approximate relation,

$$Z'' + [\zeta_0 + \zeta_1 \sin N\theta + \zeta_2 \cos N\theta]\, Z = 0 \quad (9)$$

with

$$\left.\begin{aligned} \zeta_0 &\approx -k + \frac{1}{2}\frac{\delta^2(N^2 + K^2)}{N^2 - (1 + k)} \\ \zeta_1 &\approx -\frac{\delta k N^2}{N^2 - (1 + k)} \\ \zeta_2 &\approx \delta K . \end{aligned}\right\} \quad (9a)$$

Eqs. (7) and (9) are of Mathieu type and their properties are well known. Their solutions for small amplitudes of oscillation about the closed orbit are in good agreement with accurate numerical results.

The focusing strengths are related directly to the betatron frequencies, expressed alternatively in terms of the parameters Q or μ: Q is defined as the number of complete oscillation wavelengths per revolution of the machine, and μ is the phase change of the oscillation per period of the system. They are connected by the relation,

$$\mu = 2\pi Q/N . \quad (10)$$

Radial and vertical parameters will be denoted by subscripts R and V respectively. The frequency in the first stability band of the Mathieu eq. (7) is given by

$$\cos \mu_R = \cos (2\pi\gamma_0^{\frac{1}{2}}/N) - \left(\frac{\pi}{N}\right)^2 \frac{\sin (2\pi\gamma_0^{\frac{1}{2}}/N)}{2\pi\gamma_0^{\frac{1}{2}}/N} \frac{\gamma_1^2 + \gamma_2^2}{N^2 - 4\gamma_0} . \quad (11)$$

The equation for μ_V is obtained on replacing the γ_n by ζ_n. However, for small μ, (roughly when $\mu < \pi/2$), we may approximate to the sine and cosines in eq. (11) to obtain the *smooth approximation* formula,

$$\mu_R^2 = \frac{4\pi^2\gamma_0}{N^2} + \frac{2\pi^2}{N^2}\frac{(\gamma_1^2 + \gamma_2^2)}{N^2} . \quad (11a)$$

Applying this procedure to both the radial and vertical equations, and neglecting $(1 + k)$ in comparison with N^2, we derive the approximate relations,

$$Q_R^2 = (1 + k) - \frac{\delta^2 K^2}{2N^2} + \left[\frac{\delta^2 K^2}{2N^2} + \frac{\delta^2(2 + k)^2}{2N^2}\right] \approx (1 + k) \quad (12)$$

$$Q_V^2 = -k + \frac{1}{2}\delta^2 + \frac{\delta^2 K^2}{2N^2} + \left[\frac{\delta^2 K^2}{2N^2} + \frac{\delta^2 k^2}{2N^2}\right] \approx -k + \frac{1}{2}\delta^2 + \frac{\delta^2 K^2}{N^2} . \quad (12a)$$

The terms $(1 + k)$ and $-k$ in these expressions represent the radial focusing and vertical defocusing due to the mean field. In the radial case, the other terms largely cancel; they represent the focusing effects at the ridge edges, offset by the "scalloped" nature of the closed orbit. In the vertical case, these terms reinforce each other, and are augmented by the *Thomas focusing term*, $\frac{1}{2}\delta^2$, which would still be obtained in the absence of spiralling, (for radial ridges, $\sigma = \pi/2$ and $K = 0$).

In the cyclotron, vertical focusing is necessarily weak, so that eq. (12a) should give a reasonable estimate. On the other hand, for small N, μ_R is likely to be greater than $\pi/2$, so that eq. (12) is not reliable; a better estimate is afforded by eq. (11), but as we shall see later, non-linear terms affect the value of μ_R.

However, we note that Q_R will be close to unity near the centre of the machine and will increase with energy. Owing to the difficulty of obtaining sufficient flutter near the centre, Q_V will be imaginary, (vertical defocusing), in this region; inserting suitable values for the parameters, we find that it is never likely to exceed $\frac{1}{2}$ at any time during the acceleration.

4. Resonances

Since (7) and (9) are Mathieu equations, stop-bands occur wherever $\mu = s\pi$, s being an integer. These are exceedingly serious resonance regions which it will be impossible to traverse. Thus, the *radial π-mode*

$$\mu_R = \pi, \quad Q_R = N/2 \tag{13}$$

provides a definite limitation to C.W. cyclotron operation. In fig. 2 we plot the energy at which the π-mode of eq. (7) occurs, with $N = 3$, for different values of Q_V. The limitation at about 190 MeV immediately eliminates the possibility of using $N = 3$ for the conversion.

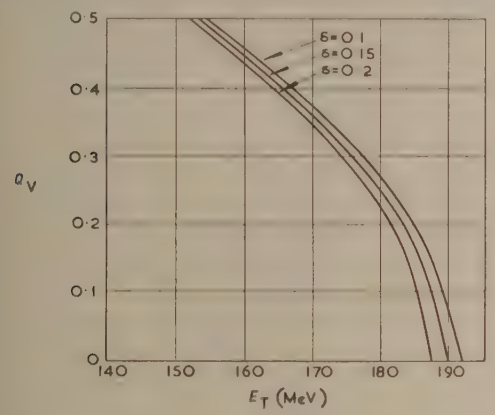

Fig. 2. Energy of radial π-mode ($Q_R = 3/2$), for $N = 3$.

Smoothing out the linearized motion into sinusoidal oscillations, we may introduce perturbing terms representing either the effects of various kinds of error, or of other terms intrinsic to the dynamics but neglected on the linear approximation. The presence of further resonances may then be deduced from the occurrence of resonance denominators, (e.g. $Q^2 - s^2$), in the solutions.

For example, field "bumps" may be analysed into azimuthal harmonics which appear in the equations and lead to resonance wherever

$$Q = s \tag{14}$$

(Q is taken to mean either Q_R or Q_V, and s is any integer).

These linear *integral resonances* are extremely serious[9]), even for very small errors, and it is not considered practicable to traverse them. In particular, the case $Q_R = 2$ is the chief limitation in a high-energy cyclotron with large N. As $N \to \infty$, $Q_R \to (1 + k)^{\frac{1}{2}} = \gamma$, so that the upper limit for C.W. operation will be 938 MeV. (For finite N, this energy is reduced:—to about 900 MeV with $N = 12$, 850 MeV with $N = 8$, and 770 MeV with $N = 6$.)

Similarly, errors in the field modulation give rise to resonance conditions wherever

$$Q = \frac{1}{2}s \,. \tag{15}$$

These linear *half-integral resonances* are also serious. In particular, the case of $Q_V = \frac{1}{2}$ may be very dangerous, owing to the small vertical aperture available in a cyclotron. The radial resonances at $Q_R = 3/2$, etc., may possibly be traversed with careful design and construction. We note that the radial π-mode coincides with either an integral or half-integral resonance, depending on whether N is even or odd.

Non-linear terms in the equations lead to a great number of resonances. When deriving the linear radial eq. (7), a complete series of terms, y^n, $n = 2, 3, 4, \ldots$ etc., was neglected. These terms appear in the equation of motion multiplied by $\cos N\theta$, $\sin N\theta$, or higher harmonics. As a result, there is a set of *intrinsic radial non-linear resonances* in the motion. For example, the quadratic terms lead to resonance conditions for

$$Q_R = N/3, \quad \mu_R = 2\pi/3 \,, \tag{16}$$

the cubic terms for

$$Q_R = N/4, \quad \mu_R = 2\pi/4 \,, \tag{16a}$$

and s^{th}-order terms for

$$Q_R = N/(s + 1), \quad \mu_R = 2\pi/(s + 1) \,. \tag{16b}$$

The quadratic $2\pi/3$-mode resonance is a major obstacle to acceleration in a four-ridge C.W. machine, and it is important to estimate the energy at which it occurs. In fig. 3 this energy is plotted as function of Q_V, μ_R being calculated on linear theory. The curve indicates that the choice of $N = 4$ may be only just possible for a 240 MeV C.W. machine. We shall see in the next

[9]) P. D. Dunn *et al.*, CERN Symposium Proceedings (1956) (this paper contains some of the material in ref. [4])).

section how this assessment is modified by the non-linear studies. The cubic resonance at $2\pi/4$-mode occurs for $Q_R = 1$ when $N = 4$; that is, at the centre of the cyclotron. Hence, operation of the conversion will take place in the range $2\pi/4 < \mu_R < 2\pi/3$.

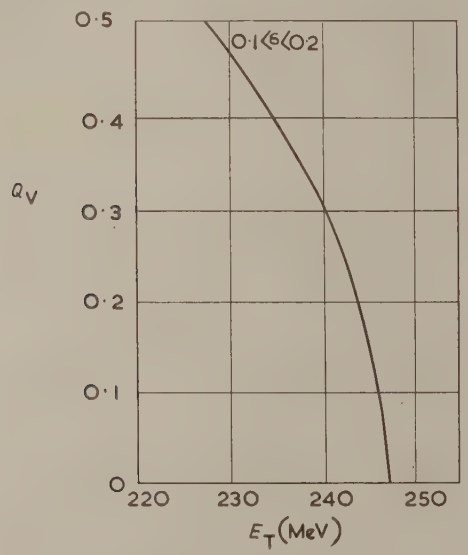

Fig. 3. Energy of radial $2\pi/3$-mode, ($Q_R = {}^4/_3$), for $N = 4$.

Similarly, the linearized treatment neglected series of coupling terms of type $y^\lambda Z^\nu \cos sN\theta$ in both the radial and vertical equations. Owing to the small vertical aperture, coupling from the radial into the vertical motion could have serious consequences. *Quadratic coupled resonances* are found to arise when

$$\left.\begin{aligned} Q_R \pm 2Q_V &= s \\ 2Q_R \pm Q_V &= s \end{aligned}\right\} \qquad (17)$$

and resonances of p^{th} order occur for

$$\left.\begin{aligned} aQ_R \pm bQ_V &= s \\ \text{with} \qquad (a+b) &= (p+1) \end{aligned}\right\} \qquad (18)$$

where a, b, p, s, are integers. In general, these resonances are intrinsic to the motion when $s = N$ or zero, and are most serious when the coefficient of Q_V is even. Errors may also give rise to *linear coupled resonances*, given by

$$\left.\begin{aligned} Q_R - Q_V &= \pm s \\ Q_R + Q_V &= s. \end{aligned}\right\} \qquad (19)$$

By far the most serious intrinsic coupled resonance is the quadratic instability $Q_R - 2Q_V = 0$. This corresponds, in conventional cyclotrons, to the well known $n = 0.2$ resonance, but is considerably more dangerous in spiral ridge machines. We shall see later that some of the higher order resonances must also be taken into consideration in the design. The linear coupled error resonance, $Q_R - Q_V = 1$, must also be borne in mind, since part of the early acceleration may take place in its vicinity.

The *resonance chart* for an $N = 4$ machine is illustrated in fig. 4; this type of diagram tends to give a distorted picture of the tolerances

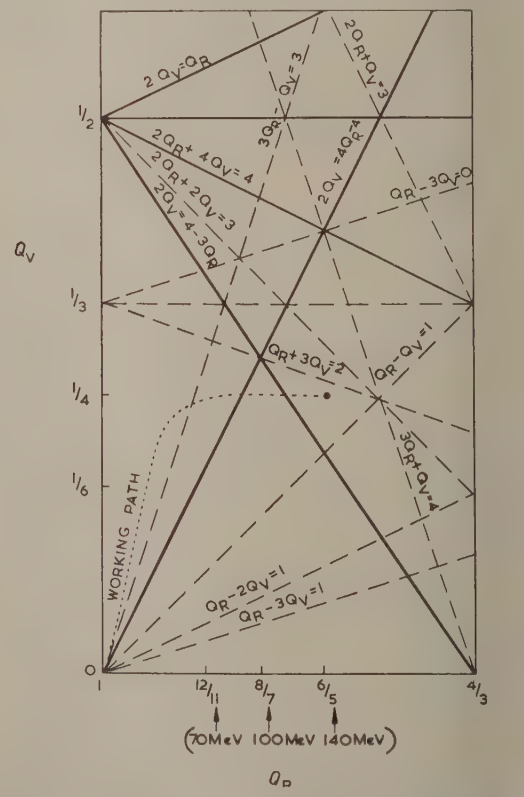

Fig. 4. Resonance chart for $N = 4$. Intrinsic resonances are drawn as full lines, error resonance are broken. Energies marked on the Q_R axis refer to C.W. operation, and a rough working path for the C.W. region is shown.

involved in moving between resonances, and a more realistic chart is obtained by plotting energy or radius in place of Q_R. In particular,

the tolerance in attempting to work between $Q_V = 0$ and the $Q_R - Q_V = 1$ error line near the centre of the machine is prohibitive.

5. Non-Linear Radial Motion

More accurate studies of the median plane motion may be carried out by numerical integration of eq. (4) or the simplified relation,

$$\rho'' + (1 + k)\rho = -\delta \sin(N\theta - K\rho), \quad \rho = R - 1, \quad (20)$$

which gives an excellent representation of the dynamics. Analysis carried out on the basis of eq. (20) has served to explain most of the features observed computationally. The effects of the non-linear resonances at $\mu_R = 2\pi/3$, $2\pi/4$, etc., have been interpreted satisfactorily[10,11]).

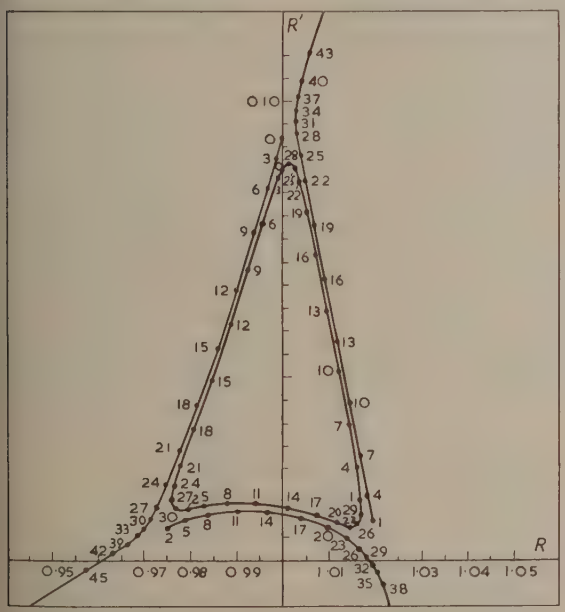

Fig. 5. Radial phase plot near $2\pi/3$-mode, for $N = 4$, $\delta = 0.15$. The proton energy is 200 MeV ($k = 0.4718$), and $Q_V = 0$, ($K = 18.0936$). Two orbits are shown, one stable and one unstable. Numbered points refer to the periodic intervals $\left(\frac{N\theta}{2\pi}\right) = 0, 1, 2 \ldots$ etc.

Many of the results have also been reproduced on a pendulum analogue[8]).

In the numerical work, the range between $2\pi/4$ and $2\pi/3$-modes has been investigated extensively for the conversion project. Orbits

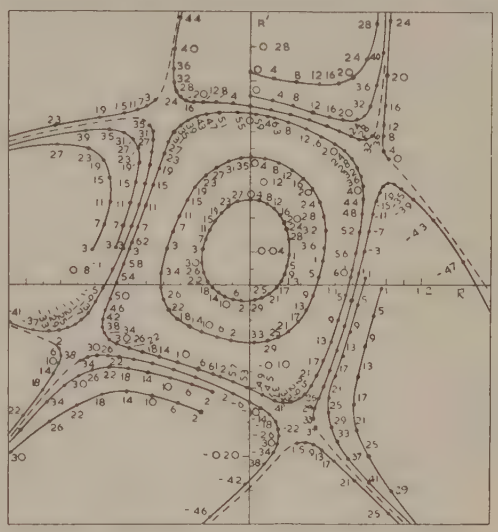

Fig. 6. Radial phase plot near $2\pi/4$-mode, for $N = 4$, $\delta = 0.15$. The proton energy is 25 MeV, ($k = 0.054003$) and $Q_V = 0$, ($K = 5.5137$). Seven orbits are represented, three stable and four unstable.

have been plotted at periodic points, $N\theta = 0$, 2π, 4π, etc., in the $(R, \mathrm{d}R/\mathrm{d}\theta)$ phase plane, the computations being carried out on a digital computer.

Fig. 5 is a typical example of the results obtained near $2\pi/3$-mode. For sufficiently small amplitudes of oscillation about the closed orbit, the periodic points lie on a closed contour. As the amplitude is increased, the oscillation frequency is affected, and approaches closer to $2\pi/3$-mode; the non-linearities cause the contours to become more angular, and they assume a pseudo-triangular form. If the amplitude exceeds a certain value, the oscillation immediately locks into resonance, and exponential growth sets in. The phase contours then break up into three separate branches.

Similarly, near $2\pi/4$-mode, the frequency changes with amplitude and eventually locks into resonance. The closed contours in this case are pseudo-rectangular and the unstable orbits have four branches, (see fig. 6). A rough survey of an $N = 6$ machine confirms the presence of analogous effects near $2\pi/5$-mode:—five-sided

[10]) M. Bell, A.E.R.E. T/R 2209.
[11]) D. Morgan, A.E.R.E. T/R 2361.

closed contours and five-branch instability. No instability was apparent near $2\pi/6$ in this case, tending to confirm the theoretical prediction that those resonances of higher order than $2\pi/3$ are conditional in character.

This behaviour has been reproduced analytically[10, 11]), and expressions for the bounding curve or *separatrix* between stable and unstable regions of phase space have been derived. The separatrix is characterised by *fixed points* at its extremities,—three fixed points for $2\pi/3$-mode, four for $2\pi/4$-mode, and so on. Orbits with initial conditions corresponding to a fixed point are *fixed point solutions*; their frequency is $2\pi/3$ or $2\pi/4$ exactly, and they continue to retrace the set of fixed points on successive revolutions, being completely represented by them. Orbits starting elsewhere on the separatrix tend towards the fixed point solutions but never reach them.

Computations have shown that the exponential growth is halted when the orbit divergence, R', becomes equal to the spiral angle, σ. This is the phenomenon of *ridge-running*, where the orbits appear to oscillate with a large amplitude modulation. However, this possible ultimate stability is of no practical consequence, since the amplitude at which it occurs is generally much too great.

Between resonance modes, further phenomena arise. In particular, *island formation* occurs, characterised by the disintegration of the contours, at sufficient amplitude, into a set of disconnected "islands" lying around the last single closed contour. This behaviour is connected with the existence of higher-order commensurabilities in the oscillation frequency. Thus, defining

$$\mu_R = 2\pi q_R\,, \quad q_R = Q_R/N\,, \qquad (21)$$

q_R is the number of oscillations per magnet period. We see that for $\mu_R = 2\pi/n$, one oscillation is carried out in n periods; e.g. $\mu_R = 2\pi/3$, $q_R = 1/3$, and the oscillation is commensurable with three periods. Between $^1/_4$ and $^1/_3$, q_R may assume an infinite number of rational fractional values, and with each of these, a higher order commensurability occurs. For example, with $q_R = 2/7$, two complete oscillations are carried out in seven periods. In the neighbourhood of this frequency we observe seven islands. Theoretically, there is no limit to the number of islands which may be formed, but as they increase in number and decrease in size, the possibility of observing them, computationally, becomes small.

Fig. 7 shows how the non-linear resonances restrict operation in the conversion. The maximum stable radial betatron amplitude, read from phase plots such as figs. 5 and 6, is plotted against machine radius and energy for two values of Q_V. (Islands have been ignored for this purpose; the outermost single closed contours were regarded as the stability limit.) It will be seen that the effects of the $2\pi/3$-mode resonance extend inwards some distance from the perimeter of the machine, and would create considerable beam loss if C.W. operation were maintained. The original proposal was therefore modified to the extent that C.W. operation should cease at about 40″ or 140 MeV, and a separate F.M. accelerating system should be employed over the last 10″. Calculations indicated that less than 2% F.M. would be required, so that the decrease in intensity should not be great. The mean field in the outer region would be power law, so that k would be constant and the working point on the resonance chart would be "frozen".

Fig. 7 also indicates that the effects of the $2\pi/4$-mode, near the centre, might be serious. At the 10″ radius, the betatron oscillation amplitude should be less than $\frac{1}{2}$″ if serious loss is not to occur. This may be a stringent requirement, since in conventional machines, oscillations initiated near the centre may certainly be greater than this value. A model of the central region is now under construction, and this problem will be investigated experimentally. It may also be remarked here that, owing to the difficulty of getting large enough δ at the centre, Q_V may be imaginary out to about 5″ or 6″. The vertical oscillations will therefore grow to some extent.

Returning to the curves of fig. 7, it is of

interest to note that, for a given Q_V, the available stable amplitude varies almost linearly with δ, provided we are not too close to the centre. For a given δ, the ampl tude varies inversely, in a complicated way, with Q_V However, we may use linear interpolation between $Q_V = 0$ and $\frac{1}{2}$ to a fair degree of accuracy.

values of ω_1, ω_2 and λ. The radial phase plots obtained do not differ essentially from those described in § 5, but the vertical phase plots exhibit new features.

For the small vertical amplitudes possible in the cyclotron, coupling from radial into vertical motion is important; the reverse process is not

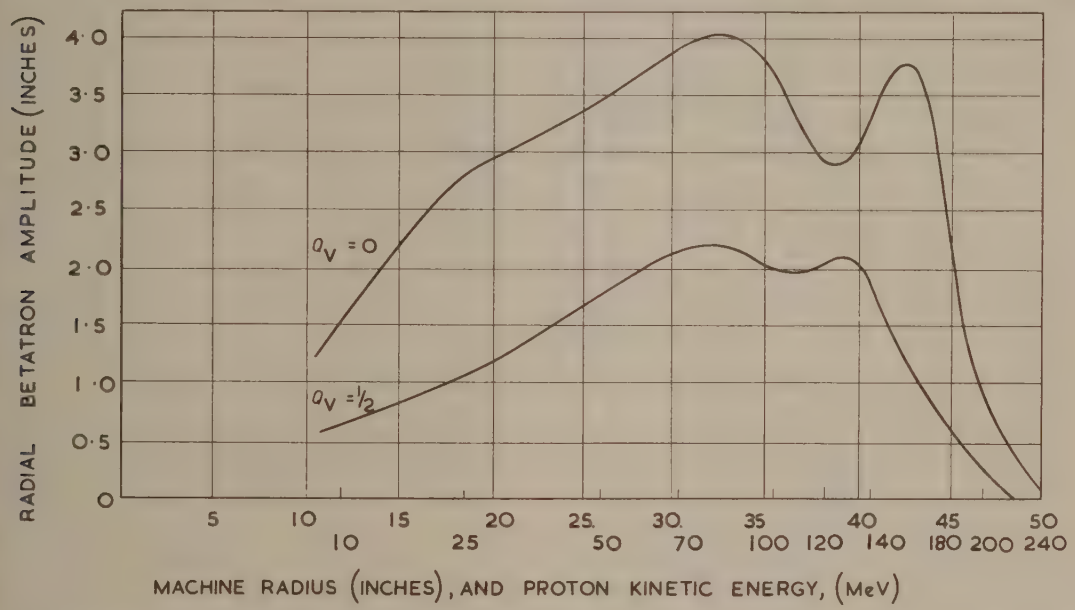

Fig. 7. Maximum available stable radial betatron amplitude in an $N = 4$, C.W. cyclotron. The dips at 0″ and 50″ are due to the $2\pi/4$ and $2\pi/3$-mode resonances respectively. Island formation is observed mainly in the range 30″–40″.

6. Coupled Motion

The coupled dynamics may be represented simply and effectively by the pair of equations,

$$\left.\begin{aligned} \rho'' + (1+k)\rho &= -\delta \sin (N\theta - K\rho) \cosh KZ \\ Z'' - kZ &= -\delta \cos (N\theta - K\rho) \sinh KZ \end{aligned}\right\} \quad (21)$$

or alternatively, defining $\xi = K\rho$, $\eta = KZ$, $\phi = N\theta$,

$$\left.\begin{aligned} \xi'' + \omega_1^2 \xi &= -\lambda \sin (\phi - \xi) \cosh \eta \\ \eta'' - \omega_2^2 \eta &= -\lambda \cos (\phi - \xi) \sinh \eta \end{aligned}\right\} \quad (22)$$

where

$$\omega_1^2 = (1+k)/N^2, \quad \omega_2^2 = k/N^2, \quad \text{and } \lambda = \delta K/N^2 . \quad (22a)$$

A great number of orbits have been computed from these equations with $N = 4$ and different values of k corresponding to operation in the conversion. However, the results may have application to other machines with similar significant. We may therefore write $\cosh \eta = 1$ in the radial equation, and $\sinh \eta = \eta$ in the vertical equation. The latter is therefore linear in η. Inserting an approximate non-linear solution ξ in the cosine term, we find eventually that the vertical stability is well represented by a Hill equation of the form

$$\begin{aligned} \eta'' + [\alpha_0 &+ \alpha_1 \sin (q_R\phi + \varepsilon) \\ &+ \alpha_2 \sin \{(1 - 3q_R)\phi - 3\varepsilon\} \\ &+ \alpha_3 \cos \{(4q_R - 1)\phi + 4\varepsilon\}]\eta = 0 \end{aligned} \quad (23)$$

where the α_n are functions of λ and A_R, A_R being a parameter representing the radial betatron amplitude; ε is a phase term, also coming from the radial motion. We now see that the periodic terms in the force bracket are controlled largely by the radial periodicity q_R. The machine periodicity plays a less significant part; this is

graphically illustrated by the vertical phase plots, which are best drawn as sets of branches whose number is determined by the radial periodicity.

as those of figs. 8 and 9, where, for a given value of k, the stable and unstable zones are plotted in terms of λ and A_R. The parameter λ is essentially a measure of the strength of vertical

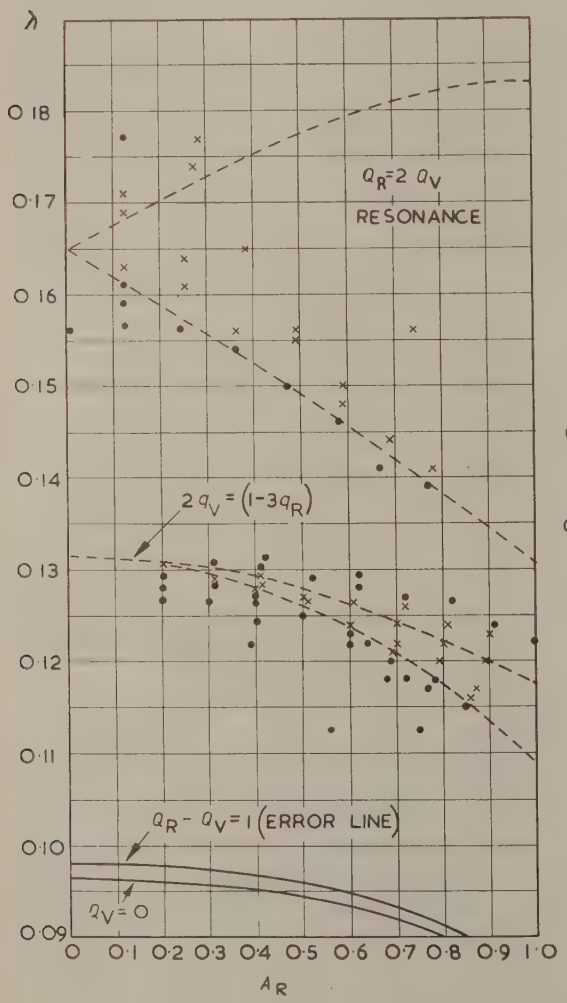

Fig. 8. Coupled resonances at 70 MeV.
$N = 4 \quad \delta = 0.15 \quad k = 0.1548$
$\omega_1^2 = 0.072175 \quad \omega_2^2 = 0.009675$

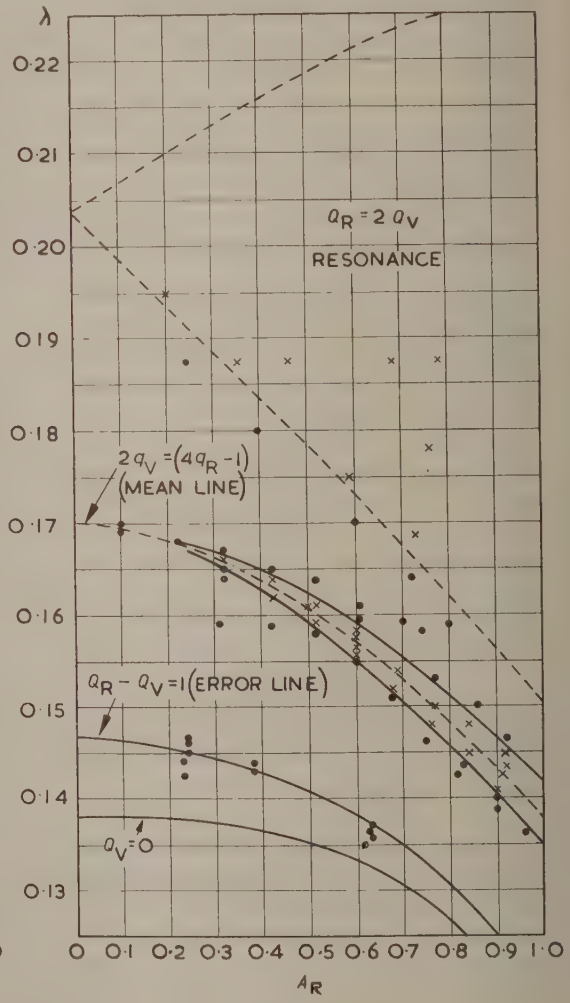

Fig. 9. Coupled resonances at 140 MeV.
$N = 4 \quad \delta = 0.15 \quad k = 0.3207$
$\omega_1^2 = 0.08254 \quad \omega_2^2 = 0.02004$

$\lambda = \delta K/N^2$; A_R is a measure of radial betatron amplitude. For the linear spiral law, $\alpha = 0.1$, the amplitude in inches is given approximately by $2.5\,A_R$. ——— Theoretical resonances edges,
• stable, × unstable } computed orbits.
$Q_R - Q_V = 1$ and $Q_V = 0$ lines are approximate.

We may plot the stop-bands of the Hill eq. (23) in a similar fashion to Mathieu stop-bands. The situation is best illustrated on charts such

focusing. Each of the oscillatory terms in eq. (23) gives rise to a stop-band whose position depends on the other two terms.

Resonance occurs for

$$2q_V = q_R, \quad 2q_V = 1 - 3q_R, \quad \text{and} \quad 2q_V = 4q_R - 1. \quad (24)$$

The first of these instabilities is simply the prohibitive quadratic coupling resonance mentioned in § 4; the others come from higher-order coupling terms.

The charts of figs. 8 and 9 have been drawn for 70 MeV, ($q_R \approx 3/11$) and 140 MeV, ($q_R \approx 3/10$), respectively; the resonance edges have been calculated theoretically. Each of the plotted points represents an orbit computed from eq. (21), dots referring to stable, and crosses to unstable, orbits. Excellent agreement between analysis and computation is evident. It will be observed that, for a given λ, the vertical frequency increases with radial amplitude, and for a sufficiently great value of A_R, the vertical motion becomes unstable.

The resonance bands have been investigated over the energy range between 70 MeV and 140 MeV. It is observed that; (a) The $2q_V = q_R$ instability is extremely serious everywhere. Therefore we should never allow the working path to approach it for reasonable values of A_R. (b) The $2q_V = 1–3q_R$ resonance width does not change appreciably up to about 120 MeV, but seems to be very narrow above that energy. (c) The $2q_V = 4q_R–1$ case only appears to be important between about 100 MeV and 140 MeV. A working path such as that sketched in fig. 4 is therefore indicated. The build-up to be acticipated in crossing the $2q_V = 1–3q_R$ resonance region has been examined theoretically and computationally; the results recommend that, if the amplitude of small vertical oscillations is not to double, then the radial betatron amplitude should not exceed about 0.5″.

The vertical amplitude build-up due to any of these resonances is eventually arrested when the vertical non-linearities become appreciable, and back-coupling begins to take place. However, in the case of the $2q_V = q_R$ resonance, this *turnover* only occurs when the amplitude has grown much greater than the vertical aperture. In the other cases, the turnover amplitude is critically close to the available aperture, and it would not be safe to rely on this effect in designing a machine.

7. Conclusions

Many aspects of the design may be illustrated on a diagram such as that of fig. 10. The chart is calculated for a chosen linear spiral parameter, α, whose value in the conversion should be in the neighbourhood of 0.1 rad/in. Plotting Q_V against machine radius, r_0, we draw contours of constant δ, and superpose the $2q_V = 1–3q_R$ and $2q_V = 4q_R - 1$ resonance lines for zero radial betatron amplitude, $A_R = 0$; the $Q_R - Q_V = 1$ error line has also been included. The sharp change in the curves at the 40″ radius is due to the switch from C.W. to F.M., power law, operation.

When selecting a working path on this diagram, the following considerations should be borne in mind:— (a) As remarked in § 6, it is best to traverse the non-linear coupled resonances below their crossover. Also, as A_R becomes finite, these lines will broaden out into bands, and will appear to shift downwards on the chart; hence the working path should not approach too close to the crossover of fig. 10. (b) In practice it is not possible to obtain the required δ at the centre of the machine; the first part of the fig. 10 working path has been selected in accordance with experimental model measurements. (c) It will not be possible at any radius in the conversion to achieve a δ greater than about 0.15. Hence, the above working path approaches the practical limit. By slightly increasing α, this condition may be relaxed, but we recall that, for a given Q_V, a smaller δ will reduce the available amplitude of stable radial oscillation. The decrease in δ over the last 10″, necessary to maintain a constant Q_V, will have this effect, but as may be deduced from fig. 7, the consequences should not be serious in this region. The required fall-off may be readily achieved in practice by proper design of poleface geometry.

The diagram amply illustrates the tolerances on δ throughout the acceleration. Near the centre, Q_V is insensitive to changes in δ, but by the time the particles have reached 140 MeV, a change in δ from 0.15 to 0.145 could bring the working point down to the $2q_V = 1—3q_R$ and $Q_R - Q_V = 1$ resonances. These extremes are

undesirable, since, having fixed K by our choice of spiral law, δ is our only remaining control on vertical focusing. Small variations in the flutter may be achieved by using correcting coils.

Summarising, the dynamical studies briefly discussed above indicate that conversion should be feasible given, (a), careful design and construction, and (b), provided that sufficient protons with less than about 0.5″ radial oscillation amplitude may be accelerated from the centre. This latter problem will be examined experimentally. The recommended design incorporates four ridges with a linear spiral law, $\theta = \alpha r$, $\alpha = 0.1$ rad/in., and should give 240 MeV protons at the 50″ radius. Fixed frequency operation should extend to 140 MeV, about 40″ radius; thereafter, a power law mean field is required, involving less than 2% frequency modulation. This degree of F.M. may be obtained readily with a conventional rotating condensor system, but the use of ferrite offers the prospect of higher repetition rates. To obtain large beam currents we require higher dee voltages, and the voltage limitation is ultimately set by the size of magnet gap. With a 6″ minimum gap, fixed from considerations of the required flutter, a dee voltage of about 50 kV should be feasible. In conjunction with a repetition rate of 1 000 c/s this should allow a beam current of between 20 μA and 100 μA to be obtained.

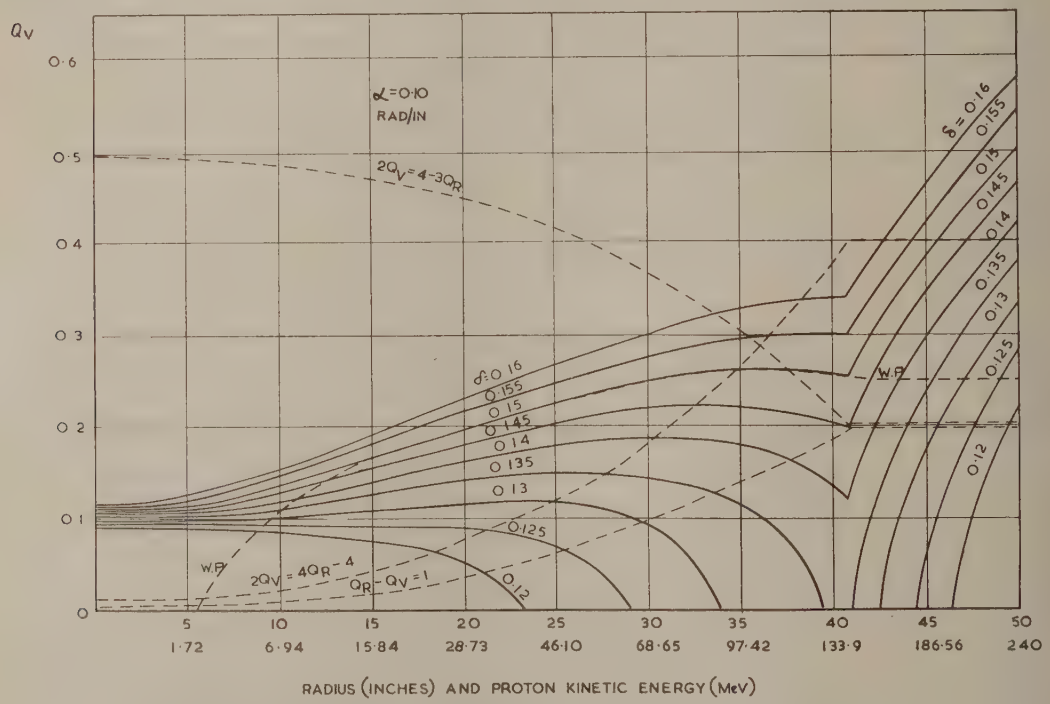

Fig. 10. Suggested working path, (W.P.), in Harwell conversion with linear spiral law, $\theta = \alpha r$, $\alpha = 0.10$ rad/in. Resonances for zero radial betatron amplitude are shown as dotted lines.

The authors wish to thank M. Snowden, who is in charge of the experimental group working on the conversion project, for many helpful discussions. J. W. Burren, D. Morgan, and Mrs. M. Bell have contributed to the non-linear theoretical studies. Most of the extensive computational programme was carried out on DEUCE, at A.W.R.E., and thanks are due to Dr. J. Corner who arranged for computing time to be made available. Some computation has also been done on DEUCE at the N.P.L., Teddington.

NUCLEAR INSTRUMENTS 2 (1958) 299–331; NORTH-HOLLAND PUBLISHING CO. – AMSTERDAM

PHOTOGRAPHIC RECORDING METHODS IN NUCLEAR PULSE SPECTROMETRY

D. MAEDER

E.T.H., *Zurich*†

Received 12 October 1957

Applications of photographic techniques as a tool in measuring pulse amplitude (PA) distributions fall into 3 general groups:

(1) Recording of individual events as they arrive from the nuclear radiation detector, with subsequent analysis based on visual or photoelectric inspection of the record.

(2) Time exposures of a large series of events, the distribution analysis being provided by the exposure-density correspondence in the photographic process.

(3) Use for permanent storage of results from counting equipment, after the pulse sorting has been performed electronically.

The first and third groups will be reviewed in sections 2 and 5, and some improvements of existing techniques suggested. Quantization of variables is discussed in §§ 2.5 and 2.6 as a simple means for removing ambiguities in automatic scanning of individual event records.

For the second group a thorough presentation of design problems and evaluation procedures is attempted (sections 3 and 4). Gray wedge (GW) techniques lead to a straightforward quantitative interpretation of photographed PA spectra.

The simplest version of a fast GW spectrometer consists of a commercial oscilloscope and a special plug-in adaptor unit. The adaptor described in § 3.3 provides double rectangular pulse shaping, various shape corrections, overload protection, and generates an exponential sawtooth voltage derived from the linear oscilloscope sweep. This simple GW spectrometer is particularly useful at high counting rates (up to 10^5 counts/sec).

For a more general use (at both high and low intensities) additional parts such as pulse stretchers, gating circuits and various sweep or wedge arrangements are needed (§ 3.4). Stretching and gating requirements will be discussed from a general point of view, and details of circuits used at the ETH will be presented in §§ 3.5 through 3.7. Various methods of producing GW effects are reviewed and the calculated wedge characteristics and light efficiencies compared (§ 3.8). Advantages of the electronic type of GW are the freedom from light losses, simplicity of construction, and versatility in selecting different wedge characteristics. Photographic procedures (§ 3.10) include the use of a printing process to obtain easy-to-read graphs of the PA spectra. Empirical calibration is described in §§ 3.11 and 3.12, and the sources of deviations from the calculated behaviour are discussed.

Absolute intensity evaluation from GW pictures is made possible, as shown in section 4, if the spectrometer is equipped with a few electronic counting channels and an automatic channel limit marker to establish the correspondence between the photographic curve and the channel counts. In coincidence measurements both individual dot recording and density recording of two-dimensional distributions are found useful. Again, combining the photographic technique with a relatively small number of counting circuits permits the determination of absolute intensities.

The high speed at which information from electronic counting equipment may be accepted for permanent storage on film makes the use of photographic techniques particularly attractive for automatic recording (section 5). Programming of a serial memory spectrometer including dead time correction is described in § 5.2. A scanning mechanism is proposed in § 5.3 to read previous results back into the spectrometer memory, with provision for semi-automatic computation of linear combinations.

1. Introduction

Numerous review articles on the art of measuring pulse amplitude (PA) distributions have been published in the past few years[1–8]; most of them concentrate on electronic counting devices which store the results in a set of mechanical registers and/or electronic scalers, or, in some recent versions, give a permanent record using a mechanical printer or plotter. The purpose of the

† Present adress: Oak Ridge National Laboratory, Oak Ridge (Tenn.).

[1]) J. H. Parsons, ORNL-Report 1827 (March 1948) Proc. I.R.E. **37** (1949) 564.

[2]) N. F. Moody ,W. J. Battell, W. D. Howell and R. H. Taplin, Rev. Sci. Instr. **22** (1951) 439 and 551.

[3]) G. G. Kelley, Nucleonics **10** (4) (1952) 34.

[4]) A. B. Van Rennes, Nucleonics **10** (7) (1952) 20; (8) 22; (9) 32; (10) 50.

[5]) E. Baldinger and W. Haeberli, Ergebn. d. ev. Natur **27** (1953) 248.

[6]) G. G. Kelley, Geneva Conference, Paper P/66 (1955).

[7]) W. A. Higinbotham, Nucleonics **14** (4) (1956) 61.

[8]) J. L. W. Churchill and S. C. Curran, Advances in Electronics and Electron Phys. **8** (Acad. Press Inc., New York, 1956) 317.

present paper is to summarize photographic techniques replacing or supplementing complex electronic and electromechanical equipment. These procedures will be described with reference to PA spectrometers, but may of course be applied to the design of time interval spectrometers as well.

Historical arrangements[9-11]), which required the use of photographic recording because electronic sorting circuits were not available, have later led to the development of the modern dot recording (DR) system including automatic scanning[14-16]). Here the photographic material serves to store the original information with essentially no loss. One single counter may then perform the analysis into channels later on, at the expense of some delay before the results are known. Although existing equipment of this type does not produce channels of accurately defined width, it seems probable that absolute counting precision can ultimately be realized with an improved DR system (section 2).

Other photographic methods depend on the evaluation of densities and their wide use is mainly due to the simplicity of equipment required[1,18-28]). In the presentation of these methods (section 3) emphasis is placed on gray wedge (GW) techniques[18-21,26-28]) which automatically yield a photographic plot of the PA spectrum. Empirical intensity calibration using samples of artificial continua will be discussed. However, methods depending on density evaluation alone will not, in general, give absolute intensity values to better than about 10% accuracy; therefore a combination with counting devices[29,30]) has been worked out at Zurich which is described in section 4. Here the photographic record is intended to interpolate, with a resolution corresponding to a large number of channels, between the absolute counts obtained from a small number of electronic counting channels which are set to monitor characteristic portions of the spectrum investigated.

In coincidence work involving PA measurement of both coincidence partners two-dimensional photographic DR offers the advantage of a resolution equivalent to about $100 \times 100 = 10^4$ channels which is at present not available in any purely electronic counting system. Individual events[30,31]) or average densities[32-35]) may be evaluated in such applications, depending on the total number of coincidences accumulated on a single frame.

Photographic recording is also of value in connection with purely electronic PA spectrometers since reading 100 or more channel counts

[9]) H. Greinacher, Zs. Phys. **36** (1926) 364.

[10]) G. Ortner and G. Stetter, Phys. Zs. **28** (1927) 70; Zs. f. Phys. **54** (1929) 449.

[11]) E. Rutherford, F. A. B. Ward and C. E. Wynn-Williams, Proc. Roy Soc. A **129** (1930) 211; Wynn-Williams and Ward, Proc. Roy. Soc. A **131** (1931) 391.

[12]) P. J. van Heerden, The Crystal counter (Thesis, Utrecht, 1945).

[13]) R. S. Stone and C. J. Borkowski, ORNL (1950) 796.

[14]) G. P. Freeman, Diamond, a Crystal Counter (Thesis, Utrecht, 1952).

[15]) W. A. Hunt, W. Rhinehart, J. Weber and D. J. Zaffarano, Rev. Sci. Instr. **25** (1954) 268.

[16]) A. B. van Rennes, Technical Report No. 3, Pulse Amplitude Analysis in Nuclear Research (Thesis, MIT, 1955).

[17]) Sm. S. Choudhury and B. M. Banerjee, Rev. Sci. Instr. **27** (1956) 1080.

[18]) D. Maeder, Helv. Phys. Acta **20** (1947) 139.

[19]) D. Maeder, P. Huber and A. Stebler, Helv. Phys. Acta **20** (1947) 230.

[20]) D. Maeder and H. Medicus, Helv. Phys. Acta **23** (Suppl. III) (1950) 175.

[21]) A. Dallos, Acta Phys. Acad. Sci. Hungar. **1** (1950) 56.

[22]) R. Hofstadter and J. A. McIntyre, Nucleonics **7** (3) (1950) 32.

[23]) E. C. Campbell and M. Goodrich, Phys. Rev. **78** (1950) 640.

[24]) H. E. Müller, Wr. Akad. Ber. IIa **159** (1950) 361.

[25]) H. Wänke, Wr. Akad. Ber. IIa **161** (1952) 151.

[26]) W. Bernstein, R. L. Chase and A. W. Schardt, Rev. Sci. Instr. **24** (1953) 437.

[27]) R. L. Chase, BNL-Report 263 (Nov. 1953).

[28]) A. W. Schardt, BNL-Report 237 (Jan. 1954).

[29]) J. Brunner, O. Huber, R. Joly and D. Maeder, Helv. Phys. Acta **26** (1953) 588.

[30]) D. Maeder and P. Stähelin, Helv. Phys. Acta **28** (1955) 193.

[31]) W. Beusch, P. Erdös, D. Maeder and P. Stoll, Helv. Phys. Acta **30** (1957) 268.

[32]) R. F. Post, Phys. Rev. **83** (1951) 886.

[33]) L. Grodzins, Rev. Sci. Instr. **26** (1955) 1208.

[34]) P. Stähelin, D. Maeder and M. Pochon, Zs. f. Phys. **140** (1955) 498.

[35]) Th. Mayer-Kuckuk, Zs. f. Naturforschung **11a** (1956) 627.

requires considerable time. This is true even with modern storage type multichannel systems equipped with mechanical printers. Here the photographic recording provides a possibility to follow rapidly decaying spectra. Most of the existing storage type spectrometers[36-46]) are based on binary coding and therefore call for a print-out system to convert the data into decimal notation. The recent development of a purely decimal multichannel memory[43]) permits us to dispense with the slow and expensive mechanical converter, since the oscilloscope display yields photographic pictures of spectra in an easy-to-read decimal digital form. These photographic records provide a space saving means of permanent storage from which data may be read automatically into a computer or into the original spectrometer by means of a photoelectric scanning device (section 5).

Discussions with many users and designers of PA spectrometers have stimulated the writing of the present article, especially of sections 2 and 5. The discussion given in sections 3 and 4 mainly reflects the author's experience with 3 different GW instruments; part of this material has been presented at a conference on kick-sorters[47]) held at Gatlinburg in 1956.

The author is indebted to the US National Research Council for the invitation to that conference, and particularly to W.A. Higinbotham for arranging visits to numerous laboratories. Finally, the author wishes to thank Prof. P. Scherrer for his encouraging interest in this work, and to Mr. W. Beusch, R. Müller and P. Schmid for their assistance in the construction of our equipment and in the measurements.

2. Photographic Recording of Individual Events

2.1. HISTORICAL DEVELOPMENT

The following abbreviations will be used in this review: CRT = cathode ray tube, DR = dot recording, GW = gray wedge, PA = pulse amplitude, MV = measuring voltage delivered at the output of a pulse stretcher.

With the application of sensitive amplifiers to ionization chamber experiments by Greinacher[9]) and their further development for quantitative work[10,11]) the problem of measuring individual amplitudes of a large number of short electrical pulses became important to nuclear spectroscopists. Since the term "short" meant $\approx 10^{-3}$ sec at that time, the pulses could be recorded by means of a string galvanometer on a moving paper or film. As long as a few thousand events were considered to represent a "large number", visual inspection of the film when projected on a graduated scale seemed to constitute a satisfactory evaluation procedure, requiring about one man-hour per 10^3 counts. The simplicity of the equipment and the straightforward coupling between the input signals and the pattern appearing on the record give this classical method a high degree of reliability and stability.

More recently the galvanometer had to be replaced with a CRT oscilloscope in order to follow the much shorter pulses produced by improved detectors such as proportional gas counters and scintillating crystals. In cases where extreme time resolution was required, also the mechanical transport of the film had to be supplemented with some fast electronic displacement, e.g. by using self-triggered and intensified sweeps so that individual fast pulses could be resolved and studied in detail on pictures taken in a conventional movie camera[48]).

[36]) G. W. Hutchinson and G. G. Scarrott, Phil. Mag. **42** (1951) 792.
[37]) G. W. Hutchinson, Nucleonics **11** (2) (1953) 24.
[38]) P. W. Byington and C. W. Johnstone, I.R.E. Conv. Record **10** (1955) 204.
[39]) T. L. Emmer, I.R.E. Conv. Record **10** (1955) 211.
[40]) J. L. McKibben, J. D. Gallagher and H. J. Lang, LADC-1835 (1955); I.R.E. Conv. Record **10** (1955) 186.
[41]) A. Tarabella, Onde Electrique **35** (1955) 985.
[42]) R. Chase, BNL-Report 401 (1956).
[43]) D. Maeder, Helv. Phys. Acta **29** (1956) 459.
[44]) H. L. Schultz, G. F. Pieper and L. Rosler, Rev. Sci. Instr. **27** (1956) 437.
[45]) R. W. Schumann and J. P. McMahon, Rev. Sci. Instr. **27** (1956) 675.
[46]) J. Reaves, NBS Semiannual Rep. 4498 (Dec. 1955).
[47]) H. W. Koch and R. W. Johnson (Editors), Proc. of the Gatlinburg Conf. on Multichannel Pulse Height Analyzers. Nuclear Science Series Rep. No. 20 (Washington DC 1957).
[48]) R. Hofstadter, Phys. Rev. **74** (1948) 100.

The common feature of these direct recording methods is that the complete information contained in the original pulses is stored in permanent form. The fact that any irregularities of the zero line show up at first sight is of great value for measurements of high precision.

On the other hand, fig. 1A illustrates two well-known drawbacks of the classical galvanometer method:

(a) Excessive consumption of photographic paper or film if counting losses are to be kept small (e.g., events 4 and 5 are hardly resolved in fig. 1A, even though their PA are widely different);

(b) Broadening of the zero line due to overexposure.

say that DR pictures can be read by automatic scanners to absolute accuracy.

2.2. DOT RECORDING (DR) SYSTEMS

With galvanometer recording, increased exposure of the pulse top may be obtained, e.g. by using stretched ($\approx 10^{-3}$ sec) rectangular pulses[25]) or by triggering a stroboscopic light source a certain time ($\approx 2 \times 10^{-4}$ sec) after the beginning of each pulse[24]), using galvanometers of a high resonant frequency ($\nu \approx 5\,000$/sec). Such arrangements, although actually used in density recording spectrometers, would seem suitable for accurate DR of pulses from a slow ionisation chamber.

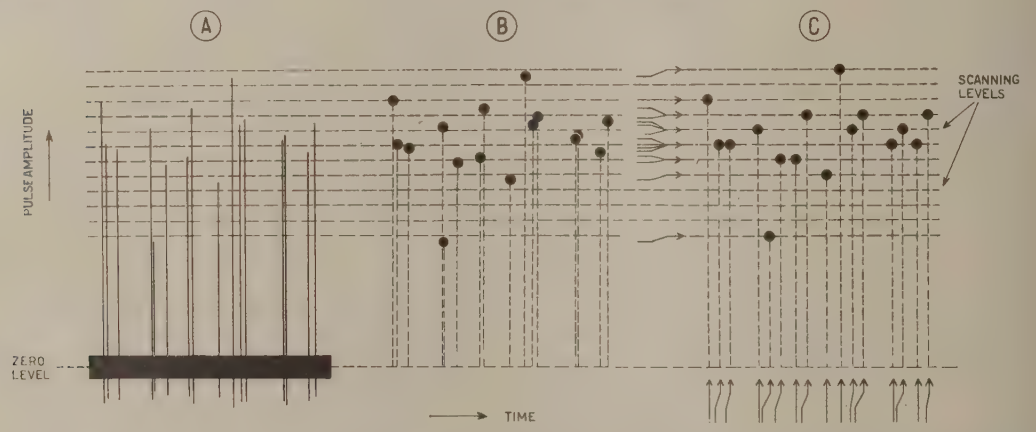

Fig. 1. Appearence of the same set of input pulses when recorded on moving film by: (A) classical method (continuous illumination). (B) proportional dot recording system (conserves original P.A. and time interval distributions). (C) quantized dot recording system (proposed in order to remove ambiguities in evaluation).

The second of these difficulties may be removed by suitably shaping the optical slit, or by using CRT oscilloscope techniques[13]). Both difficulties (a) and (b) are eliminated if only the top of each pulse is photographed. Such a procedure was introduced by Van Heerden[12]) in 1945 and has since been improved[14–17]) (see § 2.2).

The considerable amount of time spent in visual sorting and counting of photographed pulses, has led to the construction of automatic scanning equipment which will be critically reviewed in §§ 2.3 and 2.4. Further improvement is needed (as suggested in §§ 2.5 and 2.6) before one may

Published DR spectrometers are based on CRT oscilloscope display of the pulses. Selection of the pulse top is accomplished either by viewing the oscilloscope screen through a slit using a self-triggered sweep[12, 14, 16]), or by applying a delayed intensifying pulse of short duration to the grid of the CRT[15, 17]). In both cases flat-topped pulses such as those produced by delay-line clipping[49]) or by half-amplitude diode topping[50]) are preferable to RC–RC shaped pulses, in order

[49]) W. C. Elmore, Nucleonics **2** (2) (1948) 4; (3) 16; (4) 43; (5) 50.

[50]) R. S. Foote and H. W. Koch, Rev. Sci. Instr. **25** (1954) 746.

to make adjustments less critical. Well-defined dots with a diameter as small as ½% of the total PA deflection range are easily photographed on 35 mm linagraph panchromatic film if an appreciable fraction ($\gtrsim 10^{-7}$ sec) of the flat pulse top is used for exposure[15, 51]). With peaked pulses 1 μsec wide[16]), the useful part of the total pulse becomes so short that extremely high final accelerating potentials (up to 20 kV applied to a 5XP11 tube) are necessary in order to obtain dots of 0.08 mm ⌀ with a 21 mm deflection range on the film.

Since most DR spectrometers are designed for use with an automatic scanner which does not take possible fluctuations of the zero line into account, the CRT beam is usually cut off completely between pulses. Insofar as visual scanning might be considered, a faint continuous exposure of the zero level would seem to provide increased reliability of PA evaluation[13]).

2.3. SPEED LIMITATIONS

The usual DR technique resolves closely spaced pulses if their amplitudes are sufficiently different (Nos. 4 and 5 in fig. 1); however, closely spaced pairs like Nos. 13 and 14 are still unresolved in fig. 1B. If d denotes the minimum spacing, along the direction of film-motion, for two dots in the same PA channel to be separately distinguishable, and v the velocity of film motion, the fractional overlap loss in the i-th channel is approximately given by

$$\varepsilon_i \approx n_i d/V$$

at a rate of n_i input pulses per second falling into that channel. Since d is not accurately known, it is advisable to keep overlap corrections small; e.g., all ε_i could be held below 3% by choosing the film speed

$$v \geq 33\, d \cdot \mathrm{Max}\,(n_i)$$

which amounts to 0.5 m/sec if the maximum pulse rate is 100 counts/sec per channel. However, at such a film speed the persistence of the CRT screen has been observed to cause additional overlap loss[16]). Van Rennes states that in this respect the P-15 phosphor (decay to 30% within < 1.5 μsec) would be preferable to the usual P-11 phosphor, although its lower photographic activity would increase difficulties in obtaining a small spot size. We may recall that a large factor could be gained in light efficiency by using flat-topped pulses with the stroboscopic exposure technique[15]).

At a given total number of pulses recorded, the fractional losses are in general different from channel to channel and depend on the spectrum shape. E.g., a continuum containing 10^5 pulses spread evenly over 100 PA channels could be recorded on ≈ 5 m of film length with 3% overlap loss; however, 50 m of film are required to store 10^5 pulses forming a gaussian peak of 10 channels total half-width, if losses are to be kept $\leq 3\%$ in every channel. Therefore the film speed during recording should be adjusted to fit the counting rate observed at the most intense peak of the spectrum region investigated.

The time consumed in scanning was originally[14]) 5 sec/m or 1.5 msec per dot diameter. It has later been reduced to ≥ 1 sec/m, or about 0.2 msec per dot diameter[16]). Thus, a film record containing a maximum of 10^4 counts per channel requires a minimum scanning time of 3 min per channel if the recording speed had been chosen to keep overlap losses $< 1\%$.

2.4. LIMITATIONS IN CHANNEL DEFINITION

In the scanning apparatus, the image ("scanning aperture") of a small light source is projected onto the paper or film record, and the reflected[14]) or transmitted[15, 16]) light is received by a phototube. A discriminator connected to the phototube output is set to register a count when a certain fraction of the "scanning aperture" is obscured by a dot. No optimum relation between the sizes and shapes of scanning aperture and dots seems to be established; e.g., apertures of 0.04×0.85 mm², resp. 0.038×0.51 mm², resp. 0.07 mm ⌀, resp. 0.13 mm ⌀ have been combined with dots of [0.29 ± 0.04] mm × [0.7 mm or larger][14]), 0.25×0.30 mm² [16]), 0.24 mm ⌀[15]) and 0.20 mm ⌀[51]). The effective channel width and its stability depend not only on these

[51]) D. J. Zaffarano, communication to editors of [47]) (p. 138).

geometrical parameters and their constancy, but also on:

intensity of scanning light source; photographic density distribution in the dots; background density of film; efficiency of light collection on the photocathode; sensitivity of photocathode; gain in the phototube (or in external amplifier); discriminator threshold.

A thorough analysis of the channel stability problem is given by Van Rennes[16]) who stabilised several of the above factors by a feedback system, thereby reducing random variations in channel width to about $2\frac{1}{2}\%$ RMS.

2.5. QUANTIZATION OF TIME AXIS

The overlap losses discussed in § 2.3 could be eliminated if an electronic arrangement would provide for a regular spacing of dots on the film. For this purpose a unit step function with slowly decaying top may be added, for each incoming pulse, to the x deflection in the recording CRT, as proposed in the lower part of fig. 2. If the step voltage ΔV (determined by the charge pulse delivered to the capacitor C) is adjusted to correspond to the minimum resolving distance d on the film and the leak resistor R is matched to the film velocity v according to

$$v = \frac{d}{RC} \cdot \frac{\overline{V}}{\Delta V},$$

($\overline{V}$ = average voltage across R; should be $\gg \Delta V$)

no overlap losses can occur in the photographic DR†. The film velocity must satisfy the condition

$$v = \frac{v_{\min}}{x} > v_{\min} = d \cdot \sum n_i$$

($\sum n_i = n$ = total input pulse rate);

proper adjustment thus requires no knowledge of the spectrum shape, in contrast to the case discussed in § 2.3. To store a total of $N = 10^5$ pulses then requires at least $Nd = 20$ m of film length which may be scanned within about 20 sec/channel.

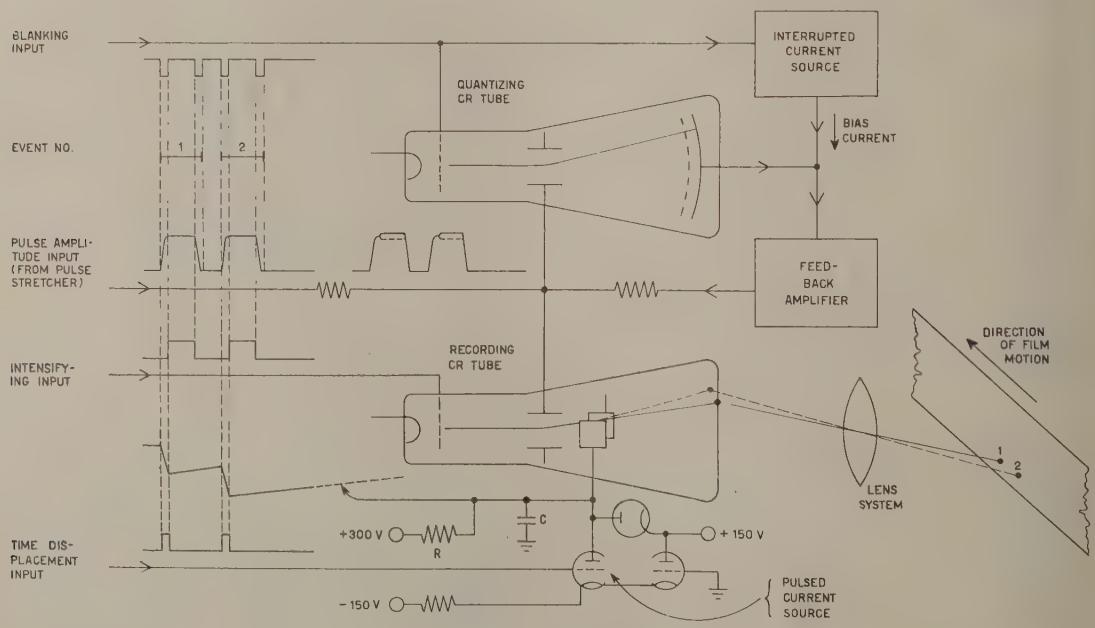

Fig. 2. Functional diagram of a quantized dot recording system.

It may be necessary to restrict the total time deflection range to kd, in order to preserve good focusing of dots. According to a formula worked

† We assume that a phosphor of sufficiently short persistence is used in the oscilloscope tube.

out by R. Müller, the probability of exceeding the limit kd on a film of length Nd is given by

$$P_k(x) = N \cdot \prod_{\varrho=0}^{\nu^*} \left[e^{-x} \sum_{\mu=0}^{\varrho} \frac{x\mu}{\mu!} \right]^2 \left[\sum_{\nu=1}^{\nu^*} e^{-\nu x} \frac{(\nu x)^k + \nu - 1}{(k+\nu-1)!} \right]$$

under the assumptions that $P_k(x) \ll 1$ and that terms with $\nu > \nu^*$ give a negligible contribution (where $\nu^* \ll N$). For example, $P_k(x) = 3.5 \times 10^{-5}$ with $k = 50$, $N = 10^5$ and $x = 0.8$ (with $x = 0.9$, P_k would already approach unity in a run containing $N = 10^5$ pulses). R must be chosen to fit the actual film speed, namely

$$R = \frac{x}{C} \cdot \frac{\overline{V}}{\Delta V} \cdot n \quad .$$

Successful application of this principle in a DR spectrometer used for visual scanning has been reported by Choudhury and Banerjee[17]).

2.6. QUANTIZATION OF PA DEFLECTION

The reliability of the scan counts from a record of the type shown in fig. 1B depends on a number of critical parameters including the uniformity of spot intensity and shape within the PA deflection range (see § 2.4). Evidently any ambiguity in channel assignment of the dots could be eliminated if the dots were made to fall on a set of discrete levels as illustrated in fig. 1C.

Of the various possible ways of obtaining a quantized output from input pulses having a continuous PA distribution, the use of Porter and Borkowski's[52]) special CRT in the manner indicated in the upper part of fig. 2 would appear to introduce the least amount of additional dead time. A negative feedback circuit has recently been described by these authors[47]) which catches the electron beam at the lower edge of the nearest aperture in the masking electrode within 0.5 μsec after the input pulse has reached its top.

A further step to increase the number of well-defined channels on a moving film record would be to represent each event by one or more dots arranged in a column according to some coding scheme. Such a technique would be especially useful for recording multidimensional information.

2.7. TWO-DIMENSIONAL DOT RECORDING

In coincidence work it is often desirable to know the PA of all partners which contribute to the accepted events. In the case of twofold coincidences, the complete information can be recorded in a single experimental run by a two-dimensional DR system on a standing film or plate. If 100 dot positions are resolved in both coordinates, the coincidences can be classified into 10^4 channels. It appears that photoelectric scanners have not developed for this pur-

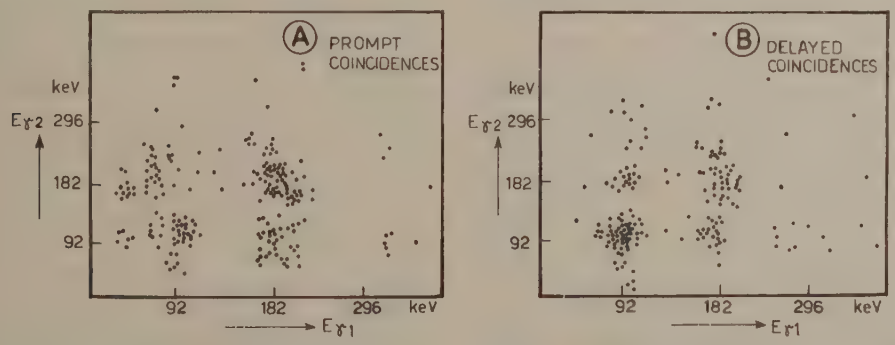

Fig. 3. Two-dimensional pulse spectrometry based on dot recording. γ-rays from the decay $Cu^{67} \rightarrow Zn^{67}$ are investigated using two NaI scintillation crystals in a coincidence arrangement. (A) Prompt coincidences between 206 and 182 keV, and between 206 and 90 keV γ-rays show that the 388 keV level in Zn^{67} (known from the Ga^{67} decay) is excited. (B) Trigger pulses associated with vertical deflections have been delayed by 1.5 μsec ahead of the coincidence mixing (window width increased to 1.0 μsec) in order to detect delayed coincidences between $E\gamma_2 = 296$ (or 90) keV and the 9 μsec isomeric γ-ray of $E\gamma_1 = 92$ keV.

[52]) F. M. Porter and C. J. Borkowski, Nucleonics **12** (3) (1954) 55.

pose, so that up to the present the analysis of two-dimensional concidence records has to be based on visual evaluation. If quantitative counting of individual coincidences is to be achieved, the overlap losses must be kept small by utilizing more than one film frame recording the data; e.g., the film should be transported automatically to the next frame whenever 64 (or perhaps 100) events have been photographed. Fig. 3 summarizes dots from about 40 pictures obtained in this manner (using a Robot Junior 24 × 24 mm camera) in an investigation of the $Cu^{67} \rightarrow Zn^{67}$ decay scheme[31]). Delayed coincidences can be displayed in the same way, as shown in fig. 3B which brings the 9 μsec isomeric transition in Zn^{67} into evidence. The gated pulse stretchers (see section 3) used in these measurements permitted intensifying each dot for 10 μsec with both prompt and delayed coincidence mixing. Thus, well-focussed dot exposures were obtained from a 5 ABP 1 tube at only 2 000 V of accelerating potential. The difference between figs. 3A and 3B, although clearly visible, is not very pronounced because of a common contribution of chance coincidences from the numerous quanta of 92 and 182 keV which, for the most part, are not emitted in a cascade.

If statistically significant data are accumulated on a single picture, dot overlap makes quantitative counting impossible. However, such pictures are extremely useful for a quick energy assignment of coincidence partners[32-35]). Qualitative interpretation of intensities is often sufficient in these applications, but semi-quantitative results may be obtained from photographic density evaluation[34]) or from a combination with electronic counting methods[30]) which will be explained in section 4.

3. Photographic Integration of Pulse Sequences

3.1. USEFULNESS OF DENSITY METHODS

In applications where the exact position of peaks and valleys in a PA distribution is the only matter of interest, it seems quite obvious to use photographic material as an integrator of the number of pulses exposed per unit area on its different parts. Since $\approx 10^4 \ldots 10^5$ image elements are well distinguishable, qualitative information on the frequency of nuclear events in a larger number of channels than available in any purely electronic counting system can be stored on a single photographic picture, if photographic density is used as an intensity indicator. Full advantage of this large number of channels is taken in two-dimensional density recording of coincidences (§ 2.7). Density records of one-dimensional spectra might be obtained, in principle, using any conventional DR spectrometer (§ 2.2) without moving the film; the round dots are then usually replaced by straight lines, e.g. slit images[24, 25]), or portions of a triggered sweep[22, 23]). However, a more quantitative indication of intensities may be obtained, in such applications, by proper use of the second coordinate, as explained in subsequent subsections of this section.

Density recording spectrometers were originally developed to eliminate the labour of scanning galvanometer records visually, at a time when electronic multichannel spectrometers or photoelectric DR scanners were not known. Although a large variety of electronic counting instruments have become available since, photographic density recording techniques are still in use today, mainly for the following reasons:

(1) Low cost of equipment.

(2) Speed of data collection.

(3) Ease of operation and maintenance.

Because of the simplicity of their operating principle, density recording spectrometers can easily be designed to work at high counting rates. In contrast to fast multichannel instruments, their proper operation does not depend on a large number of critical adjustments. On the other hand, the high counting speed and relative simplicity of single channel spectrometers is paid for by their inability to accept the complete information. It appears that the most economic and efficient instrumentation permitting quantitative measurement of a whole spectrum at high counting speeds consists of a few electronic counting channels combined with photographic GW recording (see section 4).

3.2. GRAY WEDGE (GW) SYSTEMS

Density patterns produced by photographing pulse distributions may be evaluated by densitometer analysis[13, 24]). However, the inconvenience and inaccuracy in the interpretation of densitometric measurements call for some simpler procedure which would be less dependent on the characteristics of the photographic material and on the processing conditions. If the pulses are photographed from a CRT display in which the apparent spot intensity is a suitable function $I(y)$ of the ordinate y (fig. 4A)—PA signal applied to x deflection —, the resulting two-dimensional picture gives a direct indication of the spectrum shape. The photographic negative reproduced in fig. 4B was taken using the ETH spectrograph with logarithmic energy display in connection with an investigation of the Hg → $Au^{193, 195}$ decay schemes by Dr. Halter's group.

In the original apparatus[18]), a filter having a transmission gradient along the y axis was put over the face of the CRT. In later versions, the function $I(y)$ was obtained by electronic modulation of sweep velocity[20, 21]). Bernstein, Chase and Schardt[26]) improved the filter type instrument by using a high precision glass wedge, and they introduced the term "gray wedge spectrometer". This technique has been extended recently to extremely high pulse rates[53]). Since the photographs are evaluated at one fixed density value only, the GW method is simple and reliable.

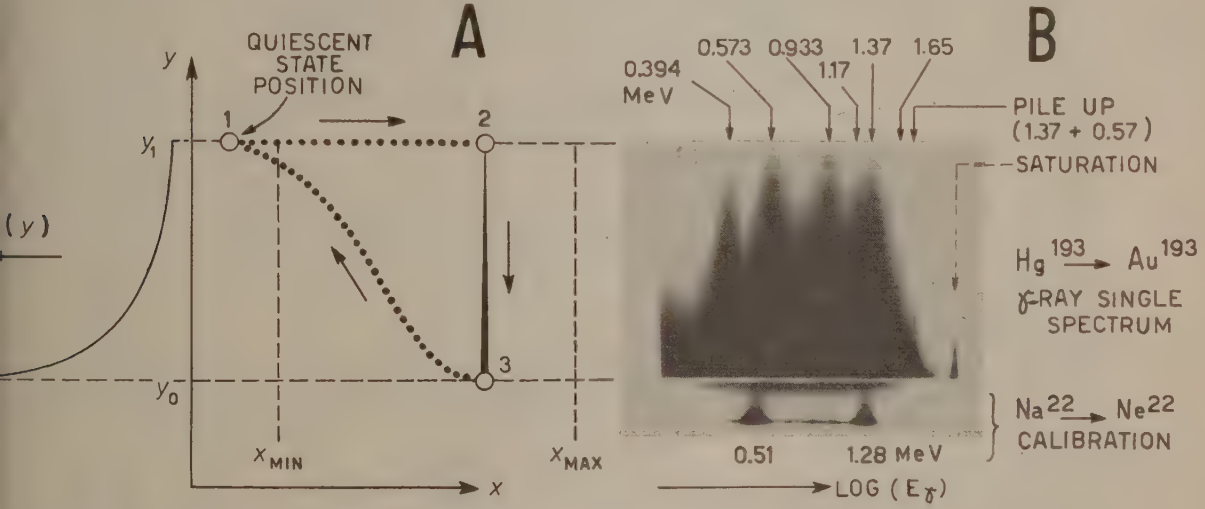

Fig. 4. Gray wedge method. (A) Path of spot on CRT screen. The abszissa x of the straight line portion 2–3 represents the variable whose statistical distribution is to be measured (e.g., pulse amplitude, or log (PA), or delay time). The spot is brightened during its passage from position 2 to 3, and its apparent intensity is made to follow a certain function $I(y)$. (B) Appearance of a negative produced by photographing 200 000 NaI scintillation pulses displayed on a CRT in the manner indicated in fig. 4 (A). The logarithmic converter used in the x-deflection circuit is described in § 3.6.

Plotting an isodensity line is an extremely simple procedure which consists merely in taking one or two contact prints (see fig. 13).

3.3. USE OF A COMMERCIAL OSCILLOSCOPE AS A SIMPLE GW SPECTROMETER

Any synchroscope[54]) can easily be adapted for GW spectrometer service. If an oscilloscope of the type fitted with exchangeable plug-in amplifiers is used, most of the extra circuits can be built into a special plug-in unit. The block diagram (fig. 5) shows how few additional parts

[53]) J. T. Flynn and F. A. Johnson, Rev. Sci. Instr. **28** (1957) 867.

[54]) V. L. Fitch and E. W. Titterton, Rev. Sci. Instr. **18** (1947) 821.

are then needed to compose a fast scintillation spectrometer. According to fig. 5, only one internal change (connection from plug-in unit to horizontal display switch) is necessary. This change can be permanent, as it does not interfere with the normal use of the oscilloscope. The arrangement of the various functions was suggested by the following considerations:

(1) In fast oscilloscopes the vertical deflection range is strongly limited by interception of the electron beam with the deflection plates, whereas the horizontal deflection can be large. In order to obtain good energy resolution, it is advisable to choose the horizontal direction for the PA display.

(2) The horizontal amplifier, when used without magnifier has strong negative feedback and will thus give good linearity up to the largest PA deflections.

(3) Although in this way the horizontal deflection amplifier cannot be utilized for amplifying the sweep, the sweep pulse itself is available at an external binding post. If it is fed to the vertical amplifier, the built-in delay line becomes useful in that it delays the beginning of the sweep sawtooth until the PA deflection has reached its top.

(4) No optical gray wedge is required if the

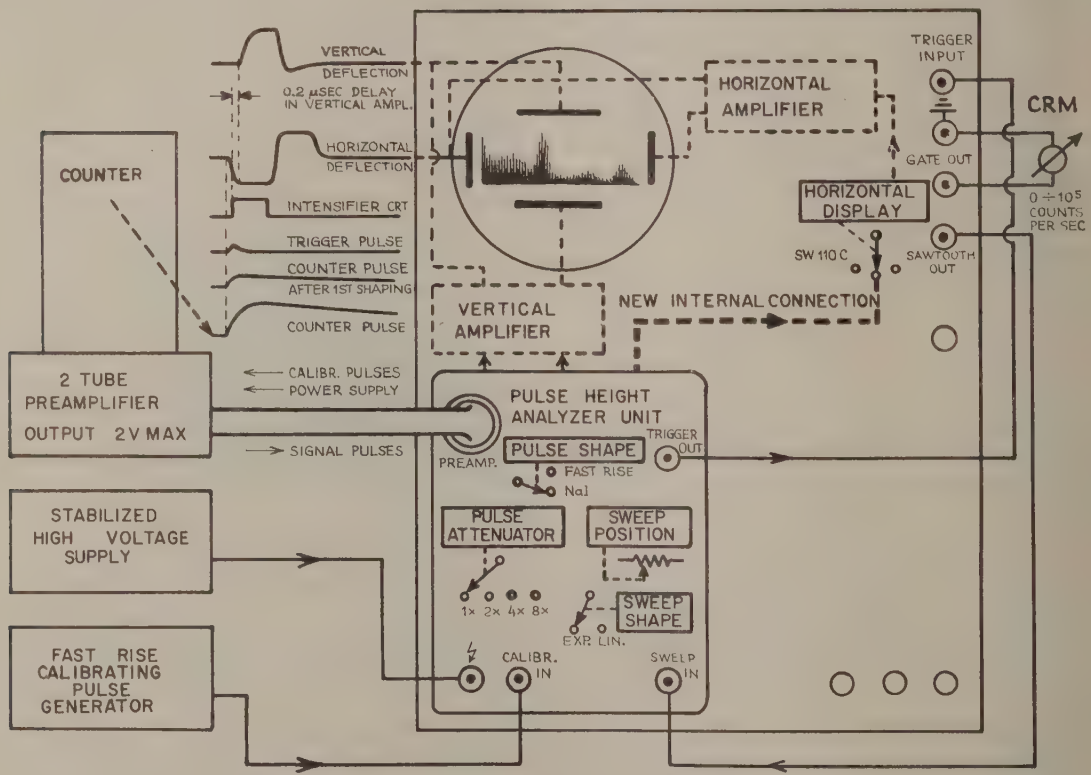

Fig. 5. Block diagram of a fast GW spectrometer of inexpensive design, using a normal laboratory oscilloscope.

(5) The external trigger lead from the adaptor unit to the oscilloscope may be used to introduce coincidence selection.

(6) The "gate output" of the oscilloscope provides a useful counting rate meter if connected to a 50 μA meter through 50 kΩ (10^5 counts per sec at full scale deflection).

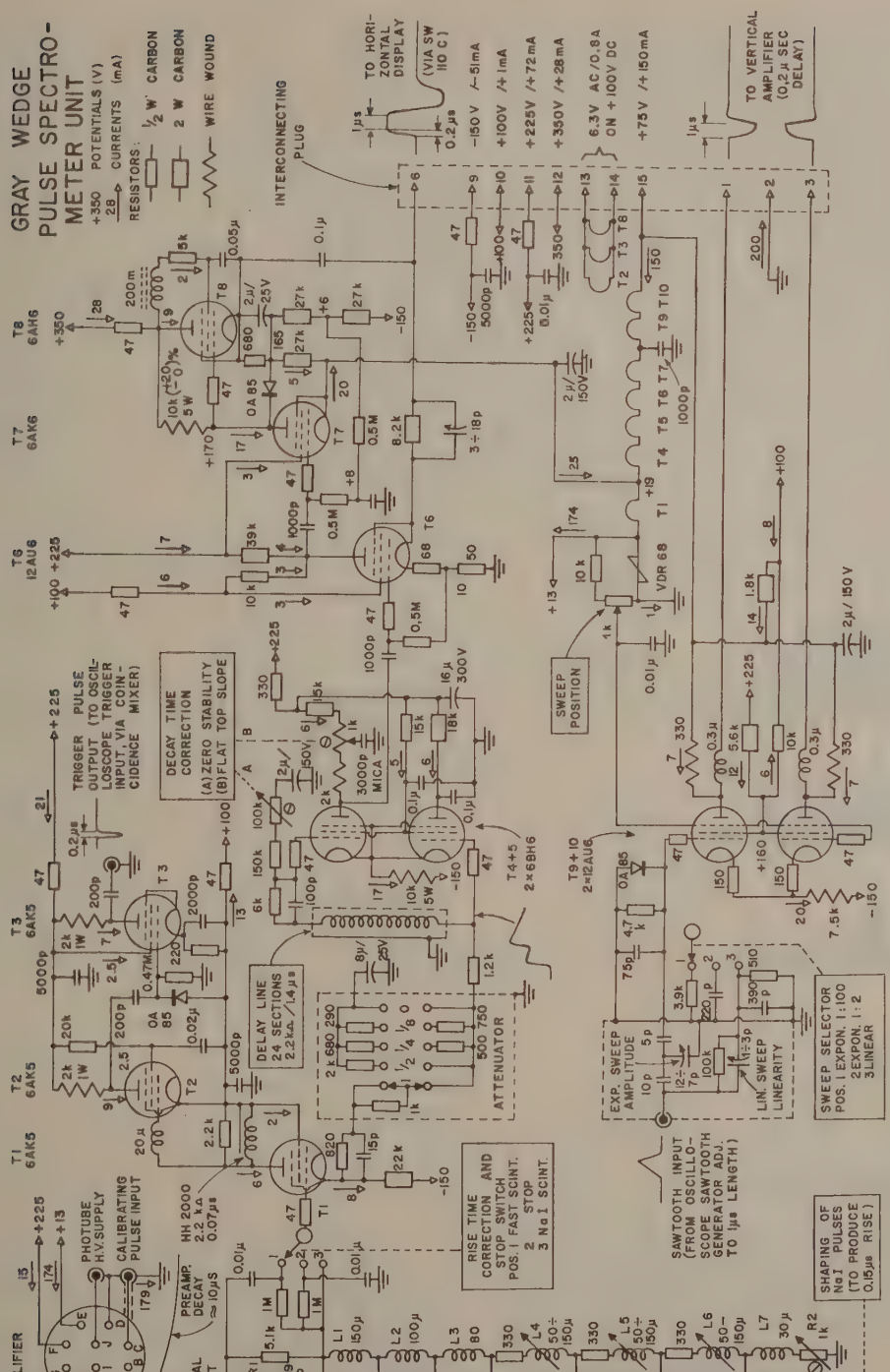

Fig. 6. Circuit diagram of plug-in adaptor. This unit converts a type 541 oscilloscope into a fast GW spectrometer having a total dead time of about 3 μsec per recorded pulse (note: sweep selector should show a connection to grid of T9).

The pulses to be displayed in such a spectrometer should have a flat top covering the whole sweep duration. Delay-line clipping and pulse shape corrections are incorporated in the plug-in adaptor unit (fig. 6) which was constructed at our laboratory to fit a type 541 oscilloscope. Since the shortest sweep available in the oscilloscope lasts for 1.0 μsec, the clipping time was made 1.4 μsec in order to keep the rounded corners outside the used portion of the trace. With NaI pulses, the effective rise time must be cut down to ≈ 0.15 μsec; for this purpose, a tapered delay-line network ($C_{1,\ldots,7}$, $L_{1,\ldots,7}$, $R_{1,2}$) is inserted at the input. The slow decay of the flat top is compensated by an integrating network in the anode circuit of the clipping stage

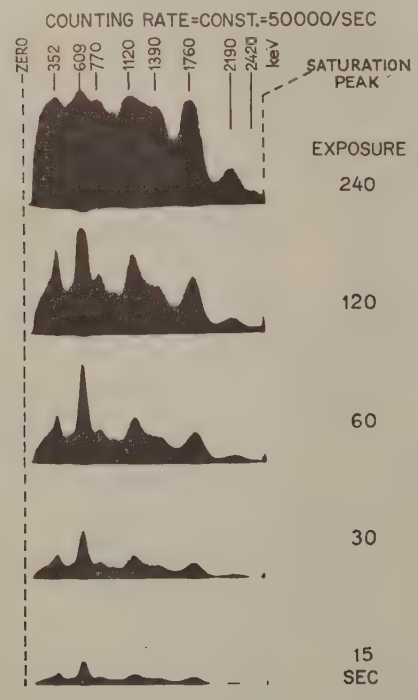

Fig. 7. Approximate linearity of GW intensity scale, demonstrated by a set of scintillation spectra (γ-rays from Ra (B + C) falling on a 4 × 5″ crystal of sodium iodide) taken with different exposure times at a fixed total rate of 50 000 counts per second.

T_5. Double clipping is used in order to obtain satisfactory zero line stability at high counting rates[55–57]). The same type of pulse shaping arrangement is used in our larger spectrometers; a more elaborate circuit which includes independent adjustments of symmetry at small PA, of symmetry at saturated PA, and of the slope of the flat top will be described elsewhere[58]).

Using this adaptor unit the two Co^{60} peaks have been resolved at counting rates up to 150 000/sec, when about 15% of the pulses overlap during the sweep interval. The dead time of the oscilloscope trigger circuit, compatible with the total duration of the double clipping, then causes about 40% counting loss. A set of spectrograms exposed for different lengths of time, using a Ra source of constant intensity, is reproduced in fig. 7 in order to show the essentially linear variation of the height of the upper contour lines with the number of pulses exposed per unit PA interval.

3.4. REQUIREMENTS IMPOSED ON A COMPLETE GW SPECTROMETER

Instead of adapting a laboratory oscilloscope as described in § 3.3, one may prefer more elaborate equipment for certain applications, for the following reasons:

(a) Since the fixed 1 μsec sweep requires a total of $\approx 10^5$ counts to produce a high contrast GW picture, experiments with low activity sources or with coincidence selection would be difficult, unless a selection of different sweep durations were available.

(b) When using a slow sweep, the flat top of the 1 μsec pulses must be prolonged beyond the practical limit of linear shaping networks. Apart from coincidence gating, which is already available in the simple oscilloscope version (§ 3.3), additional gating circuitry is necessary to avoid pile up of neighbouring pulses if a stretcher circuit is used.

(c) For high precision energy measurements

[55]) E. Fairstein, ORNL-Report 1335 (Jan. 1952) and Rev. Sci. Instr. **27** (1956) 475.

[56]) J. E. Francis, P. R. Bell and G. G. Kelley, Nucleonics **12** (3) (1954) 55.

[57]) D. Maeder, Helv. Phys. Acta **29** (1956) 265.

[58]) D. Maeder and R. Müller (to be published in Helv. Phys. Acta).

it may be desirable to expand a portion of the spectrum.

(d) To assure reproducibility of intensity calibration, the beam intensity in the CRT should, if at all, be adjustable only in fixed steps. Any possibility of leaving the spot "turned on" in the quiescent state should be eliminated.

(e) In order to obtain absolute intensity results, at least one counting channel should be incorporated, with provisions for automatic marking of channel limits on the GW pictures.

ments which are contradictory to simplicity of circuit structure.

3.5.1. *Basic concepts of pulse stretcher design*

An ideal pulse stretcher would

(1) Produce a d.c. voltage (called "measuring voltage" = MV) which has a definite relationship (e.g., linear or logarithmic) to the amplitude of an input pulse beginning at t_0, provided that t_0 satisfies the timing requirements listed below.

(2) Deliver a signal ("ready pulse") to the

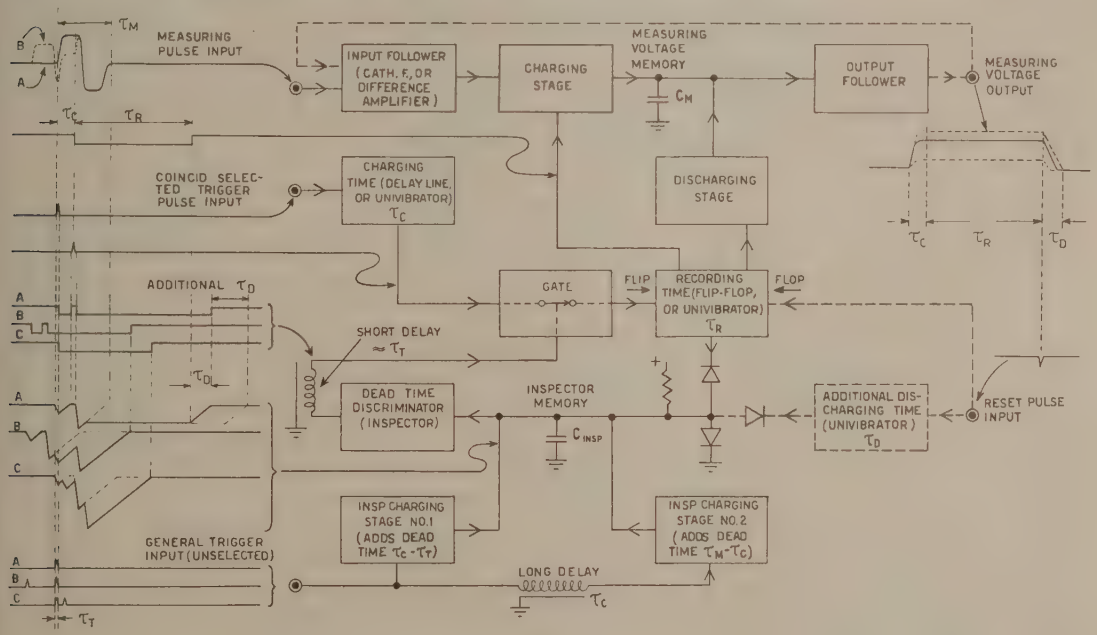

Fig. 8. Basic components of pulse stretchers.

Circuits developed to meet requirements (a)...(d) will be discussed in the following sections, while (e) is deferred to section 4.

3.5. PULSE STRETCHERS

Pulse stretchers form an essential part of almost every spectrometer. Some of the simpler circuits have recently been summarized by Meyer[59]) in this journal. We wish to stress here the importance of fulfilling a number of require-

[59]) M. A. Meyer, Nuclear Instruments **1** (1957) 62.

recording equipment at an instant t_1, indicating that the MV is available.

(3) Be able to perform (1) within a short "charging time" $\tau_C = t_1 - t_0$, whose minimum setting should be determined by the finite slope of the input pulses rather than by limitations in the stretcher circuit.

(4) Hold the MV constant for an indefinite length of time, until a signal ("reset pulse") is received from the recording equipment at an instant t_2. $\tau_R = t_2 - t_1$ will be called "recording time".

(5) Return to a standard condition within a short "discharging" "time" $\tau_D = t_3 - t_2$ (comparable with the interval τ_C).

(6) Be intensitive to another input pulse during $(\tau_R + \tau_D)$.

(7a) Reduce the recording time τ_R to zero for each input pulse which is not, within τ_C, accompanied by a signal which identifies it as a "pulse of interest", satisfying some coincidence or anticoincidence imposed by the particular experiment.

In place of (7a), which permits the measurement of delayed coincidences in a window adjustable in width and position between t_0 and t_1, the stretcher may be required to

(7b) Reject those pulses which are preceded within τ_M (= total duration of an input pulse), or followed within τ_C, by another (possibly unselected) input pulse in the case of prompt coincidence selection. The block diagram (fig. 8) presents the basic structure which fits case 7b. The critical part in most stretchers is a memory capacitor (C_M in fig. 8) together with its charging and discharging circuits. Input PA usually ranges from about 1 to 100 volts; the lower limit being set by the behaviour of the nonlinear circuit elements. Difficulties generally arise from the necessity of combining large τ_R (up to several msec in certain serial memory spectrometers) with small τ_C and τ_D values (usually $\lesssim 1$ μsec). For the subsequent discussion (§§ 3.5.2 through 3.5.5), existing stretcher types will be classified according to the charging elements used.

We may finally mention here the possibility of realizing ideally drift-free stretchers by deriving an analog voltage from a scaler whose count is proportional to the PA; however, continuous stretchers seem preferable to quantized ones (see § 2.6) for GW display of pulses.

3.5.2. *Secondary emission charging circuit*

Requirements (3) and (5) in § 3.5.1 call for a small memory capacitor and heavy charging currents whereas (4) calls for a large capacitor and small leakage. Secondary emission tubes like the EFP60 are ideally suited to provide heavy current pulses (up to ≈ 0.1 A) and have been used successfully in GW[27,28]) and other spectrometers[60]), even in delay line memory instruments[44]), although it seems difficult to reduce leakage much below 10^{-6} A. Lowering the EFP60 screen voltage during τ_R might overcome this limitation; however, this idea has not been tried so far. Recently, Chase[42]) has eliminated this difficulty by cascading two similar stretchers having different storage capacity values. Without this artifice, the measuring voltage will usually drop by several volts per msec if a C_M value is chosen (≈ 100 pF) which is consistent with $\tau_C \approx 0.1$ μsec. Discharging is usually done by a conventional sharp cutoff pentode (EF80 or 6AH6), and therefore takes somewhat more time ($\tau_D \gtrsim 3\ \tau_C$).

3.5.3. *Diode charging circuit*

In another type of stretchers diodes are used for charging, insulating, and sometimes also for discharging the storage capacity. Either a d.c. restorer[25]) or a cathode follower[3,26,45]) is then necessary to supply the diode current. Crystal diodes are often preferred to vacuum diodes in this application because of their low voltage drop during conduction, although their limited back resistance calls for special guard potential circuits[3]) to reduce leakage to $\lesssim 1$ μA. With the charging currents supplied by a low impedance cathode follower, similar performance as quoted in § 3.5.2 is obtained.

Leak currents through the discharging element (either a vacuum diode, or a sharp cutoff pentode) can usually be kept much smaller than those drawn by the charging elements. Positive ion grid current in the output cathode follower tube has occasionally been found to cause leakage troubles[39]).

3.5.4. *Cathode follower charging circuit*

The cathode follower used as the charging element in an early version of pulse stretchers[18]) has later been modified as shown in fig. 9, in order to obtain a low charging impedance throughout the interval τ_C. Thus, nonlinear

[60]) R. Patzelt, Wr. Akad. Ber. IIa **165** (1956) 229.

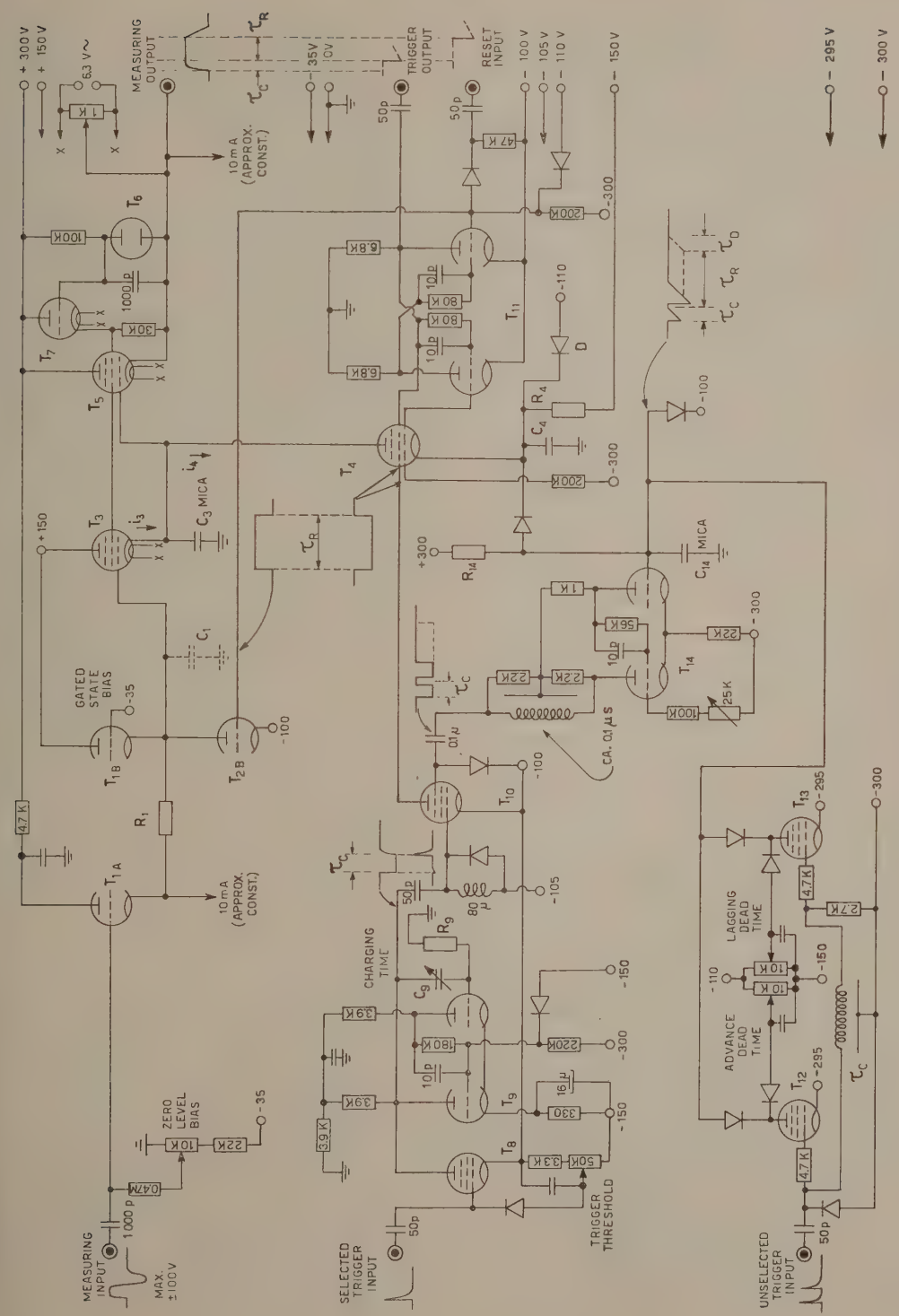

Fig. 9. Linear pulse stretcher of the cathode follower type. The diagram has been simplified by omitting DC biasing networks and constant current sources.

errors caused by the rapid increase of diode impedance near the peak of the pulse[3]) are avoided. The indefiniteness of source impedance, which is characteristic of all unidirectional charging devices on approaching the equilibrium, is usually counteracted by 1:1 feedback from the MV output to the input cathode follower (see fig. 8). The input stage then acts as a differential amplifier (overall gain ≈ 10) whose output drives the charging stage[26-28, 42, 44, 45, 60, 61]). With our modified cathode follower circuit a two-directional charging impedance of a few hundred ohms is maintained during τ_C by allowing a steady current to flow through the discharging tube (T_4 in fig. 9). This arrangement simplifies the discharge circuitry in that T_4 has to be switched off only during τ_R, complementary with the gating tube T_{2B}. On the other hand, it implies that triggering of the τ_R generator (T_{11}) must occur at a well defined phase of the pulse near its top. Therefore, input pulses fed to a stretcher of the type described here should have a flat top at least a few tenths of a μsec wide. The gating resistor R_1 in series with the parasitic capacity C_1 provides for a linear integration of fast oscillations which might be superimposed on artificially sharpened NaI pulses (see § 3.3).

Leakage sources in this circuit are: Residual anode currents in T_3 and T_4, heater-cathode insulation in T_3, and positive ion grid current in T_3 and T_5. T_3 is switched off, during τ_R, by clamping the grid to about 30 volts below the zero PA level by means of T_{2B} and T_{1B}. In order to reduce leakage in T_3 and T_5, a relatively low screen grid-cathode voltage is applied via the d.c. shifter and follower arrangement $T_6 + T_7$. Heater leakage is eliminated by connecting the filament of T_3 to the MV output. T_4 is switched off by negative pulses applied to grids 1 and 2 simultaneously. During cutoff, the cathode is caught by the noncritical diode D. With selected tubes residual currents have been reduced to below 10^{-8} A.

The following choice of critical parameters represents a reasonable compromise between speed of response and slowness of drift:

$R_1 =$ 8.2 kΩ, requiring that the input cathode follower T_{1A} be capable to deliver an extra current of at least $(100 + 30)\, V/R_1 \approx 15$ mA without drawing grid current if a large input pulse arrives during τ_R.

$C_1 =$ as small as possible; e.g. $R_1 C_1 \lesssim 0.16$ μsec.

$\tau_C =$ 1.2 μsec, determined by the adjustable univibrator T_9. Within 1.2 μsec of a flat topped input pulse, the grid potential of T_3 can approach its asymptotic value to better than 50 mV (since $\exp(-1.2\ \mu\text{sec}/R_1C_1) \lesssim 0.05\%$) if there is no grid current in T_3.

$T_{2B} =$ $\frac{1}{2}$ E88CC, conducting during τ_R ($\gtrsim 15$ mA), nonconducting during τ_C. Contributes < 80 mV to MV error if cut off to < 10 μA.

$T_3 =$ 6AU6, selected for low leak current, (e.g. $i_3 < 10^{-8}$ A at $V_{grid} - V_{cath} < -15$ V). With 90 volts applied between screen grid and cathode, T_3 must be capable of cathode current surges up to $i_{3max} \approx 16$ mA without drawing appreciable grid current. In equilibrium with T_4, i_3 is much smaller and the transconductance becomes $S_3 \approx 3$ mA/V.

$T_4 =$ 6AH6, with the steady state anode current i_4 determined by R_4. The screen grid-cathode voltage is lowered to about 40 V during τ_R in order to facilitate cutoff. If $i_4 = {}^1/_4 i_{3max}$, charging currents between $+ {}^3/_4$ and $- {}^1/_4$ of i_{3max} can be supplied to C_3 (e.g. $+12 \ldots -4$ mA).

$C_3 =$ 82 pF, or $C_3^* \approx 100$ pF including stray capacitances, requiring at most 0.9 μsec to be charged from the quiescent state near the MV. The remaining 0.3 μsec left for the transition into equilibrium are more than sufficient since $C_3^*/S_3 \approx 0.03$ μsec.

$\tau_R =$ limited by sum of leak currents in C_3^*. If $i_{leak} \leqslant 10^{-8}$ A, the drift becomes $\leqslant 0.1$ V/msec. If necessary, a drift compensation derived from the MV output may be applied across a small resistor in the return lead of C_3.

[61]) G. G. Kelley, reported in [47]) (p. 64).

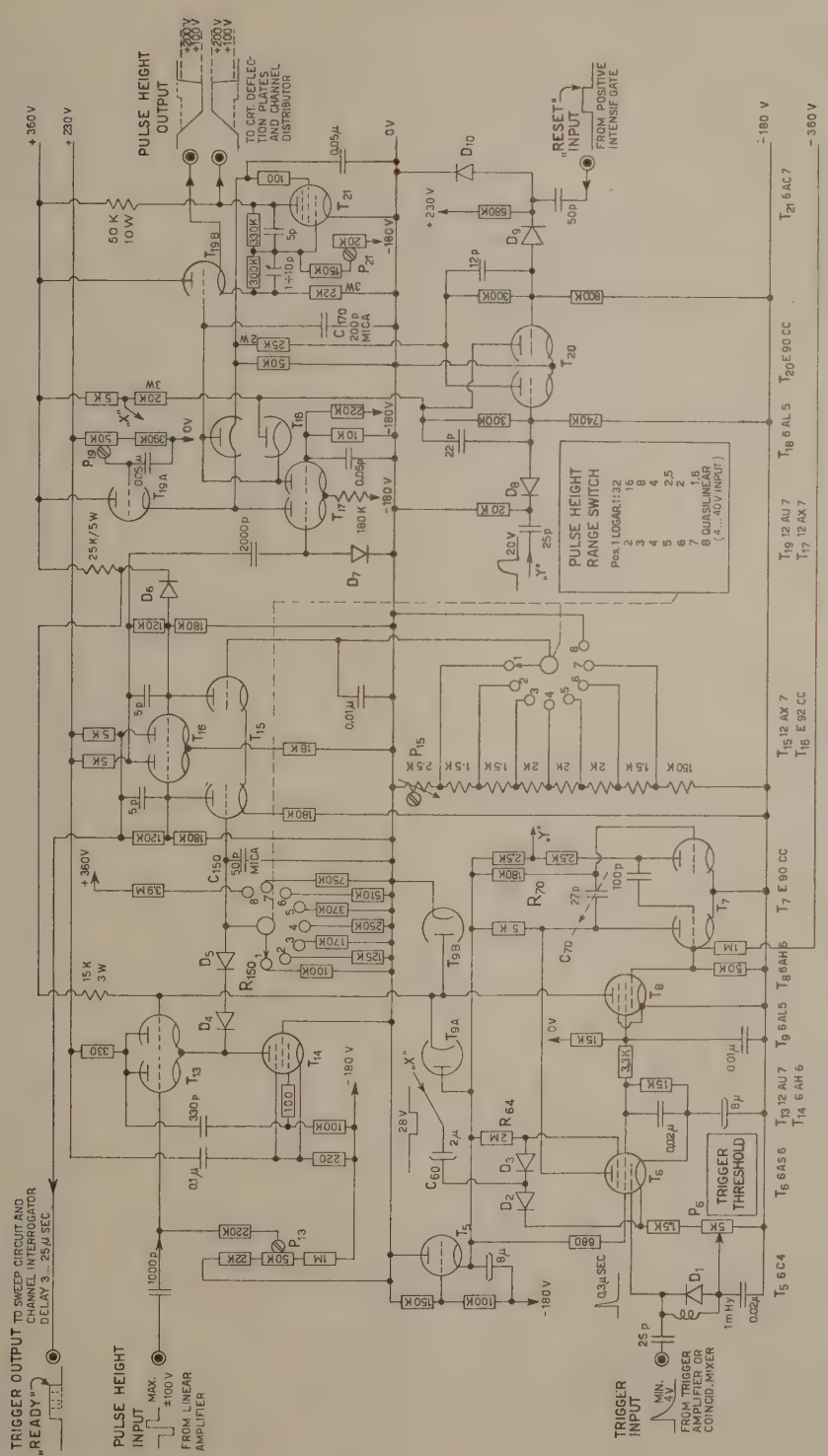

Fig. 10. Pulse amplitude-to-logarithm converter and stretcher.

$\tau_D =$ $\leqslant 3$ μsec if i_4 is limited to the steady state value. Can be reduced to $\leqslant 1$ μsec by proper choice of C_4 ($\approx 10\, C_3$) which is recharged during τ_D.

3.5.5. *Pentode charging circuit*

Most of the known charging circuits are designed to supply positive charges to the memory capacity. Use of an EFP60 to charge C_M negatively would have to be paid by less efficient d.c. feedback since the anode would be at a higher d.c. level. A diode stretcher, on the other hand, may be driven negatively by a modified cathode follower[62]), as exemplified in fig. 10. (see § 3.6). The further possibility of using a pentode for charging and a cathode follower for discharging has been realized by Dallos[21]) in an extremely simple circuit ($\tau_C \approx 1$ μsec, $\tau_R \approx 100$ μsec, $\tau_D \approx 10$ μsec) in which no arrangement was provided to ensure linearity and zero level stability.

3.6. LOGARITHMIC EXPANSION AND COMPRESSION OF PA SCALE

Linear expander amplifiers have been incorporated in some GW instruments[18, 28]), although the PA resolution of nuclear radiation detectors usually does not necessitate increased dispersion in the spectrometer. On the other hand, with scintillation detectors it is often desirable to compress the high energy region in order to record, at one time, the whole spectrum between X-rays and hard γ-rays with adequate resolution at all energies. Both compression and expansion of the energy scale can be produced in a logarithmic converter-stretcher circuit. The principle of operation and some advantages of the logarithmic energy display have been explained elsewhere[63]); fig. 10 shows the detailed circuit which is in use at our laboratory.

Two OA85 diodes in series are used to charge the auxiliary memory capacitor, C_{150}, to the negative peak of an input pulse. The equilibrium near the peak depends on the current drawn through R_{150}. Although the present circuit does not provide constant current during τ_C, charging errors may be reduced by proper bias adjustment (P_{13}), so that even a 1:50 PA range is covered within $\pm$ 4% relative accuracy. In view of the role played by the ohmic leak (R_{150} in fig. 10, or R_2 in ref.[63])), no tube is required for discharging C_{150}. Since R_{150} never exceeds 750 kΩ, except in position 8 (quasilinear range) which is not intended for precision measurements, the diode back resistance is not too critical.

The choice of negative pulses to charge C_{150} allowed us to gate the input White follower ($T_{13} + T_{14}$) by switching off the right half of T_{13} during τ_C (≈ 1.5 μsec, determined by C_{70} R_{70}), and facilitated the design of the highly sensitive and stable discriminator ($T_{15} + T_{16}$). If the PA at C_{150} is too small to trigger T_{16} via T_{15}, the diode D_6 ensures that a pulse of minimum size appears at the output each time the gate has been opened. The "X" pulse transmitted to T_6 prevents T_7 from triggering during $\tau_R + \tau_D$ (with τ_D being determined by R_{64} and the stray capacity of grid 3 in T_6).

The final memory capacitor, C_{170}, is charged negatively by a constant current source T_{17} which is switched off ($< 10^{-7}$ A) during τ_R, and discharged by a vacuum diode T_{18} as soon as the flip-flop tube T_{20} flops back to the stand-by state after reception of a reset order from the GW sweep circuit or other recording equipment (e.g., of the Hutchinson-Scarrott type[36])). Drift during τ_R can be kept very small by chosing C_{170} sufficiently large, since intervals of 3...25 μsec are available for charging C_{170}.

In the 1:1.6 PA range position, the logarithmic converter may be used in place of a linear expander with the advantage that differential counting rates dN/dx become independent of detector and amplifier gain settings. The conservation of the shape and intensity of a spectrum, as its different parts are shifted through the useful PA range, is characteristic of the logarithmic energy display.

3.7. SWEEP, INTENSIFYING, AND GATING CIRCUITS

Use of a linear sweep in connection with a wedge filter is described in the literature[18, 26–28]).

[62]) E. L. C. White, unpublished, quoted in[2]) (p. 557).
[63]) D. Maeder, Rev. Sci. Instr. **26** (1955) 805.

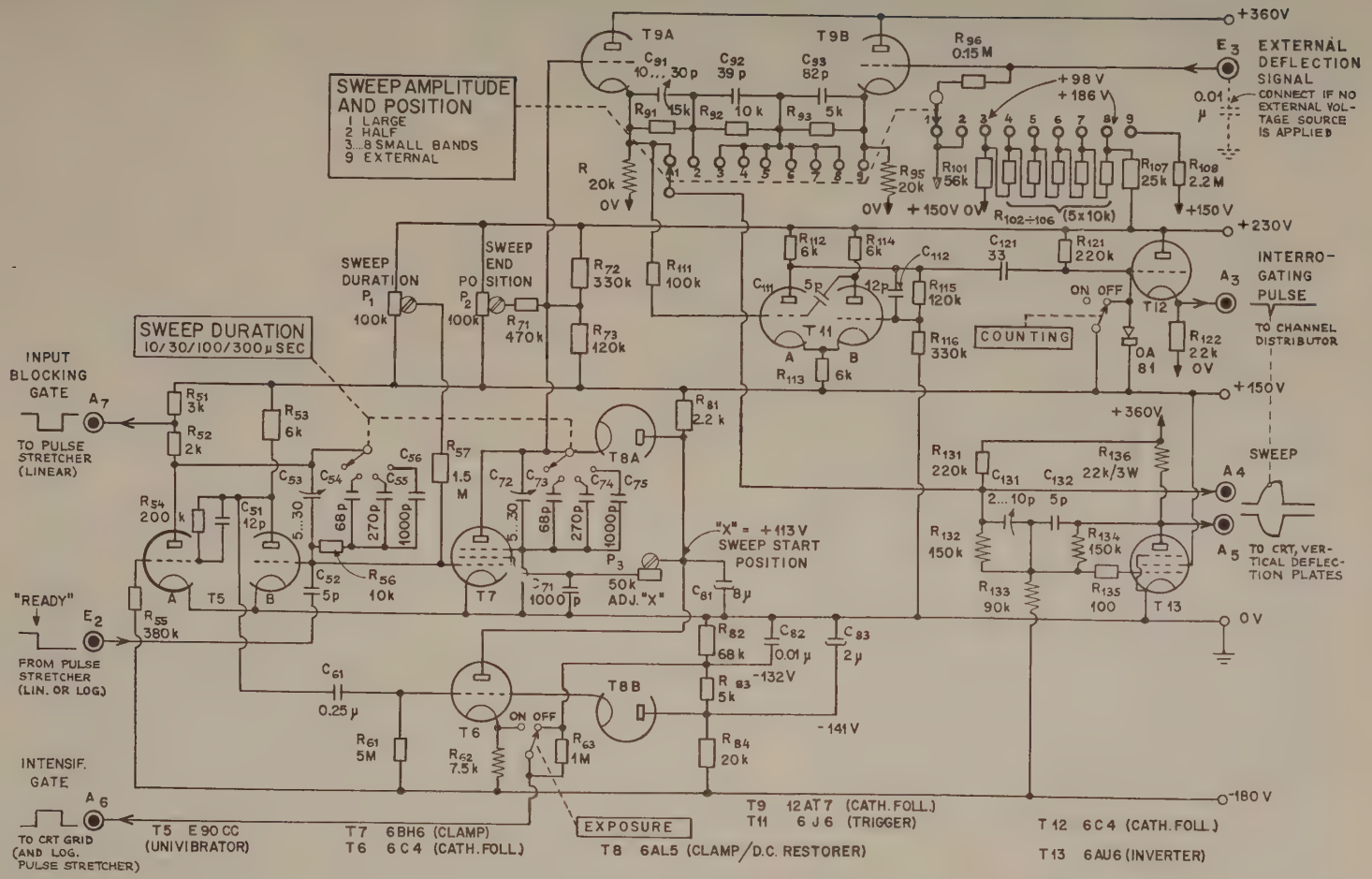

Fig. 11. Exponential sweep, intensifier gate and interrogating pulse generator of a combined GW and counting channel spectrometer.

The exponentials sweep circuit presented here (fig. 11) dispenses with the optical GW and its inherent loss of light, and at the same time provides simple switching between various positions and widths of the equivalent GW for quick energy comparisons of different spectra in the same picture (e.g., a small calibration band may be photographed above or below the main spectrum; compare fig. 4). In our present apparatus, an additional switch (not shown in fig. 11) can increase the leak impedance ($R_{71,72,73}$) so that the GW intensity range is changed from 100:1 to 10:1 with a slight gain in light intensity (see § 3.8). Proper selection of the sweep duration ($\tau_R = 10 \ldots 300$ μsec) makes it possible to obtain a high contrast spectrogram within 5 min from any source which gives $\gtrsim 10$ pulses per second in a 10% interval of the total PA range, and to keep dead time losses $< 5\%$ (see below).

Coupling from A_6 to the CRT grid must be designed to preserve the flat top of the positive pulse delivered by T_6. The same output is used to derive a "reset" signal for the pulse stretchers of figs. 9 and 10. For gating other types of stretchers, a negative counterpart of the intensifying pulse is available at A_7.

Blocking the input during $\tau_R + \tau_D$ for each recorded event causes a fractional loss equal to $N_R(\tau_R + \tau_D)$ where N_R pulses per sec are finally recorded. However, this type of gating does not exclude superposition of pulses during τ_C. Such a pile-up is especially troublesome in coincidence measurements where only a small fraction ε of the input pulses is accepted for PA analysis. Kelley[3]) therefore designed an inspector circuit in which a memory (corresponding to C_{Insp} in fig. 8) receives a fixed amount of charge from every input trigger pulse. This memory is used to gate the same (or possibly coincidence selected) trigger pulses after a suitable delay adjusted to fit the total duration of a measuring input pulse (τ_M in fig. 8). With $\tau_R < \tau_M$, this scheme would make input gating from the recording end unnecessary[3]). However, the purpose of our pulse stretchers is to make $\tau_R \gg \tau_M$ and to avoid introducing a long dead time with each input pulse. Collection of different gating orders on a common memory (C_{Insp} in fig. 8, or C_{14} in fig. 9) permits a combined rejection of pulses which are preceded (within τ_M), or followed (within τ_C) by any (possibly non-coincident) other input pulse, together with conventional $\tau_R + \tau_D$ gating. If τ_M is effective with $N_0 - N_R$, and τ_C with N_R pulses per second, the fractional counting loss becomes $N_0\tau_M + N_R(\tau_C + \tau_R + \tau_D - \tau_M)$, or

$$1 \qquad \frac{N_R}{\varepsilon N_0} = N_0 \frac{(1-\varepsilon)\,\tau_M + \varepsilon\,(\tau_C + \tau_R + \tau_D)}{1 + \varepsilon\, N_0\,(\tau_C + \tau_R + \tau_D - \tau_M}$$

where ε = coincidence efficiency, and $N_0 \approx$ total input pulse rate ($N_0\tau_M$ assumed $\ll 1$). Without input inspection, an additional fraction

$$N_0\,(\tau_C + \tau_M)\left[1 - \frac{1}{2}N_0\,(\tau_C + \tau_M) \pm \ldots\right]$$

of pulses falsified by overlapping would be counted.

The pulse generated in $T_{11} + T_{12}$ of fig. 11 when the sweep deflection reaches about half of its final height is used to interrogate electronic counting channels (see section 4).

3.8. DISCUSSION OF GRAY WEDGES

For the following comparison, we shall assume the spot intensity on the CRT screen to be $I_0 =$ constant during τ_R, the sweep deflection to cover a fixed range $y_0 \ldots y_1$ at a certain resolution width δy, and the optical lens system to accept the same solid angle Ω in all cases considered. F will denote the GW range factor which is usually chosen between 100:1 and 10:1, and $T = T(y)$ the transmission of a filter type GW.

3.8.1. *Optical wedge of exponential transmission characteristic*

From a single sweep of constant velocity, $v = (y_1 - y_0)/\tau_R$, every image element along the trace would receive the exposure $\Omega\ I_0\ \delta y/v$ if a filter was not inserted into the light path. With a filter obeying the transmission law

$$T(y) = T_0\, e^{-a\,(y - y_0)}, \quad \text{where} \quad a = \ln F/(y_1 - y_0)$$

the total exposure delivered by $\delta N(x)$ pulses

(per resolution width in the x direction) becomes

$$\tau_R \, \Omega \, I_0 T_0 \frac{\delta y}{y_1 - y_0} \cdot \delta N(x) \cdot e^{-a(y - y_0)} .$$

Therefore, if we neglect failure of the reciprocity law (§ 3.12.4), we expect to find constant photographic density along a curve given by

$$\log \delta N(x) = \text{const.} + ay .$$

In order to compare light efficiencies, we note that the exposure produced by a single pulse near the upper edge of the spectrogram ($y = y_1$)

$$B_1^{\text{exp. filter}} = \tau_R \, \Omega \, I_0 T_0 \, \delta y / (y_1 - y_0) \, F$$

decreases in inverse proportion to the range factor F. The fractional intensity error is $\delta y \log F/(y_1 - y_0)$. A useful feature of the logarithmic intensity scale is the insensitivity of the shape of isodensity curves on processing and printing conditions.

3.8.2. *Other types of optical wedges*

A linear intensity scale would permit graphical analysis of complex spectra into areas proportional to the intensities of the components. However, manufacture of a glass filter having the required transmission

$$T(y) = T_0 y_0 / y, \quad \text{where} \quad y_1/y_0 = F$$

would be much more complicated than to construct the equivalent electronic GW discussed below.

3.8.3. *Electronic GW producing linear intensity scale*

An exponential sweep (as described in § 3.7)

$$y = y_1 e^{-t/RC}, \quad \text{where} \quad \begin{aligned} y_1/y_0 &= F < y_1/\delta y \\ RC &= \tau_R / \log F \end{aligned}$$

has a variable velocity $v = -y(t)/RC$ and therefore delivers to an image element at position y the exposure $\Omega I_0 RC \delta y/y$. With $\delta N(x)$ pulses the total exposure becomes

$$B(x, y) = \tau_R \, \Omega \, I_0 \, \delta N(x) \, \delta y / y \log F .$$

Constant exposure is produced along curves of the form

$$\delta N(x) = \text{const.} \cdot y .$$

Exposure per pulse at $y = y_1$ exceeds the corresponding $B_1^{\text{exp. filter}}$ by a factor

$$\frac{B_1^{\text{exp. sweep}}}{B_1^{\text{exp. filter}}} = \frac{(y_1 - y_0) F}{y_1 T_0 \log F} = \frac{1}{T_0} \frac{F - 1}{\log F}$$

which amounts to $\approx 5 \ldots 30$ for $F = 10 \ldots 100$. Further advantages of the electronic type of GW are that its characteristics (width, position, and range factor) can easily be changed and that it is located in the plane of the CRT screen. The relative error varies between $\delta y/y_1$ and $\delta y/y_0$.

3.8.4. *Other intensity scales*

Use of a parabolic sweep[21])

$$y = y_0 (1 + bt^2), \quad \text{where} \quad \begin{cases} \sqrt{y_1/y_0} = F < \sqrt{y_1/\delta y} \\ b = (F - 1)/\tau_R \end{cases}$$

whose derivative is $v = 2b\sqrt{y(t) \, y_0}$, results in an exposure distribution

$$B(x, y) = \frac{1}{2} \tau_R \, \Omega \, I_0 \, \delta N(x) \cdot \delta y / \sqrt{y y_0} \cdot (F - 1)$$

with constant exposure curves of the shape

$$\delta N(x) = \text{const.} \cdot \sqrt{y} .$$

Single pulse exposure at $y = y_1$ exceeds $B_1^{\text{exp. filter}}$ by a factor

$$\frac{B_1^{\text{par. sweep}}}{B_1^{\text{exp. filter}}} = \frac{y_1 - y_0}{y_1 T_0} \frac{F^2}{2 (F - 1)} = \frac{1}{T_0} \frac{F + 1}{2}$$

which becomes ≈ 7 for $F = 10$. Larger range factors are excluded by the finite resolution δy of the CRT.

In order to cover a large intensity range with a more uniform sensitivity, a sweep shape giving a logarithmic intensity scale would be of interest. The appropriate function

$$y = y_1 - a \log (1 + bt), \quad \text{where} \quad \begin{cases} a = (y_1 - y_0)/\log F \\ b = (F - 1)/\tau_R \end{cases}$$

which would lead to the same exposure formula as in § 3.8.1, apart from a constant factor

$$\frac{B_1^{\log. \text{ sweep}}}{B_1^{\text{exp. filter}}} = \frac{1}{T_0} \frac{F \log F}{F - 1} \quad (3 \ldots 9 \text{ for } F = 10 \ldots 1\,000),$$

may be approximated by subdividing an exponential sweep, by means of diodes, into a number of sections having different RC time constants. However, the slight gain in light

efficiency does not seem to justify such complications in the sweep circuit, considering that an accurately logarithmic scale is easily obtained by means of a glass wedge.

A two-section exponential sweep, displaying relative intensities from 1...10 in the lower half, from 10...100 in the upper half of the total deflection, has occasionally been used at our laboratory.

3.9. OPTICAL SYSTEM

Any standard camera could be used for taking GW spectrograms, provided that the aperture diaphragm is stopped down to such an extent that vignetting effects are eliminated. However, a large aperture is necessary if high contrast type films or plates are to be used, and if the accelerating voltage is restricted to $\lesssim 2$ kV in order to protect the CRT phosphor.

ment, the $\cos^4$ law[66]) and the angular dependence of reflection losses cause a substantial decrease of brightness towards the margin of the image, and a corresponding nonuniformity in the GW calibration along the x-axis. A blackened metal strip (E in fig. 12) inserted between the lens and the image plane compensates for this effect.

3.10. PHOTOGRAPHIC PROCEDURES

3.10.1. *Negative*

High contrast material is best suited for GW recording, although it usually has a low sensitivity. Gevaert Process Extra Ortho (0 5) plates are normally used at our laboratory[20]) since they give excellent contrast ($\gamma \approx 5.5$) at a sensitivity of 4/10 DIN; whereas Kodak Contrast Process Ortho sheet film, which gives $\gamma \approx 4$ at about 8/10 DIN, is applied only in cases where extremely poor statistics have to be

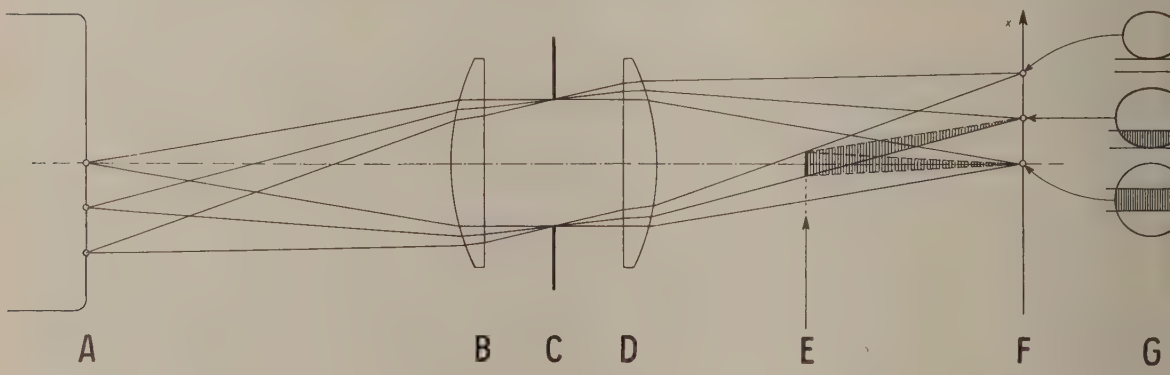

Fig. 12. Optical system with intensity equalizer, compensating for $\cos^4$ law along x axis. (A) Object (CRT screen), (B and D) Lens system (symmetric doublet with spacing adjusted to minimize image curvature), (C) Diaphragm, (E)Equalizing strip, (F) Image plane, (G) Lens aperture seen from different points of the image, Note: (E) and (G) are not drawn to scale.

An aspherical lens system of simple design[64]) has been constructed for the Basle and Zurich GW instruments, in order to obtain a 1:1 image which is large enough for direct visual inspection of a contact print. With about 50 cm distance from the screen to the image plane, it provides adequate resolution over a 5×7 cm^2 area at a 1:1.5 aperture ratio. Fig. 12 shows a cross-section of this lens system; further details are given in[65]).

Although no vignetting occurs in our arrange-

recorded. For the latter case Agfa Isochrom plates (18/10 DIN) are used at Basle[67]). The Brookhaven group recommends Kodak IV-F[26]), or Kodak IV-O[28]) spectrographic 35 mm film, with a Wratten C5 blue filter to eliminate the

[64]) D. Maeder, Helv. Phys. Acta **23** (1950) 476.

[65]) D. Maeder, Optik **9** (1952) 49.

[66]) O. Eppenstein, Handb. d. Phys. (Geiger & Scheel) XVIII, p. 210 (Berlin 1927); A. König, Handb. d. Phys. (Wien & Harms) **20** (2), (Leipzig 1929) p. 234.

[67]) E. Würger, K. P. Meyer und P. Huber, Helv. Phys. Acta **30** (1957) 157.

light from the CRT cathode. A special processing method is recommended for Kodak IV-O film[28]).

With plates or sheet film of large size (9 × 12 cm), precautions should be taken to ensure uniformity of development[19]). The gradation of an original plate negative (Process Extra Ortho) is not as sharp as it appears in fig. 13A.

The Polaroid-Land process is often used with GW instruments[26, 28]), although it gives much less contrast than the materials quoted above. However, the information available from Polaroid film is usually sufficient to procede with an experiment without waiting for the prints from high contrast records.

3.10.2. *First print*

Isodensity lines are made visible most easily by means of photographic printing[19]). Conventional high contrast paper, such as Agfa Lupex Extra Hart (similar to Kodak Velox F5) gives the positive print shown in fig. 13B (exposure 1 min from a 60 watt bulb at 40 cm distance). For producing transparent prints, we have found Gevaert Diaflex Contact paper useful; alternatively, Kodalith paper and film may serve the same purposes. A transparent calibration grid may be superimposed directly on the print[28]) in order to facilitate tracing of an isodensity line.

3.10.3. *Higher order prints*

The definition of the contour line may be further improved by taking a print from a Diaflex positive, producing a second order negative. An alternative procedure, consisting in an exposure of Lupex paper through both the original negative and a transparent positive print, gives directly a curve plot of the spectrum ("double print", fig. 13C). The positive print should in this case be made of a plate instead of paper in order to minimize shrinking.

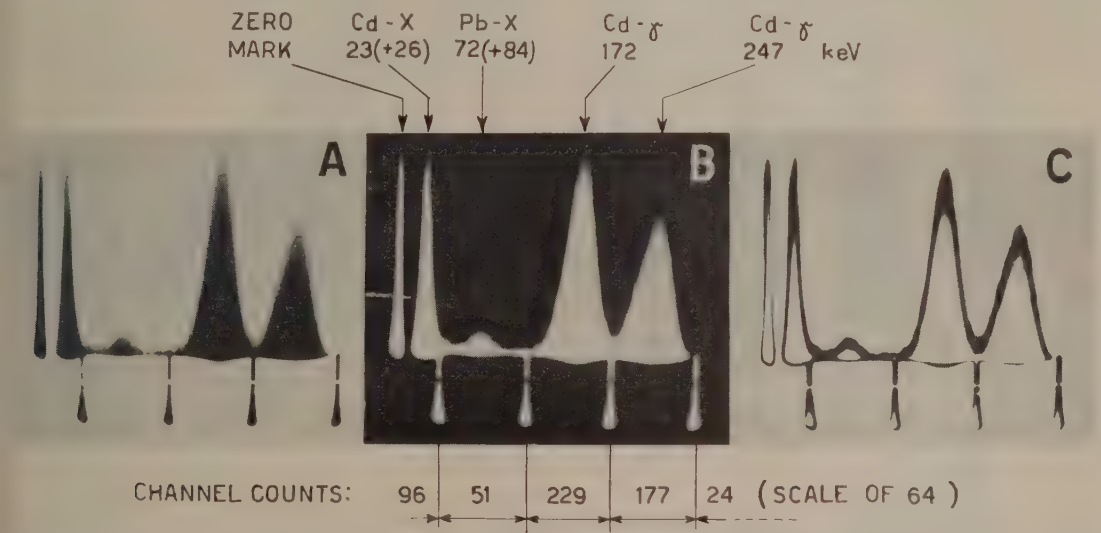

Fig. 13. Printing of GW spectrograms. (A) Appearance of film or plate negative. (B) First positive print. (C) Double print, exposed through (A) and (B). The example chosen ($In^{111} \rightarrow Cd^{111}$) demonstrates a combination of GW with electronic counting methods, which is applied here to split 4 peaks into 4 counting channels. Channel limit marks below the spectrum were produced by artificial pulses of automatically regulated amplitude. (scintillation spectrum produced by γ- and x-rays from

3.11. ENERGY CALIBRATION

Artificial pulses of proper shape and duration are fed capacitively to the output electrode of the radiation detector, in order to test the overall *linearity* and *stability* of all parts contributing to the final PA display. PA *resolution* is checked most effectively by superimposing artificial

pulses on a real spectrum received at approximately the same counting rate as expected in the actual experiment. Radiation measurements using standard sources are in general necessary to convert PA into energy. The "small sweep" positions available in our apparatus (fig. 11) permit to photograph up to 6 comparison spectra on the same plate in rapid succession.

the photographic picture). Thus, a definite intensity cannot be assigned to the peak of an ideally sharp line; therefore, if artificial pulses are to be used for intensity calibrations, their amplitudes must be varied uniformly over an interval which is large compared with the PA resolution of the spectrometer. Generators producing pulses of monotonously varying

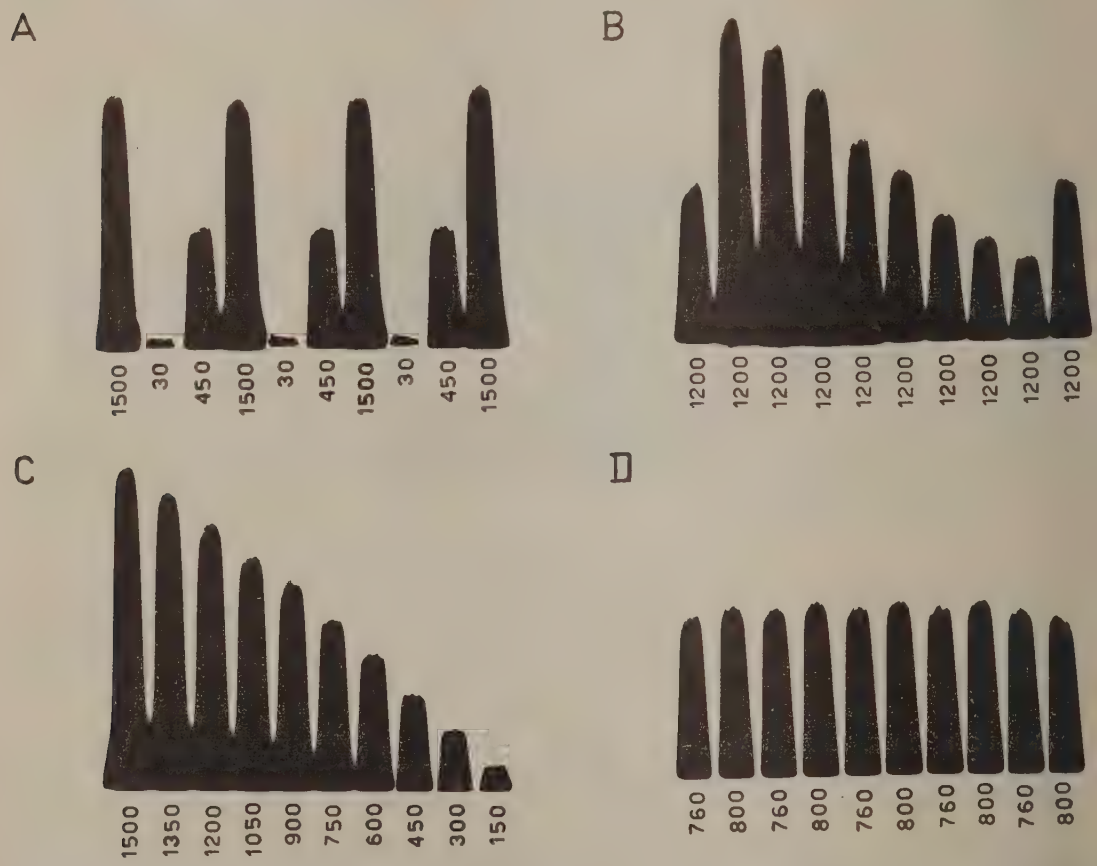

Fig. 14. Intensity calibration of electronic GW (exponential sweep of 30 μsec duration, $RC = 7$ μsec), using samples of a quasistatistical uniform PA distribution. The number of pulses exposed (divided by 64) is indicated below each sample. (A) Uniformity test: 3 samples of fixed intensities were shifted to various positions (300/sec). (B) Sampling time effect. A fixed number of pulses was delivered at different counting rates (from left to right: 40/800/400/200/80/40/20/10/4/40 per sec). (C) Calibration for a fixed run duration (5 min). (D) Difference sensitivity test (5 min).

3.12. INTENSITY CALIBRATION

3.12.1. *Experimental equipment*

By the term "intensity" we shall denote the number of pulses per unit interval of PA (measured, e.g., in millimeters of deflection on

size[68]), as they are in common use for adjusting multichannel equipment, may be applied to the calibration of GW spectrometers as well.

[68]) G. G. Kelley, P. R. Bell and C. C. Harris, ORNL-Report 1975 (Febr. 1956).

However, in the latter case, a rapid up and down variation of pulse size appears preferable to a monotonous increase in order to simulate more closely the irregular occurence of pulses in a statistical distribution. For the calibration measurements reproduced in fig. 14 a regular 100 c/sec oscillation of triangular shape was superimposed on a d.c. voltage applied to the horizontal deflection system, while the (sweep + intensifier) circuit was triggered independently by statistical pulses from a radioactive source. Ten samples of known intensity were produced in this manner on each of these calibration pictures.

3.12.2. *Uniformity check*

The uniformity of illumination over the image area is shown in fig. 14A. Samples of the same intensity positioned at different regions within the horizontal deflection range are compared in order to check for proper adjustment of the $\cos^4$ correction strip (fig. 12).

3.12.3. *Intermittency effect*

The dependence of the photographic density on the pulse frequency, if an exposure of given total duration is delivered in a number of bursts or "pulses", has been shown to become rather large at frequencies below 10 c/sec for Gevaert process plates[18]). Although Müller[24]) found no such effect between 2 and 100 c/sec for Ilford Selochrome Ortho plates, its occurence in GW spectrometers is to be suspected with most types of photographic material since a differential pulse amplitude interval in a spectrum usually receives pulses only at low counting rates. Fig. 14B demonstrates the influence of pulse frequency on the density produced by a fixed number of pulses. Each sample contains $N = 76\,800$ pulses delivered in a statistical sequence at counting rates ranging from 4.3 to 850 c/sec. Since each of these pulse frequencies corresponds to a certain duration of photographing one intensity sample, we may term the apparent intensity variation the "sampling time effect".

3.12.4. *Reciprocity law failure*

In order to obtain an empirical intensity scale which is valid for the interpretation of a particular GW picture, different calibration samples produced at constant sampling time (equal to the duration of a measurement) are required. In addition to the sampling time effect, the breakdown of the photographic reciprocity law[69]) at large variations of exposure time causes appreciable deviations from the simple relations predicted in § 3.8. The combined deviations can be represented, to a reasonably good approximation, as the result of a modified reciprocity law $I\,N^q = \text{const.}$, in order to produce constant density where the exponent q is nearly constant for a given photographic material. Thus we may expect the intensity scale of a spectrometer equipped with an *optical* gray wedge(exponential transmission law) to remain practically logarithmic over a wide range of intensities, with the slope

$$\mathrm{d}\log N/\mathrm{d}y = 1/qy_0$$

depending on the type of film or plate used[18]). This behaviour has been confirmed with improved accuracy by Bernstein, Chase and Schardt[26]) for Kodak IV spectrographic film at sampling times from a few minutes up to several hours ($q = 0.72$).

On the other hand, the empirical intensity characteristic of an *electronic* gray wedge (exponential sweep) may deviate appreciably from the ideal straight line predicted in § 3.8. From the slight nonlinearities present in the set of intensity samples reproduced in fig. 14C we conclude that q deviates by less than 10% from unity for Gevaert plates at a sampling time of 5 min. Fig. 15 summarizes analogous results obtained with different sampling times from 90 sec up to 1 hour.

3.12.5. *Fading effect*

The intensity calibration may further be influenced by any delay in the processing of the exposed plate or film. We have found an increase of the apparent intensity of about 5% during the first 3 hours, followed by a similar decrease within one day after exposure of the Gevaert plates.

[69]) C. E. K. Mees, The Theory of the Photographic Process (McMillan, New York, 1948).

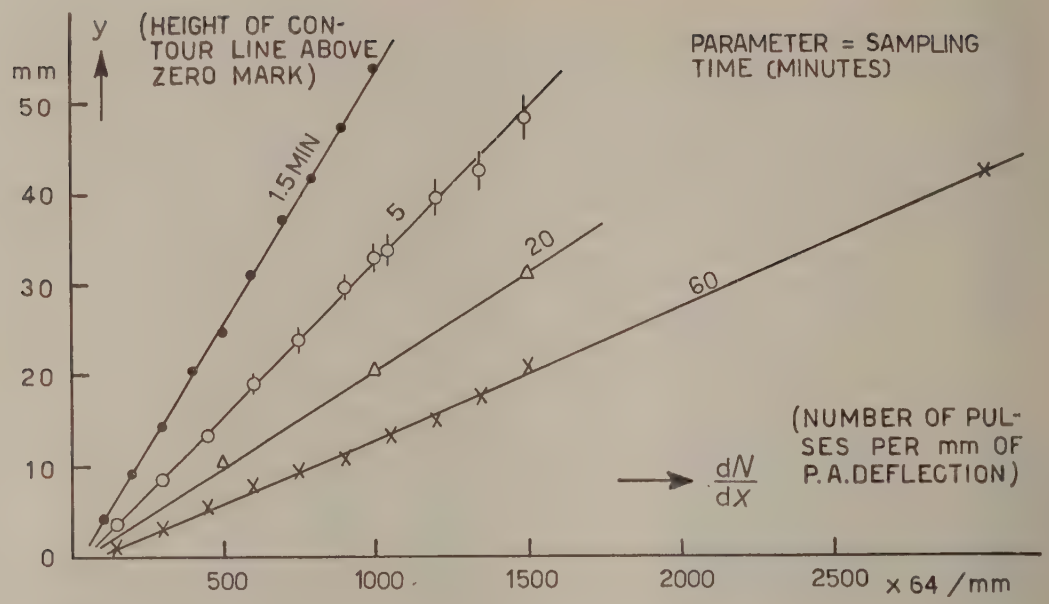

Fig. 15. GW calibration (30 μsec exponential sweep, with $RC = 7$ μsec) at different run durations.

3.12.6. *Accuracy limitations*

By standardising the processing and printing conditions, absolute *reproducibility* (using plates from the same batch) to better than 20% is attained[18]). On the other hand, *ratios* between intensities recorded at different regions in the same picture can be determined more accurately; use of a high precision optical wedge leads to a limiting accuracy of 5% over a 1:100 range[26]). With an exponential sweep type electronic wedge the relative accuracy depends largely on the absolute intensity. Fig. 14D suggests a limiting sensitivity of about 3% for revealing small *intensity differences* near the upper end of the intensity range. In view of these limitations it is of interest to point out that the simultaneous use of a relatively small number of counting channels permits accurate evaluation of *absolute intensities* from GW photographs (see section 4).

4. Combination of Photographic Density and Electronic Counting Methods

With the simultaneous use of electronic counting and GW recording equipment, the latter mainly serves to determine the fraction of each channel count, which is to be attributed to a particular peak in the spectrum. In principle, we need as many counting channels as there are peaks to be resolved, in order to enable quantitative evaluation of a complete GW spectrogram.

4.1. TOTAL INTENSITY OF AN ISOLATED PEAK

In the case of a single peak of gaussian shape, the integrated intensity is easily extrapolated from a single channel count. σ, the half-width of the peak, is assumed to follow an empirically determined function of the peak position. Channel positioning is not critical if its width is chosen sufficiently large; e.g., a properly centered channel of width $\varkappa = 1.5\sigma$ already covers 98% of the total area, and errors caused by an uncertainty of $\pm$ 0.1 σ in channel width and in channel position are $< 0.7\%$ and $< 0.03\%$ respectively. At $\varkappa = \sigma$, the channel would count 76% of all pulses and the corresponding errors would increase to 6% and 0.45%.

4.2. SEPARATION OF TWO PEAKS INTO TWO CHANNELS

The two peaks are assumed to have the same half-width σ, since corrections necessitated by

this simplification usually are quite small (see § 4.1). To separate the two peaks efficiently, the common channel limit is set midway between

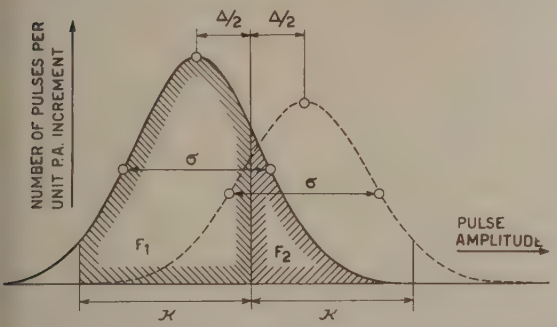

Fig. 16. Resolving two gaussian peaks into adjacent counting channels of width $\varkappa$. The half-widths τ of both peaks are assumed to be equal.

the two peaks (see fig. 16), and the channel widths $\varkappa$ are adjusted to cover most of their respective peaks, although their choice may in practical applications be influenced by the presence of other peaks. The distance Δ between the two peaks, expressed in units of σ, is the independent variable for fig. 17, in which the fractions of pulses counted in the proper channel (F_1) and in the neighbour channel (F_2) are plotted, with the reduced channel width $\varkappa/\sigma$ as a parameter. The curves show that a discrimination by a factor > 2 can be obtained, provided that Δ exceeds about 40% of σ and that no other peak is present within 150% of σ.

4.3. AUTOMATIC CHANNEL LIMIT CALIBRATION

In order to relate the channel counts to the GW record, the channel limits are photographed on the same picture, above or (see fig. 13) below the main spectrum. These marks are produced by feeding artificial pulses to the spectrometer input and adjusting their amplitude until two adjacent channels are counting at about half the

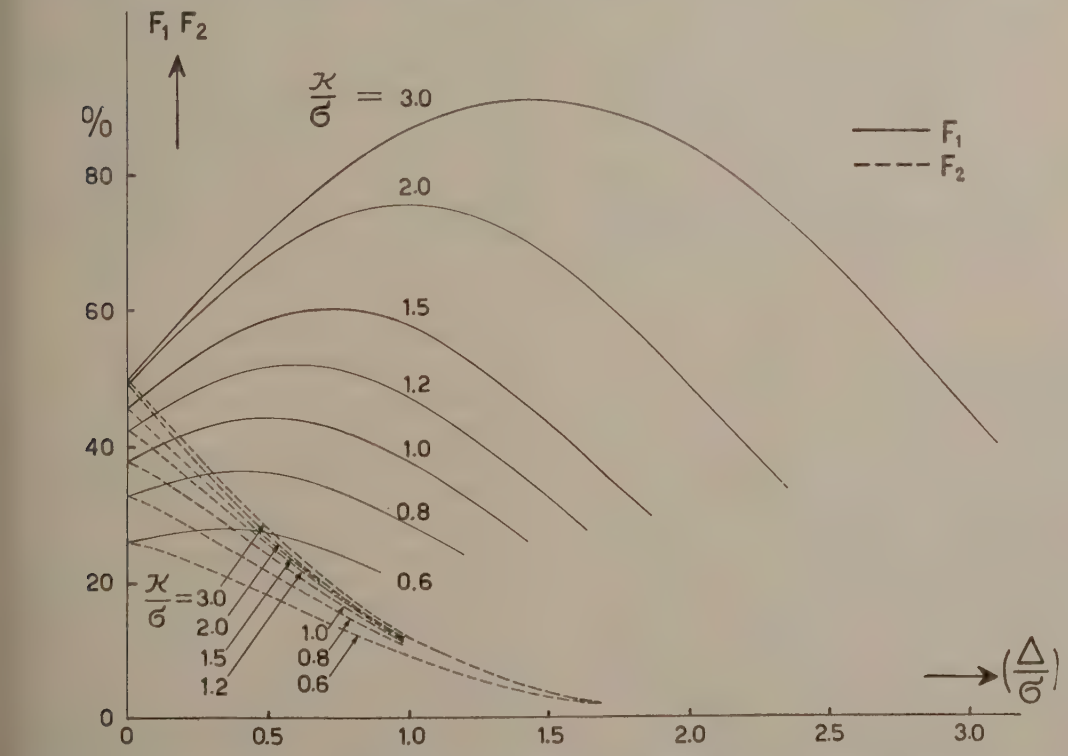

Fig. 17. Fractions of total area from the main peak (F_1) and from the neighbouring peak (F_2) which fall into counting channels positioned according to fig. 16.

input pulse frequency. The pulse generator shown in fig. 18 ($T_{60....64}$) provides automatic PA adjustment, guided by signals received from any selected pair of adjacent counting channels[30]). The lock-in feature not only facilitates circuit, fig. 11) to its respective output. In order to reset all discriminators at the end of τ_R, the MV is suitably biased, e.g. by making T_{2B} of fig. 9 conduct not only during τ_R, but also in the quiescent state.

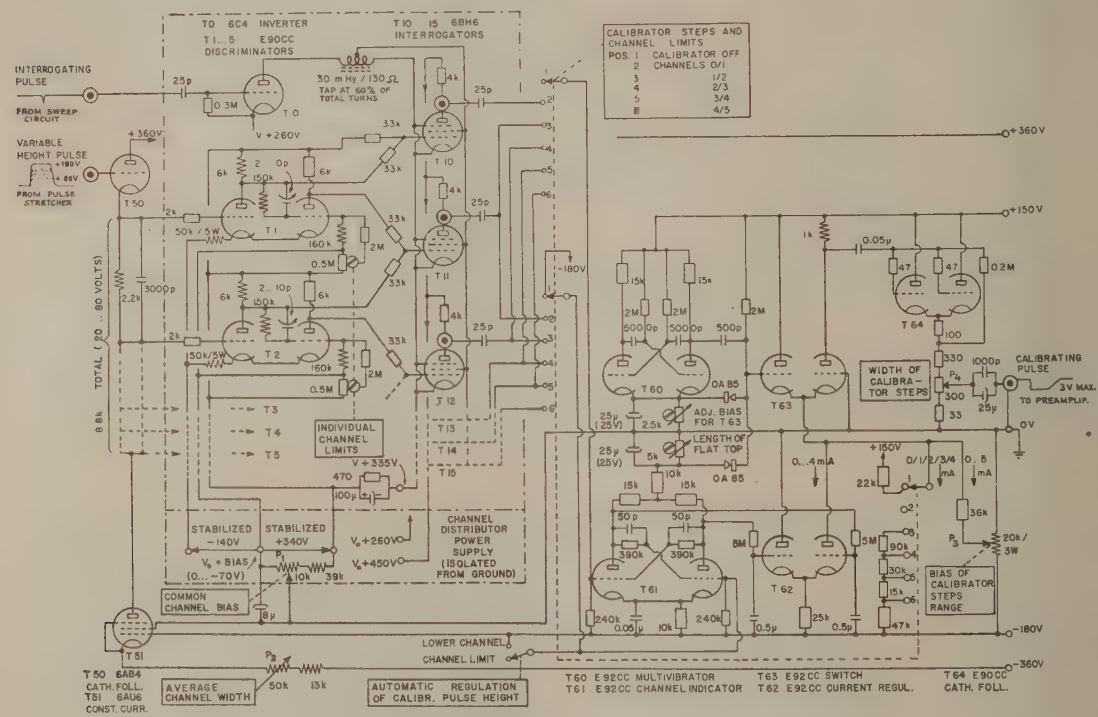

Fig. 18. Channel distributor and automatic limit marker circuit.

monitoring of the channel system, but is also helpful in the previous positioning of channels with respect to the spectrum seen on the CRT screen. In order to fit the grouping of peaks in any given PA spectrum, the channel limits in the distributor circuit ($T_{1....5}$ and $T_{10....15}$ in fig. 18) are made individually adjustable. Discriminators of a very simple design have been found satisfactory for this application, since their levels are set to non-critical positions and the channel widths usually exceed 10 volts. When the discriminators have settled to their final states (upon arrival of an MV pulse from the stretcher), only one of the tubes $T_{10....15}$ can transmit the interrogating pulse (from the sweep

4.4. COINCIDENCE APPLICATIONS

Two-dimensional DR (§ 2.7) gives only qualitative results if used as a density method (i.e. when recording large statistics on a single frame[32-35])). Again, a combination with a relatively small number of electronic counting channels permits absolute intensity evaluation when channels are properly positioned with respect to peaks and valleys in the two-dimensional distribution[30]). The photographic record provides sufficient resolution ($\gtrsim 10^4$ channels) for adjusting channel limits in such a manner that the essential information contained in the coincidence distribution may be collected in a matrix of channels (say 10×10) which fits the

capacity of existing counting equipment. A simplified circuit diagram of our 4 × 5 channel distributor is given in fig. 19. Each output signal is fed to an E1T decimal counter via an E90CC scale-of-two stage[70]). Calibration marks at the 4 recording is well suited for such applications, and the use of a modified movie camera for measurements of type (a) is considered as a common practice. The possibility of photographing, together with counting registers and

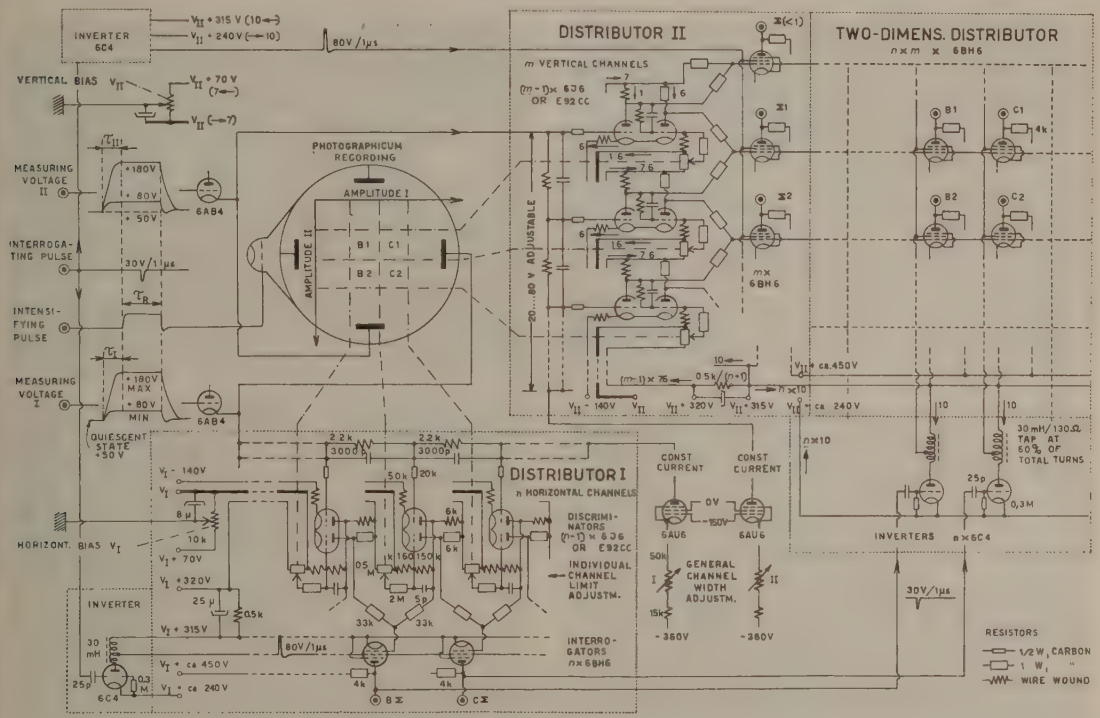

Fig. 19. Electronic counting channel arrangement used in two-dimensional coincidence spectrograph.

corners of each channel were produced by means of two automatically regulated pulse generators (§ 4.3). Evaluation procedures are described in[30]).

5. Photographic Recording of Digital Information

5.1. METHODS OF READING AND STORING COUNTER RESULTS

Digital counting, which is essential in many nuclear measurements, calls for an efficient method of producing a permanent document in cases where either

(a) a large number of successive readings from one or more counters is required, or where

(b) readings from a large number of counting channels at a time have to be taken. Photographic scaler lamps, other instruments like clocks, sample or absorber indicators, voltmeters etc., provides extreme flexibility for automatic experiments.

In recent years mechanical printers have come into use[2]), especially in connection with modern storage type spectrometers[38, 40, 42, 45]), although their low printing speed (≈ 1 channel/sec) is a serious limitation in recording multichannel information. One of the main reasons for using the expensive mechanical printers is the desire to obtain a permanent record of the data in decimal form. The recent development of a decimal memory circuit[43]) makes it possible to obtain an easy-to-read record directly by photographing the CRT display of the memory

[70]) W. Beusch and D. Maeder, Z.A.M.P. VII (1956) 520.

contents (see fig. 20), without resort to converting circuits and mechanical devices. The advantages of photographic recording, namely

(1) the speed of accepting data (up to $\approx$ 20 frames per sec), and

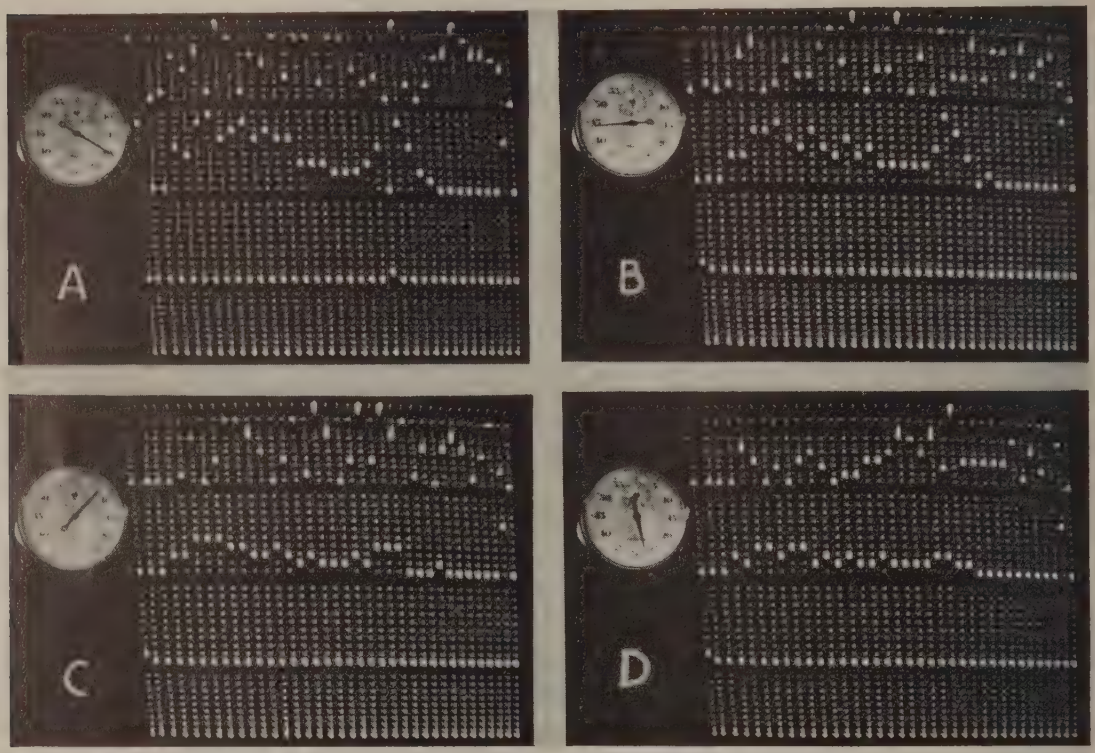

Fig. 20. Automatic photographic recording of multi-channel information. Successive frames are exposed whenever a predetermined count (e.g., 10^2) is reached in any one of the channels. The lowest channel (to the left) counts the "on time" elapsed during each measurement (clock oscillation 5 c/sec). The example chosen (A–D) shows the 24 sec decay of the γ- and bremsstrahlungs-spectrum from Ag 110 $\rightarrow$ Cd 110.

(2) the compactness of the record (1 frame of 35 mm film per 100 channels) become fully evident when a large number of successive spectra is investigated automatically (§ 5.2).

Although the decimal presentation of multi-channel results seems indispensable if data reduction is to be based on manual computation, there is a trend towards producing permanent records in a form which can be fed directly into an electronic computer. Punched card[71]) and punched tape output[72,73]) have been developed at various laboratories. Higher read-out rates would be possible with the use of magnetic tape or photographic techniques, as suggested by R. J. Klein[47]). One may expect that a photoelectric scanner of the type discussed in § 2.4 could be applied to read the contents of digital photographs into a large computer. As an alternative solution, a CRT scanner will be proposed in § 5.3. with the aim of converting the PA spectrometer itself into an inexpensive computer suitable for linear arithmetic operations involving all PA spectra previously stored in the large memory of a few meters of photographic film.

[71]) E. H. Cooke-Yarborough, reported in[47]) (p. 137).

[72]) W. B. Herrmannsfeldt, University of Illinois, Urbana (Private Communication).

[73]) R. W. Detenbeck, reported in[47]) (p. 134).

To conclude this survey, we may mention the various possibilities of obtaining mechanical or photographic records from an analog display[37,38,44,45]), where the loss of digital accuracy is the price paid for simplicity and convenience in the presentation of data.

5.2. AUTOMATIC RECORDING WITH ELECTRONIC MEMORY TYPE SPECTROMETERS

The principles of automatic counting in a single channel are thoroughly discussed by Moody *et al.*[2]). One of the major difficulties encountered by these authors (namely, the mixed electronic and mechanical storage of data) is eliminated in modern counting instruments based on purely electronic storage[36-46]). Such instruments are easily adapted for fully automatic operation, either by means of an additional programming apparatus, or by an internal arrangement in the channel distributor part of the spectrometer. The functions of the programming arrangement are

(1) to stop the counting when a predetermined time, or a predetermined count is reached,

(2) to initiate either a photographic exposure or a mechanical print-out,

(3) to change experimental conditions if required (samples, absorbers, detectors, etc.),

(4) to clear the memory, and

(5) to start the counting again.

The simplicity, reliability and speed of photographic recording is not generally appreciated because of inconveniences introduced by the binary notation used in most spectrometer memories. Even with a modified hexadecimal coding system[40]) or when using graphical conversion aids[39]), it will take ≈ 10 min to translate (modified) binary 100 channel information into a more convenient form. Our decimal memory system[43]) eliminates conversion problems and is therefore well suited for automatic photographic recording. All programming functions except (3) are incorporated in the spectrometer itself, and both time-controlled and count-controlled operation have recently been made available by adapting the lowest channel (first to the left in fig. 20) for independent counting of pulses from an external clock oscillator. Counting in all channels is stopped automatically whenever a channel reaches a preset score (e.g., 10^2 in fig. 20); a Robot Junior 24×24 mm camera (f 1/3.5) is actuated for a 1/25 sec exposure on 24/10 DIN panchromatic film, and after an interval determined by a univibrator (0.2...2 sec to allow for sample changing etc.), the counting is started again. Fig. 20 demonstrates an application to the analysis of a rapidly decaying activity; the first picture (A) was count-controlled, and the duration of that run can be measured in channel 1 (which was counting a regular 5 c/sec oscillation). For the later pictures the programming became time-controlled (20 sec for each picture) because the activity had decreased, as seen from the height of the prominent peak in the 23rd channel. As the dead time of serial memory type spectrometers is not usually negligible, we have gated the external clock oscillation before feeding it into channel no. 1, which therefore counts only during the "live time" of the apparatus. Although deadtime corrected results are thus obtained, an additional indication of standard time is required to evaluate radioactive half-lives. It is therefore planned to count ungated clock pulses (scaled down by a sufficient factor if "standard time-controlled" operation is not desired) and other external signals (e.g. from a monitoring detector) in channels nos. 2 and 3, which are provisionally left empty (in fig. 20 standard time is indicated by a stop watch). In its present state the spectrometer (without power supply and television display unit) comprises 67 tubes.

5.3. SEMI-AUTOMATIC EVALUATION OF PHOTOGRAPHED MULTICHANNEL INFORMATION

Fig. 21 shows an arrangement by which a spectrum photographed from the CRT display of a Hutchinson-Scarrot instrument may be read, after reversing development of the film, back into the spectrometer memory. With the operation switch (M/R) in position "R", pushing the press-button will release the intensification, in the CRT, of the first digit in each

channel in the course of the next memory cycle. If a particular channel carried a "one" when the original photograph was taken, the film positive will transmit the corresponding light pulse to a phototube, instructing the memory circuit to add one (or subtract one) at the appropriate place in that cycle, i.e. to change zeros into ones

A more rapid multiplication procedure is indicated in fig. 21 with a switch to select a digit displacement in the CRT which will correspond to multiplying the scanned spectrum by a given power of 2. Any desired multiplier may be composed from a few such contributions (e.g. to 1% accuracy in 4 properly selected (+

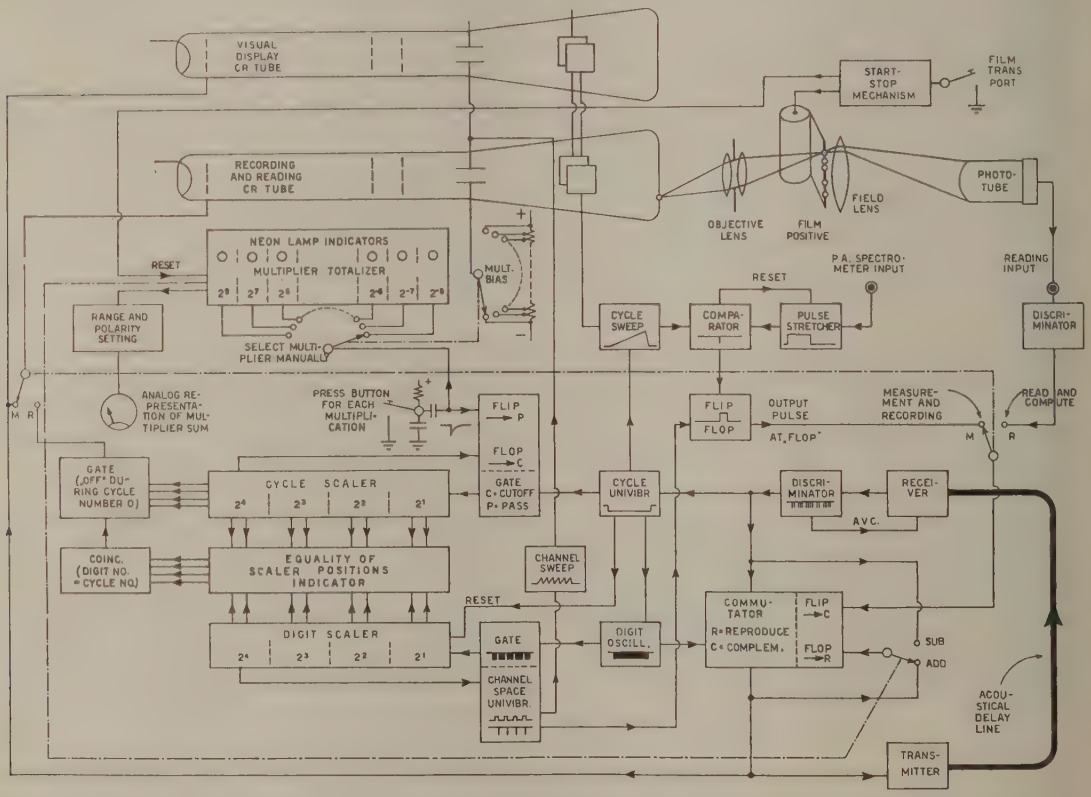

Fig. 21. Proposed photoelectric method of re-reading multichannel information, stored on film, back into the memory of the same spectrometer which was used in the original measurement, with provision for semiautomatic computing of linear combinations. Note: A pulse at an input denoted "Flop" in this diagram switches the circuit in the respective box into the quiescent state, provided that a "Flip" pulse had previously thrown it into the opposite state.

or vice-versa until the first "one" will have appeared either at the output ("ADD" position) or at the input ("SUB" position) of the reproduce-or-change network. In subsequent cycles the other digits will be intensified in turn, until the scanning is terminated when the cycle scaler returns to its zero position. The same process might be repeated in order to multiply the scanned spectrum by any integral number.

or —) steps). Thus, it will take a few seconds to add a complete multichannel spectrum, multiplied by an arbitrary positive or negative factor (limited only by the requirement that loss of information must be confined to the side of insignificant digits), into the memory. An unknown pulse distribution received from a nuclear radiation detector (switch position "M") may immediately be analyzed into a set of

standard spectra stored on film by subtracting each standard spectrum from the measured spectrum as many times as is required to clear the memory. If a signal produced when a specified channel becomes cleared were used for an automatic adjustment of coefficients and for programming the film transport, an unknown spectrum could be decomposed into contributions from several hundred calibration spectra within about 1 min, the result of the analysis being given as a record of successive multiplier totalizer readings (lamp indicators, or analog representation). For semi-automatic computation, a somewhat different scanner fitting a decimal memory spectrometer might be more convenient, thus reducing the number of manual operations required in multiplying.

NUCLEAR INSTRUMENTS 2 (1958) 332–341; NORTH-HOLLAND PUBLISHING CO. – AMSTERDAM

ON A SET OF PERMANENT MAGNET BETA-RAY SPECTROMETERS

HILDING SLÄTIS

Nobel Institute of Physics, Stockholm

Received 15 January 1958

The advantages of the use of a set of at least three permanent magnet beta-ray spectrometers, each spectrometer designed for a certain energy interval, are emphasized. It is found that a design which gives good homogeneity for strong magnetic fields might fail to do so for weak ones. A simplified construction of high resolution spectrometers is given. Reproductions of conversion line spectra of ThB + C + C″ and of $Hg^{195, 195m, 197, 197m}$ illustrate the efficiency of the spectrometers. The suitability of a high resolution permanent magnet beta-ray spectrometer for use also in the low energy region (about 6–15 keV) is demonstrated by a record of more than 50 L-Auger lines in the electron spectrum of ThB + C + C″.

1. Introduction

The permanent magnet beta-ray spectrometers for photographic recording of conversion lines are arousing an increasing interest and are being put more and more in use. They are particularly suitable for spectra containing a large number of conversion lines, and give valuable information on the origin of the lines when dealing with several half-lives in the same sample. The high resolution (up to about 1 part in 10 000) makes it possible to resolve the different L, M, N, O-conversion lines, and thus to determine the multipole order of the radiation as well as the atomic number of the element responsible for the conversion.

It is not possible here to give a review of investigations, where the permanent magnet beta-ray spectrometer has been used. It may be mentioned that at the Nobel Institute of Physics the inherent half-widths of the K-conversion lines were measured for some lines in the beta-ray spectrum of ThB + C + C″,[1,2]). A method for the determination of the relative intensities of conversion lines recorded photographically in a semicircular beta-ray spectrograph was developed by Slätis[3]). The method was tested on conversion lines in the beta spectra of ThB and RaB. The energies and the intensities of 142 Auger- and conversion lines in the active deposit of radon were measured (Mladjenović and Slätis[4])) and compared, when possible, with the corresponding values obtained by Ellis and Cork *et al.* The energies of five RaB + C lines as determined by Muller *et al.* and by Mladjenović and Slätis were compared, the differences always being < 1 part in 10 000. The same authors[5]) investigated the Auger transitions in Bi^{212} (ThC). Stockendal, McDonell, Schmorak and Bergström[6]) have obtained nice conversion line spectra of $Bi^{203} + Bi^{204} + Bi^{205} + Bi^{206}$ recorded in the permanent magnet spectrometer. The low energy part of the conversion electron spectrum is reproduced in another paper[7]). The advantage of the permanent magnet beta-ray spectrometer[8, 9]) has furthermore been enhanced by an evaporation device for beta-spectrometer samples[10]).

[1]) H. Slätis, Arkiv f. Fysik **6** (1953) 415. This paper will hereafter be referred to as I.

[2]) H. Slätis and G. Lindström, Phys. Rev. **88** (1952) 1429.

[3]) H. Slätis, Arkiv f. Fysik **8** (1954) 441.

[4]) M. Mladjenović and H. Slätis, Arkiv f. Fysik **8**(1954) 65.

[5]) M. Mladjenović and H. Slätis, Arkiv f. Fysik **9** (1954) 41.

[6]) R. Stockendal, J. A. McDonell, M. Schmorak and I. Bergström, Arkiv f. Fysik **11** (1956) 165.

[7]) M. Schmorak, R. Stockendal, J. A. McDonell and I. Bergström, Nuclear Physics 2 (1956/57) 193.

[8]) C. J. Herrlander, R. Stockendal, J. A. McDonell and I. Bergström, Nuclear Physics 1 (1956) 643.

[9]) J. A. McDonell, R. Stockendal, C. J. Herrlander and I. Bergström, Nuclear Physics 3 (1957) 513.

[10]) R. Stockendal and K. E. Bergkvist, Nuclear Instruments **1** (1957) 53.

A review of previous permanent magnet beta-ray spectrometers has been given earlier[1]). Among recently described spectrometers of this type is that of Mladjenović[11]) and that of Rosenblum *et al.*[12]). In the last mentioned spectrograph the electrons are accelerated in the neighbourhood of the sample by means of an electric field created by a potential difference of the order of magnitude 10 keV. By this device a considerable gain is achieved in the efforts to reduce the time of exposure, when records are made in the low energy region (say below 20 keV).

The strength of the magnetic field in a permanent magnet beta-ray spectrometer is easily changed by a short current pulse in the coils of the spectrometer. However, as is well known, there will at first be a "creeping"-effect, i.e. after the magnetization the field strength changes slowly the first minutes, hours or days, approaching a certain constant value after some time. This time can be appreciably shortened, if the magnetization is made in the following way. Suppose that a field strength H is desired. One starts, for instance, with a field strength of $H + H = 2H$, then one chooses $H - 4/5H = 0.2\,H$, $H + (4/5)^2\,H = 1.64\,H$, $H - (4/5)^3\,H \approx 0.5\,H$, and so on, ... 1.4 H, 0.67 H, 1.26 H, 0.8 H, 1.2 H, 0.9 H, 1.1 H, ... When well magnetized, the field is almost immediately constant for years. It was found in I, that the change over a period of one year was not larger than about 1 part in 10 000.

After having achieved a constant, well known field, it is of course of interest not to destroy it again. The advantage of a set of spectrometers, each covering a certain energy region is, therefore, obvious. At the same time the question arises, if the spectrometers can be given a simpler construction, and hence become cheaper. In addition one has to study, if a construction which is good for a certain energy region, also is the best one for another energy region. For instance, is it possible to use a smaller amount of magnetic steel when working in the low energy region?

2. Design of the Permanent Magnet Beta-Ray Spectrometers

Fig. 1C shows a schematic drawing of the iron yoke Fe of the earlier spectrometer (described in I) as well as the position of the magnetizing coils, Z, the pole pieces, I, and the permanent

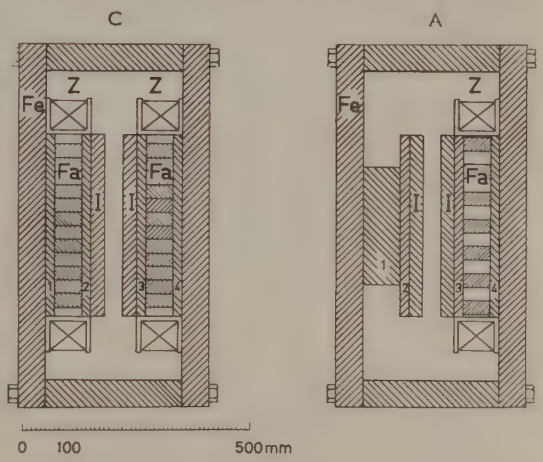

Fig. 1. C. Schematic drawing of the iron yoke Fe, 1, 2, 3, 4, the pole pieces I, the permanent magnet pieces Fa and the magnetizing coils Z in the earlier permanent magnet beta-ray spectrometer, called C. – A. Schematic drawing of the iron yoke, pole pieces, permanent magnets and the magnetizing coil in the new simplified spectrometer type.

magnet pieces, Fa. The corresponding parts in the new design are shown in fig. 1A. It is seen that the permanent magnet pieces are only at the right hand side of the pole pieces, and that these pieces are not closely packed. Only one magnetizing coil is used. Fig. 2 shows the source- and the plate- (or film-) holder. The details are described in the text of the figure. Fig. 3 demonstrates the principle of measuring the diameter 2ρ of the electron paths. The distance d_ν between the source (usually a thin wire) and a number of calibration edges ($\nu = 6$, 7, 8, ... 32) is measured directly by means of a comparator. The diameter 2ρ of the electron paths corresponding to a conversion line is computed from the distance x of the line from

[11]) M. Mladjenović, Bull. Inst. Nucl. Sciences "Boris Kidrich" **6** (1956) 54.

[12]) S. Rosenblum, J. Sant'ana Dioniso et M. Valadares, J. Phys. Rad. **17** (1956) 112.

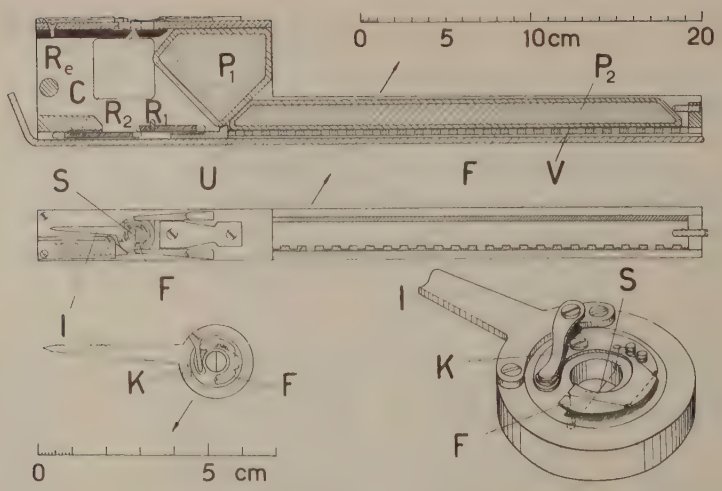

Fig. 2. 1. The source- and film-holder. R_e = ebonite baffle, R_1, R_2 = adjustable brass baffles. P_1, P_2 = lead shieldings, F = photographic plate or film, 19 × 270 mm. V = calibration edges 10 mm apart. S = source = activated wire. U = cover. 2. 1 = Source holder for ThB + C + C″ or RaB + C + C″ when extremely high resolution is desired. K = ground contact for the activated platinum or tungsten wire S, 25 or 12 μ thick. F = spring used in order to keep the wire stretched.

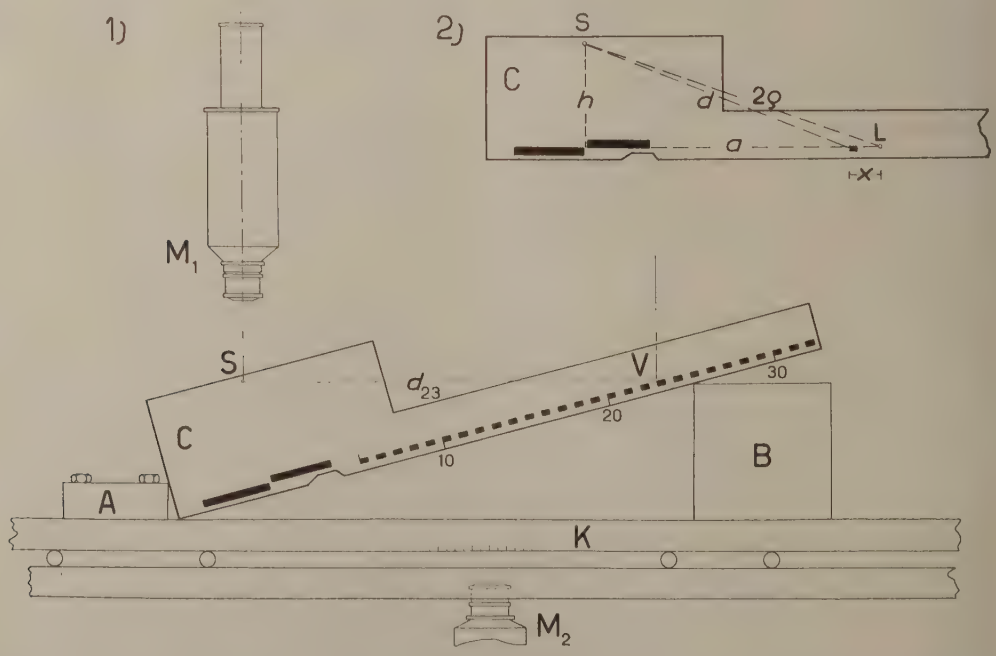

Fig. 3. 1. Method of measuring the distance between the active wire and the calibration edges. K = comparator. M_1, M_2 = microscopes. 2. Principle for measuring the diameter 2ϱ of the electron paths. x = distance between a conversion line L and a neighbouring calibration edge. For the calculation of 2ϱ accurate values of d and x, approximate values of a and h are used.

an adjacent calibration edge ν, using the distance d_ν and the distances a and h of the baffle R_1R_2 from the edge and the source, respectively (fig. 2). It is not necessary to know a with high accuracy. The details of the method are given already in I.

sample- and film-holder is seen on the left hand spectrometer (called A). A vacuum gauge rests on the right hand spectrometer (B) †.

3. Measurements of the Magnetic Field

The form of the magnetic field between the

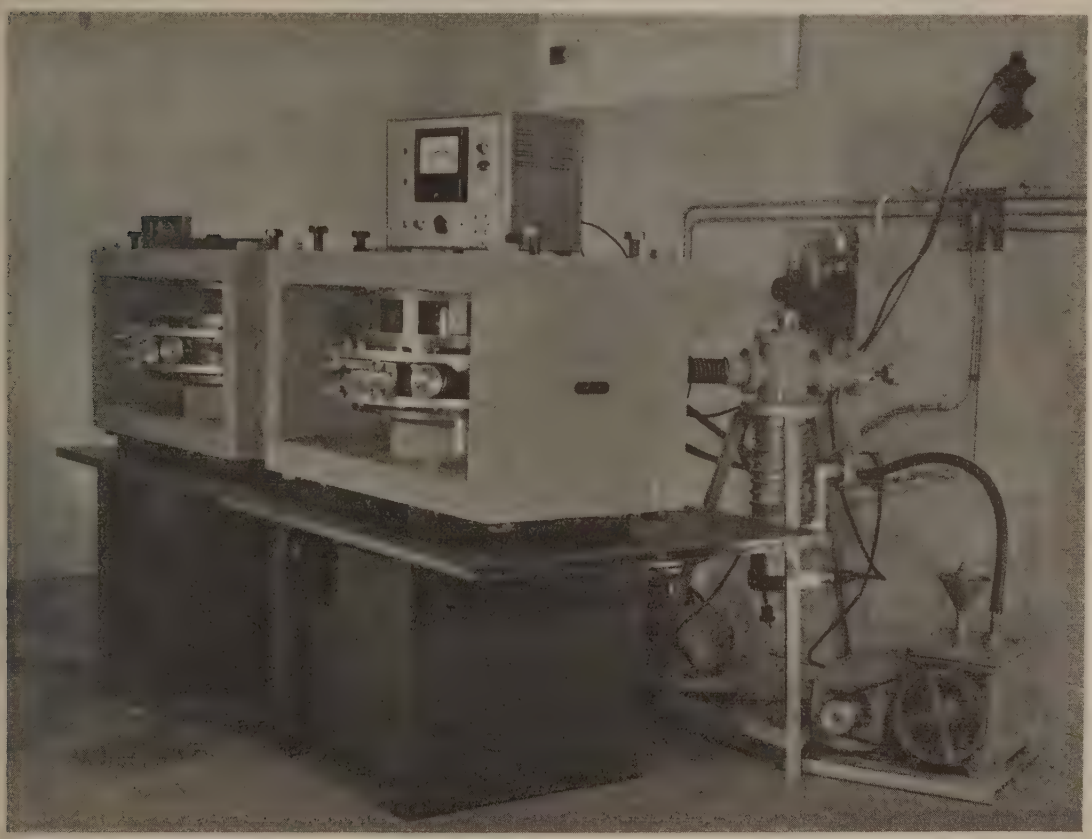

Fig. 4. Photograph of the two new permanent magnet beta-ray spectrometers, A and B. The walls and the roof of the cabinet, built to contain the spectrometers and the thermostat, are removed. The magnetization coils are also removed in order to show the permanent magnets.

Fig. 4 gives a photograph of two new permanent magnet beta-ray spectrometers A and B built in accordance with the diagram, fig. 1A. The walls and the roof of the cabinet, built in order to contain the spectrometers and the thermostat, are removed. The magnetization coils are also removed in order to show the position of the permanent magnet pieces. A pole pieces was measured by means of two antiparallel coils, mounted at a mutual distance of 5 cm on a rod, which was inserted between the pole pieces in positions, the differences of which were 2.5 cm. Turning the rod 180° about its own

† Spectrometers of the type described here will be made commercially by the Swedish firm "LKB-Produkter", Stockholm 12.

axis, the difference between the charge pulses induced in the two coils was measured by means of a fluxmeter.

the number of magnetic steel pieces, the diagram also shows the influence of the number of pieces. It is interesting to see that the spectrometers C

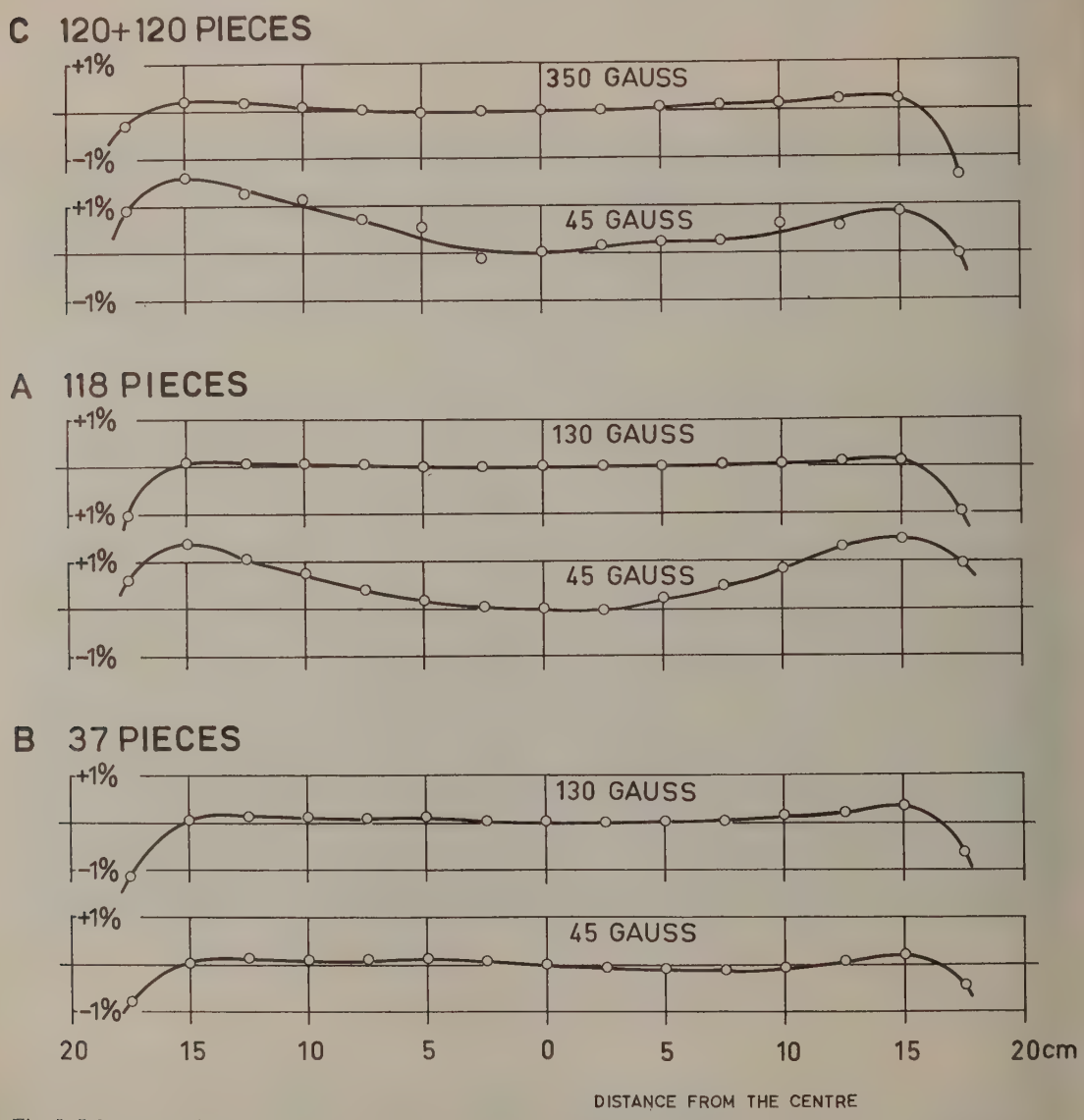

Fig. 5. Inhomogeneities of the magnetic field for different field strengths and for different numbers of magnet pieces.

Fig. 5 shows the results obtained for the three spectrometers C (described in I), A and B (described above), as well as for different field strengths given in the figure. Because of the identical construction of A and B, except for

and A, which have closely packed magnet pieces, possess a nice field form for higher field strengths, 350 and 130 gauss, respectively, whereas for 45 gauss the field strength in both spectrometers has a parabolic shape for $r \leq 15$ cm (r is the

radial distance from the axis of the pole pieces). For $r = 15$ cm the field strength is about 1.3% higher than in the center ($r = 0$), and it decreases again for $r > 15$ because of the rim effect. The reason for the parabolic field form is, obviously, the strong demagnetization effect on the inner magnet pieces, which are all surrounded by neighbouring closely packed pieces, whereas the peripherical pieces have a lower number of neighbours. This, of course, is valid for all field strengths, but for a low magnetization the coercive force is very small. It should therefore be more advantageous to create a weak field by using a lower number of magnet pieces, separating them from each other, and using a higher individual flux density. Then each piece also possesses a higher coercive force, while the demagnetizing field is the same as for closely packed pieces with corresponding lower individual flux density. This reasoning was confirmed by the use of only 37 pieces in spectrometer B, as compared with the 118 pieces in A. Fig. 5 shows that for 45 gauss the field form in the spectrometer B has achieved the same standard as for a strong field. In spite of this spectrometer B still has a good field shape for strong magnetic fields.

Experiments were made in order to investigate, if it would be possible to avoid using the magnetizing coil, instead inserting permanent magnet pieces already magnetized. It was observed that the insertion of the pieces caused a disturbing residual magnetism in the pole pieces along the line of insertion. The greater number of times the experiment was repeated, the worse was the field form in the gap. However, it was found that the magnetizing coil can be removed after the magnetization of the inserted permanent magnetic pieces. The coil is removed by first opening the iron yoke very carefully, the upper part of the yoke in Fig. 4 is lifted and kept horizontal under the whole operation, the coil is removed, and the iron yoke again closed. However, the field strength in the

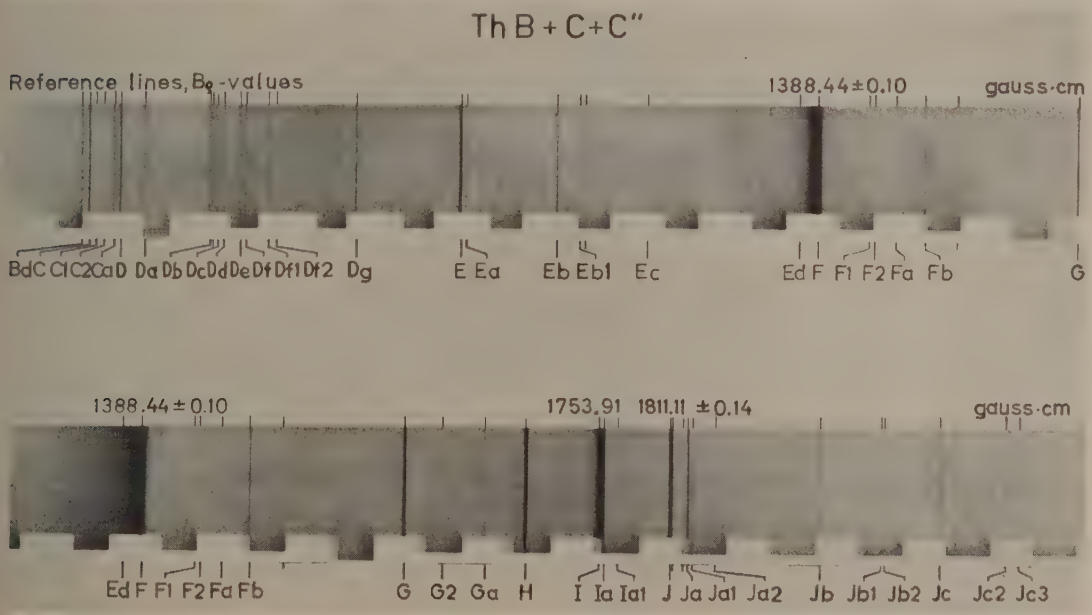

Fig. 6. Beta-ray spectrum of ThB + C + C''. The γ-activity was about 300 μC at the start of the exposure (24 hours). The activity was deposited on a platinum wire 25 μ diameter, length 4 mm. Baffle $R_1R_2 = 4$ mm. The $B\varrho$-values for the reference lines F and I are given in ref. [13]).

spectrometer was observed to decrease by about 20 percent.

It was also stated that the behavior of the individual permanent magnet pieces, when magnetized, depends strongly on the prehistory of the pieces in question. After demagnetization of the spectrometer, the individual residual magnetism of each permanent magnet piece was measured. It was observed that the residual magnetism was not zero for each piece. Instead, residual magnetism of very different size and direction was found. In order to get a homogeneous field, the spectrometer should therefore first be demagnetized very carefully, starting with high amplitudes of the alternating fields, and letting the amplitudes decrease very slowly. When magnetizing, it should be made as mentioned above.

TABLE 1

Comparison of the $B\varrho$-values given by Suruge, Siegbahn *et al.*[13]) and the $B\varrho$-values measured by Slätis and Tarjanne for some conversion lines in the beta-ray spectrum of ThB + C + C″. The comparison is made in order to study the influence of a maximum deviation of 0.32 % from a uniform magnetic field

Ellis' notation	Surugue and Siegbahn	Slätis and Tarjanne	Difference %
D_g	1030	1031.08	—0.10
E	1110	1110.28	—0.03
E_a	1114	1114.25	—0.02
E_b	1183	1184.16	—0.10
F	1388.44	1390.34	—0.14
G	1596	1598.18	—0.14
H	1697	1694.90	—0.12
I	1753.91	1753.91	0
I_a	1757.07	1757.15	—0.00
J	1811.11	1810.98	0.01
J_a	1824	1824.57	—0.03

4. Illustrations of the Use of the new Spectrometers

In this paper we are not dealing with extremely high resolutions. It was shown already in I, that resolutions of about 1 part in 10 000 are obtained with field-forms corresponding to the first curve C in Fig. 5, if suitable samples and wires are used.

In order to test the spectrometer region A (130 gauss) the $B\rho$ values of some well known lines in the spectrum of ThB + C + C″ were measured. Such a spectrum is seen in fig. 6. Tarjanne† found the values given in Table 1. For comparison the values obtained by Surugue, but adjusted by Siegbahn and Gerholm[13]) in order to match neighbouring accurately measured standard lines, are given. The differences between the $B\rho$-values given by Surugue, Siegbahn *et al.* and our values are of the order of magnitude 0.1 %. However, the magnetic field was not yet that given in fig. 5. The errors in the actual field were about three times the errors in the field described by the curve A (130 gauss). The authors experience is that field forms of the later kind make $B\rho$-determinations possible with an accuracy of a few units in 10 000. Of course, the best thing is to keep a good field form and, if necessary, to determine the small corrections which have to be added to the measured $B\rho$-values. Then it is possible to make energy determinations with errors smaller than 1 unit in 10 000.

Fig. 7 shows the conversion lines belonging to the decay of Hg^{195} (9.5 h) Hg^{195m} (38 h), Hg^{197} (65 h) and Hg^{197m} (23 h), recorded by J. Halter[14]) (Zürich) and Slätis. The active mercury was produced by bombarding gold with deuterons (dosage 110 μA hours, deuteron energy 25 MeV). The bombarded gold was heated in vacuum and thus the active mercury was evaporated and absorbed in a thin gold layer, previously evaporated on a thin wire of stainless steel. This wire, which of course was kept at a lower temperature under the mercury evaporation process, was then used as a sample in the permanent magnet beta-ray spectrometer.

In order to show the use of the very low energy region corresponding to the last curve, B (45 gauss) in fig. 5, it was decided to study the L-Auger lines in the beta-ray spectrum of

† P. Tarjanne, On leave from the Finland Institute of Technology, Helsingfors, Finland.

[13]) See Beta- and Gamma-Ray Spectroscopy, edited by K. Siegbahn (Amsterdam, 1955) the article by K. Siegbahn and T. Gerholm, p. 920.

[14]) O. Huber, J. Halter, R. Joly, D. Maeder and J. Brunner, Helv. Phys. Acta **26** (1953) 591.

ThB + C + C″. These lines were first found by Black[15]), who used sources of RaB + C + C″ and also ThB + C + C″. As these elements are isotopes of the same atomic number, 82, 83, and 81, respectively, the same Auger lines should be expected. The lines were recorded on Schumann plates in a semicircular beta-ray spectrometer. Black found 15 lines in the energy region considered, and interpreted 11 of them as due to the ejection of M, N, or O-electrons by LX-rays in the element 83. However, two of the lines were supposed to have their origin in the platinum wire, used as backing for the active deposit. Flammersfeld[16]) employed a semicircular beta-ray spectrometer with a Geiger-Müller counter. He observed four lines in the energy region of interest for the L-Auger electrons in the beta spectrum of ThB + C + C′. Butt[17]) accelerated the electrons before the Geiger-Müller counter in his magnetic lens beta-ray spectrometer. Investigating the L-Auger spectrum of ThB + C + C″, he found 8 lines. Five of these lines were interpreted as due to the element 83, the rest to the element 81. Rosenblum *et al.* [12]) report 31 lines of energies from 6.20 to 14.76 keV. Among these two are unresolved bands (7.43–7.73 and 13.51–14.23 keV, respectively). In addition they found a band between 1–3.6 keV. Bellicard[18]) used an ironfree double focusing spectrometer with a Geiger-Müller counter. He observed 26

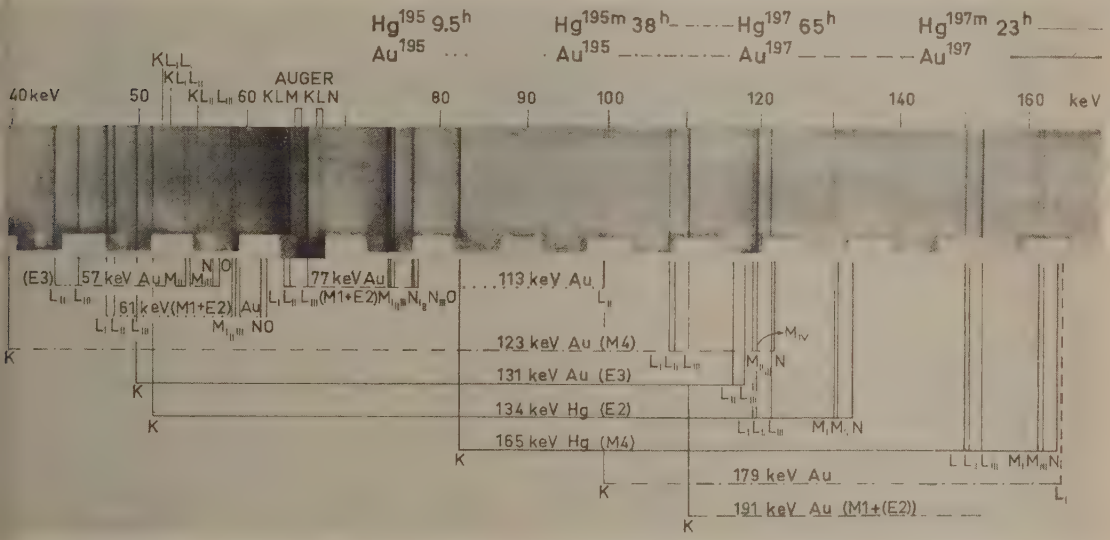

Fig. 7. Conversion line spectrum of Hg^{195} (9.5 h), Hg^{195m} (38 m), Hg^{197} (65 h), and Hg^{197m} (23 h), recorded by Halter and Slätis. The activity of the mercury was situated in an evaporated thin gold layer on a 50 μ diameter wire of stainless steel, length 6 mm. Baffle R_1R_2 = 2 mm. The γ-activity was about 120 μC at the start of the exposure = two days after the activation. Exposure time = 24 hours.

Auger lines of energies 5.920–12.500 keV. 21 of these lines were interpreted theoretically. According to the spectrum reproduced the resolving power was about 0.5%. Burde and Cohen[19]) found 30 L-Auger lines in the beta spectrum of ThB in equilibrium with its decay products. They used a thin-magnetic-lens electron spectrometer. The L-Auger spectrum coincident with alpha particles from ThC was also measured. In this case 15 L-Auger lines were observed and ascribed mainly to ThC″. By subtraction of the normalized L-Auger spectra the 15 lines

[15]) D. H. Black, Proc. Camb. Phil. Soc. **22** (1925) 832, 838.
[16]) A. Flammersfeld, Z. Physik **114** (1939) 227.
[17]) D. K. Butt, Proc. Phys. Soc. **63** (1950) 986.
[18]) J.-B. Bellicard, Ann. de Phys. **2** (1957) 419.
[19]) J. Burde and S. G. Cohen, Phys. Rev. **104** (1956) 1085.

belonging to ThC were obtained. Most of the measurements were carried out at about 1% resolution.

It is obvious that these earlier investigations are partly incomplete and partly inconsistent. This fact was a further reason for a study of the above mentioned L-Auger lines in the permanent magnet beta-ray spectrometer. The author has previously mostly employed "Ilford Selochrome 120"-film in the permanent magnet spectrometers. For instance this film was used for recording the spectra reproduced in figs. 6 and 7. However, no L-Auger lines are usually observed on these films after the ordinary one-day exposure. The author observed an Auger line for the first time when the active deposit was carried on a carbonum wire (diameter 0.13 mm). Carbonum was chosen in order to reduce the back-scattering and in order to avoid external conversion electrons coming from the backing. Because the Auger electrons stop already in the protecting layer of common films, plates were prepared using "Ilford Nuclear Research Emulsions in Gel Form, G.5." The emulsion was made as thin as possible. This has the advantage of reducing the X-ray blackening of the background, and, which is most important, of reducing the fixing time. It was observed that weak Auger lines, which were seen when the fixation started, disappeared after some minutes. The silver, situated in the outmost layer of the emulsion, was obviously dissolved in the fixing bath.

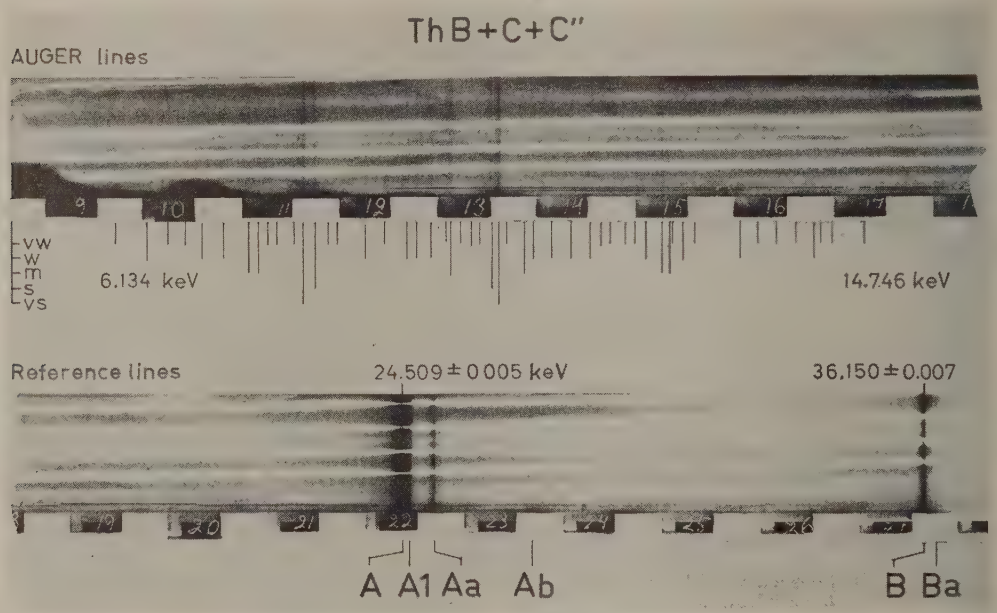

Fig. 8. 51. L-Auger lines in the beta-ray spectrum of ThB + C + C'' (Slätis). The positions of the Auger lines are marked by vertical lines, the lengths of which indicate the visually estimated intensity. vw = very weak, w = weak, m = medium, s = strong, vs = very strong. The active deposit was on a carbonum wire, diameter 130 μ, length 8 mm. Baffle R_1R_2 = 2.4 mm. Exposure 3 weeks. The plate is prepared with "Ilford Nuclear Emulsion in Gel Form, Type G.5" The energy values for the reference lines A and B are given in ref. [13]).

Fig. 8 shows such a plate, prepared with Ilford Nuclear Research G.5-emulsion in Gel, and exposed under 3 weeks. Two similar carbonum wires, length 8 mm, diameter 0.13 mm, were used alternately. While one of the wires was activated, the other one was used in the spectrometer. Changes were made every day. When activated, the activity was almost always about 500 μC.

About 40 L-Auger lines were immediately seen on the plate. Using reflected light, over 50 L-Auger lines in the energy region 6–15 keV could be measured. In order to determine the energies of the lines the well known value[18]) for the A-line in the spectrum of ThB in equilibrium with its decay products was used. The lines A, A1, Aa, Ab, B and Ba are also seen in fig. 8. The line A is strongly over-exposed, but thanks to the varying thickness of the emulsion, the position of the line is well defined in the regions of very thin emulsion.

A more detailed treatment of these L-Auger lines will be given elsewhere in a forthcoming paper[20]).

Acknowledgements

The author is indepted to the foundation "Magnus Bergvalls Stiftelse" for financial support which made the construction of the two new permanent-magnet beta-ray spectrometers possible. He would also like to express his thanks to Mr. Pekka Tarjanne (Finland Institute of Technology, Helsingfors) for valuable assistance in many experiments.

[20]) Z. Sujkowski and H. Slätis, Arkiv f. Fysik (in print).

NUCLEAR INSTRUMENTS 2 (1958) 342–347; NORTH-HOLLAND PUBLISHING CO. – AMSTERDAM

SIMPLE ČERENKOV DETECTOR FOR THE MEASUREMENT OF THE ENERGY OF RELATIVISTIC CHARGED PARTICLES

M. HUQ

Physics Department, The University of Birmingham, England

Received 23 December 1957

A detector using a cone-shaped perspex radiator for the measurement of the energy of protons from the Birmingham Proton Synchrotron is described in this paper. The overall resolution obtained was ± 13% most of which is contributed by the sensitivity of the detector to the width and angular spread of the beam. With ideal beam conditions the resolution is expected to be ± 6%.

1. Introduction

The Čerenkov process has been utilised in recent years to measure the energy of relativistic charged particles. Mather[1]) used a photographic method to detect Čerenkov radiation from protons and applied his work to the measurement of energy of the external beam of the 184 inch cyclotron at Berkeley, California. Marshall[2]) devised a Čerenkov detector, with which he obtained considerable accuracy. Both Marshall and Mather's methods need good collimation and high intensity of beam. Jelley[3]) suggested a much simpler Čerenkov detector, suitable for use in the Birmingham University proton synchrotron. A cone-shaped radiator was first proposed by Getting[4]) as early as 1947, but Getting and later Dicke[5]) failed to show any conclusive results with this type of radiator. This paper reports the results of investigations of the properties of this detector.

It is seen that the system is self-collimating, i.e. its counting efficiency decreases rapidly for off-axis particles. Consequently it is not very good for counting single particles in an initially divergent beam. In the present experiment the mean energy of the whole beam of protons, rather than in single protons, has been measured by integrating the pulse over a single "burst" from the synchrotron.

[1]) R. L. Mather, Phys. Rev. **84** (1956) 181.
[2]) J. Marshall, Phys. Rev. **86** (1952) 685.
[3]) J. V. Jelley, A.E.R.E. (Harwell, U.K.) NP/R. 1770 (1955).
[4]) I. A. Getting, Phys. Rev. **71** (1947) 123.
[5]) R. H. Dicke, Phys. Rev. **71** (1947) 737.

2. Detector Design

2.1. GENERAL

The radiator (perspex) is shaped in the form of a cone, whose semi-apex angle ϕ is equal to $\theta/2$, where θ is the Čerenkov angle for a proton with velocity v (corresponding to the Synchrotron proton energy). For protons with velocity

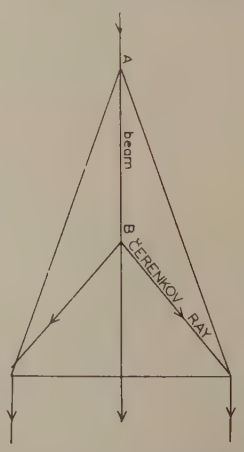

Fig. 1. A cross section of the cone-shaped radiator. Čerenkov rays from the right-energy proton travelling along the axis emerge out parallel to it.

"v" travelling along the axis the Čerenkov rays will emerge parallel to the axis (fig. 1). These may be brought to a point focus by a convex lens. For protons with velocities greater or less than "v", the Čerenkov rays come to a ring focus (fig. 4). For off-axis protons either parallel or at an angle to the axis the Čerenkov rays come to a disc-focus. Thus a small aperture placed at the focus of the lens can isolate the Čerenkov rays from on-axis and right energy protons from those off-axis and wrong-energy protons. The cone-shaped radiator thus provides a very simple velocity (i.e. energy) and direction selective device.

A photomultiplier was used for detecting the Čerenkov light. The output pulses from the photomultiplier were integrated by an RC network (see fig. 3) whose time constant was much shorter than the repetition rate of the Synchrotron pulse (10 sec) but much longer than the pulse duration ($\approx$ 10 msec), and the integrated pulse was displayed on an oscilloscope screen where it was photographed. The height (or more accurately the area) of the integrated pulse gave a measure of the Čerenkov light incident on the photomultiplier and thus a measure of the number of protons with the right energy and direction for the cone.

The cone, as it is, selects a single energy. To explore a range of energies, cones with effectively different angles are necessary. This was

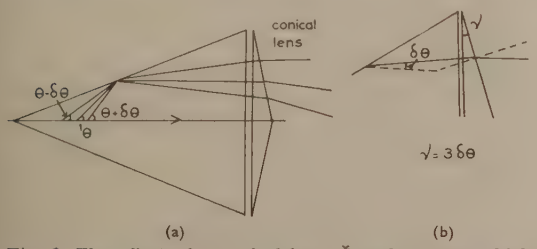

Fig. 2. The effect of a conical lens. Čerenkov rays which make an angle (θ — $\delta\theta$) with the axis (a) finally emerges parallel to it. The relation between $\delta\theta$ and (the angle of the conical lens) is shown in (b).

achieved by placing conical lenses behind the cone so that the value of θ for which the Čerenkov-rays emerged parallel to the axis was altered (fig. 2). By using both convex and concave lenses the system was made to select a range of energies. The design of the whole detector is shown in fig. 3. A frontsurfaced plane

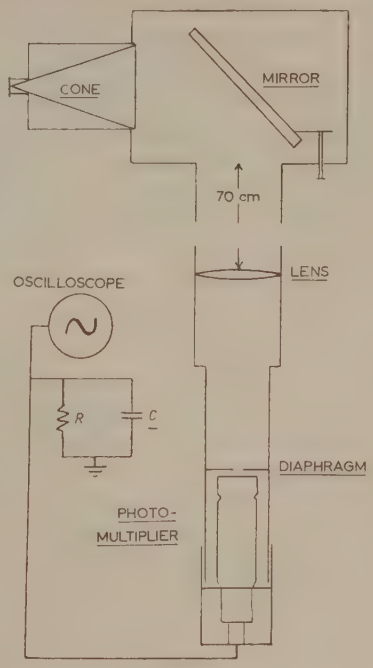

Fig. 3. The detector, the integrating circuit (RC) and oscilloscope.

mirror was placed at 45° to the axis of the cone in order to deflect the Čerenkov rays through 90°. A convex lens was placed at a distance 70 cm from the mirror. A circular aperture diaphragm was placed at the focus of the lens and a photomultiplier placed behind the diaphragm. The 90° deviation of the Čerenkov rays enabled the lens and the photomultiplier to be kept away from the main beam of protons, thus minimising the background counts due to Čerenkov rays produced in the lens and the glass envelope of the photomultiplier, and also those due to secondary emission in the photocathode. The distance of 70 cm of the lens from the mirror was determined by the minimum distance from the synchrotron at which the function of the photomultiplier (heavily shielded) was not seriously disturbed by the magnetic field of the machine. The whole apparatus, from the cone to the

photomultiplier, was enclosed in a light-tight chamber.

2.2. THE CONE AND THE CONICAL LENSES

In view of the desirability (a) of high refractive index for better light yield, (b) good transmission characteristics, (c) easy machining and (d) low Z (to minimise multiple scattering of the proton), Perspex (rfr. index = 1.5) was chosen as the most suitable material. For 950 MeV protons θ in Perspex = 39°48′ i.e. the semi-apex angle of the cone should be

$$\phi = \frac{\theta}{2} = 19°54'.$$

The cone was designed with a base diameter of 10 cm for which the effective path length (AB in fig. 1) is 7.8 cm. For this path length the effects of slowing down and magnetic bending of the proton beam are very small and the Coulomb scattering does not affect the resolution more than other unavoidable factors.

The conical lenses, with one side plane and the other side conical (convex or concave) and having the same diameter as the cone-base, were also made of Perspex. Six such lenses, three convex and three concave, gave a range from 750 to 1100 MeV in steps of about 70 MeV.

2.3. THE LIGHT DETECTOR AND ELECTRONICS

The number of photons emitted by Čerenkov process is given by[6]):

$$N = \frac{2\pi Le^2}{137}\left[\frac{1}{\lambda_1} - \frac{1}{\lambda_2}\right]\left(1 - \frac{1}{\beta^2 n^2}\right)$$

where e = charge of the particle in units of electronic charge

L = path length

$\beta = \dfrac{\text{velocity of the particle}}{\text{velocity of light}}$

n = refr. index of the radiator

λ_1 and λ_2 are the two limits of wavelength.

[6]) I. Frank and I. G. Tamm, C. R. Acad. Sci. U.S.S.R., 14 (1937) 109.

In the present case $e = 1$, $L = 7.8$ cm, $\beta = 0.8679$, $n = 1.5$. The light detector was an E.M.I. 6260 type photomultiplier
for which $\lambda_1 = 3500$ A.U.
$\lambda_2 = 5500$ A.U.
so that $N = 1500$.

We now calculate the expected pulse height of the integrated pulse. As we shall see in the next section, the light acceptance drops down rapidly as the particle distance "d" from the axis increases and for particles further than 0.5 cm the acceptance is negligible. Over a circle of 0.5 cm radius with the axis as the centre the overall acceptance is $\approx 16\%$. Taking the proton flux in the beam = 10^5 protons/cm^2 the total number of photons incident on the photocathode of the photomultiplier (assuming a light loss of a factor of 2 in the optical system) is $\approx 10^7$. Taking the photocathode emission to be 10% (10 electrons for 100 photons) and an overall gain of the photomultiplier = 10^6 we get a total charge at the collector of the photomultiplier $Q = 1.6 \times 10^{-7}$ Coulomb. This charges the capacitance 0.02 μF (in the RC integrating network) to a potential difference of 8 volts, which is approximately the final pulse height.

3. Theoretical Performance

The general performance of the cone-detector depends on its response to particles which are not in the ideal condition. By ideal condition we mean the protons travelling along the axis of the cone with the right energy to produce Čerenkov light which will be brought to a point focus. For particles with either a different energy or direction, the point-focus condition will not hold. We shall consider these deviations, one parameter at a time.

3.1. PARTICLES WITH THE WRONG ENERGY BUT TRAVELLING ALONG THE AXIS

In such conditions the Čerenkov angle will be different from θ. Let us denote this difference by $\delta\theta$, so that for a particle of higher energy the Čerenkov angle will be $(\theta + \delta\theta)$. The reflection from the side of the cone will not alter this angular deviation but on emergence from the

base of the cone the ray (fig. 4a) will be refracted and outside the cone the ray will be at an angle $n\delta\theta$ (assuming $\delta\theta$ to be small) to the axis.

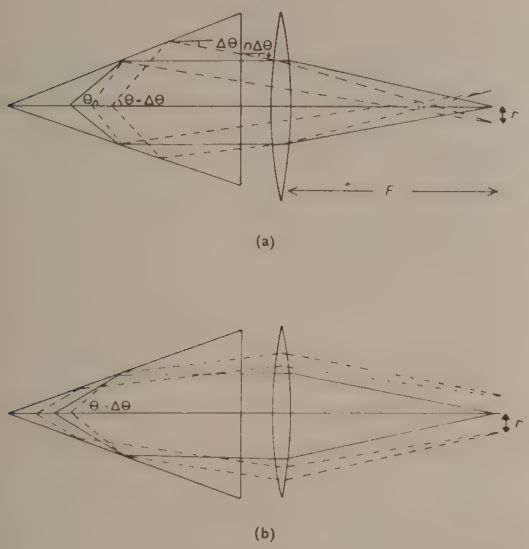

Fig. 4. The Čerenkov rays from protons with too high (a) or too low (b) energy.

Assuming that there is no change in the direction or the velocity of the proton during its passage through the cone, the Čerenkov rays will come to a sharp ring focus whose radius is given by

$$r = Fn\,\delta\theta \quad \text{where } F = \text{focal length of the lens.}$$

Similarly, taking the case of a proton of lower energy other conditions remaining the same, the Čerenkov rays come to a ring focus of radius given by the same relation (fig. 4b). Thus for protons with θ equal in magnitude but not in sign, the focussed rings of Čerenkov rays overlap but these overlapping images are widely separated by the conical lenses. Because, if, say a concave and conical lens brings the Čerenkov rays with angles $\theta + \delta\theta$ to a point focus (these would be focussed in a ring with a radius without conical lens) it would at the same time deviate the Čerenkov rays with angles $\theta - \delta\theta$ and these will be focussed in a ring with radius $2r$.

3.2. PROTONS WITH RIGHT ENERGY TRAVELLING PARALLEL TO THE AXIS BUT DISPLACED FROM IT

For such protons all the Čerenkov rays do not emerge from the cone parallel to the axis. In fact only the rays in the plane containing the proton track and the axis of the cone come out parallel to the axis. Other rays are deviated from the parallel, the degree increasing with the deviation of the ray from the above mentioned plane. Thus a fraction of the rays is lost, being either missed by the lens or cut off by the diaphragm. The fraction of the Čerenkov light reaching the photocathode from such particles was calculated, by actually determining the fraction of light reaching the photocathode reflected from consecutive sections of the cone and then taking the average. The calculation was made for three different apertures of the diaphragm corresponding to angular acceptance of $\frac{1}{2}°$, 1° and 2° for particles up to a distance of 1 cm from the axis beyond which the acceptance is found to be negligibly small.

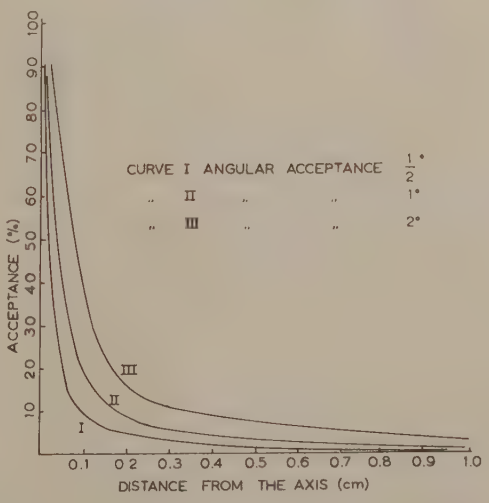
CURVE I ANGULAR ACCEPTANCE ½°
" II " " 1°
" III " " 2°
ACCEPTANCE (%)
10 20 30 40 50 60 70 80 90 100
I
II
III
0.1 0.2 0.3 0.4 0.5 0.6 0.7 0.8 0.9 1.0
DISTANCE FROM THE AXIS (cm)

Fig. 5. Shows how the Čerenkov light reaching the photomultiplier (shown as % acceptance) falls off rapidly as the distance of the proton from the axis increases. I, II and III are for three diaphragm apertures corresponding to $\frac{1}{2}°$, 1° and 2° angular acceptance.

The percentage of acceptances for particles at different distances from the axis and for different

aperture settings are shown in fig. 5. This effect reduces the effective beam width to about 2 mm.

3.3. OFF ANGLE PARTICLES

For a proton with right energy travelling along the axis, the Čerenkov rays emerge from the cone in a solid cylinder of parallel rays. If the path of the proton makes an angle θ with the axis and also crosses the axis at the mid-point of its effective length (fig. 6a) there will be light loss due to (a) deviation by the angle θ of the emergent beam and (b) due to the off-axis position of the proton. The fractional light loss F due to (a) is given by (see fig. 6b),

$$F = \frac{2L\theta}{r},$$

where r = radius of the lens

L = distance of lens from cone vase.

The fractional light loss due to (b) is given by "f" where "f" is the fractional light loss of the particle at average distance "d" ($= \frac{1}{2}\,\mathrm{PP'}$ — fig. 6c) from the axis (see fig. 5).

The overall fractional light loss $= F \times f$.

tribution to the resolution in the present case is given in table 1 for a path length of 7.8 cm, an effective beam width of 2 mm (section 2b) and a beam divergence of $\pm$ 1°.

TABLE 1

Factors affecting resolution	Estimate
Finite beam width (2 mm)	± 6.4%
Angular spread among the protons in the beam (± 1°)	± 9.6%
Curvature of the beam (due to fringing field of the synchrotron magnet)	± 3%
Multiple Coulomb scattering	± 3.4%
Slowing down of the protons in the detector	± 0.7%
Dispersion	± 2%
Overall resolution	± 12.6%

4. Results and Discussion

Two sets of observation were performed to test (a) the direction selectivity and (b) the energy selectivity of the detector.

The 5° scattered beam from the synchrotron

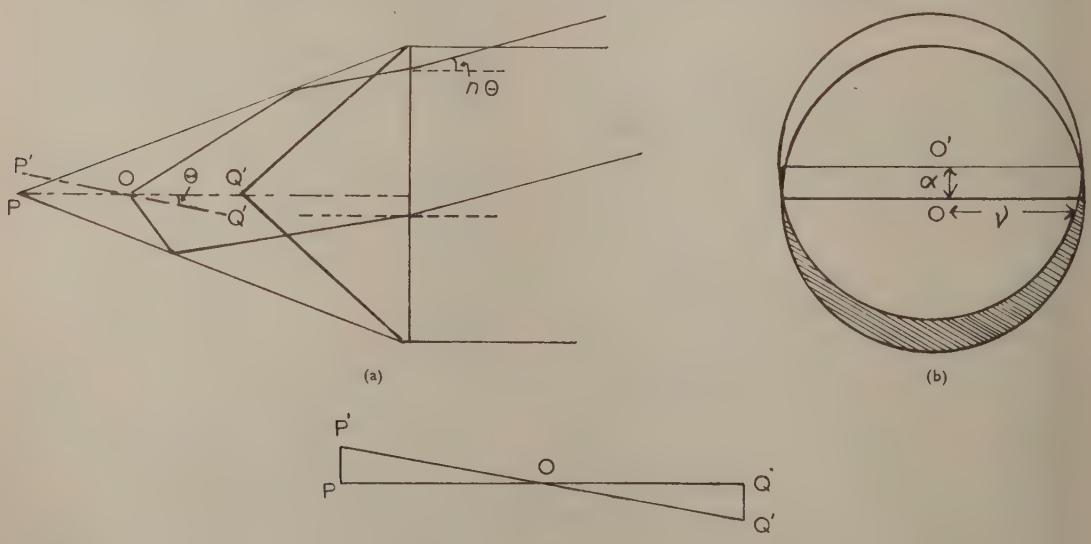

Fig. 6. Loss of Čerenkov light from a proton travelling at an angle to the axis of the cone.

3.4. OVERALL RESOLUTION OF THE DETECTOR

The factors that affect the resolution of the detector are discussed by Jelley[3]) and their con-

target was collimated at a distance of about 4 metres from the target. The beam came to a horizontal line focus due to the fringing field

of the magnet a few centimetres after the collimator and the cone was placed so that the centre of its effective path length was at the focus. At the focus the beam had a vertical width of 1 cm, and a horizontal width of 4 cm. The angular spread was of the order of $\pm$ 1°. The axis of the cone was roughly made to coincide with the direction of the beam. The integrated pulse was recorded photographically. The whole apparatus was rotated around a vertical axis passing through the effective centre of the cone, in steps of 1° and the result is shown in fig. 7.

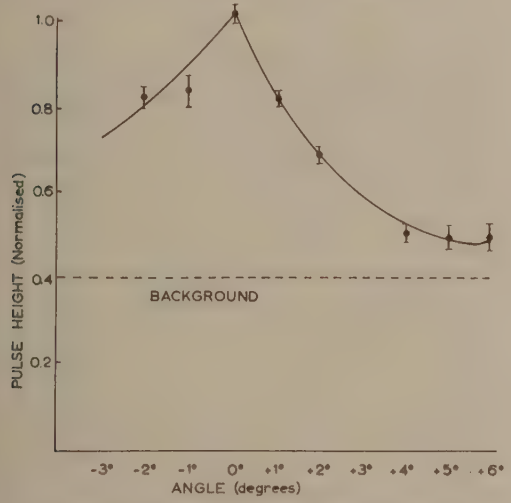

Fig. 7. Direction selectivity of the detector.

For the energy selection test the apparatus was kept fixed at the optimum position found from the direction selective curve. Different conical lenses were inserted behind the cone and the result is shown in fig. 8. The resolution as shown in fig. 8 is $\pm$ 13.2% which is very close to the 12.6% resolution predicted theoretically.

As maybe seen from the calculation of the light acceptance of the off-axis particles, a very small percentage of the total Čerenkov light produced is effective, even for a small angular or lateral displacement of the particle from the axis. This characteristic of the cone reduces its utility as a single particle counter. This may

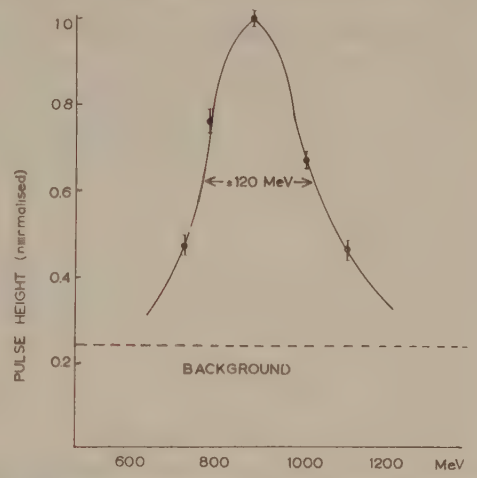

Fig. 8. The energy selectivity of the detector. Response to 950 MeV protons of detector when adjusted for proton energies from 750 to 1100 MeV.

partially explain the failure of Dicke[5]) to detect Čerenkov radiation from cosmic ray particles.

On the other hand the virtual rejection of the Čerenkov rays from the off-axis particles make the cone self-collimating and it would be very useful in experiments where a good degree of energy and direction selection is necessary. It should be noted that the major fraction of the total resolution in this apparatus is due to the width and divergence of the beam. With a better beam condition the resolution of the detector could be brought down to about $\pm$ 6%.

Acknowledgements

The author wishes to express his thanks and gratitude to Dr. G. W. Hutchinson, Professor W. E. Burcham and Dr. J. V. Jelley for many helpful discussions and criticism. The author is also grateful to the East Pakistan Government for the award of a Graduate Research Scholarship.

NUCLEAR INSTRUMENTS 2 (1958) 348–360; NORTH-HOLLAND PUBLISHING CO. – AMSTERDAM

MAGNETIC-MEMORY SCALING-SYSTEM WITH MAGNETIC COUNT INDICATION

E. FRANKLIN and J. B. JAMES

Atomic Energy Research Establishment, Harwell, Didcot, Berks

Received 7 December 1957

Circuits are described which have many advantages over those at present being used in scaling equipment. Principally they make possible the desing of scaling equipment which is small, light, cool running, of low power consumption, and very reliable.

1. Introduction

The development of magnetic materials with rectangular hysteresis loops, i.e. high remanence, sharp saturation and well defined magnetising force, has introduced the possibility of employing magnetic cores as bistable elements in the performance of logical functions and the storage of information. Many such cores are now employed in place of other bistable elements such as valve flip-flops, etc., in electronic computers, data handling equipment etc.. The two stable states generally employed are the states of magnetic remanence existing after saturation in either of two directions, though in a few cases intermediate states are used to give a multi-stable element.

Such bistable elements have many advantages over types previously available. The energy required to change the stored information is small, and no energy is consumed in retaining it, since it is stored in the form of remanent magnetic flux. This results in great power economy and also gives the useful feature that the information can be retained even when the equipment is switched off. Further advantages are small size and high reliability of the bistable elements. This paper describes the application of such elements to electronic scaling of random pulses.

It is possible to use a single rectangular loop core as a decade counting device[1]), by arranging for each incoming pulse to change the flux level of the core by a tenth of the total flux change. The core saturates after ten pulses, when the circuit then passes on a pulse to the next counting core and resets the first core so that it starts again on the eleventh pulse. To use the core in this manner does however call for close tolerances and therefore introduces a measure of unreliability. It is preferable, therefore to use circuits employing the cores only as two-state elements. A scale-of-ten may then consist of a ring of ten magnetic cores in which the polarities of the remanent flux of nine are all the same, while that of the tenth is reversed. The coupling circuits between the cores are such that, on the application of a driving pulse (a pulse to be counted) the pattern of polarities moves round the ring by one core position. A pulse is passed to the next scale-of-ten on each passage of the pattern through one particular position. A number of circuits capable of bringing about this progression of the pattern of polarities have been described in connection with shifting registers for electronic computers[2,3,4,7]).

The current pulses to operate the scale-of-ten

[1]) G. F. Pittman, A.I.E.E., Pt. 1 (Communications and Electronics), Vol. **74**, No. 17 (1955) pp. 54–58.

[2]) An Wang, Proc. I.R.E., Vol. **39**, No. 4, pp. 401–407.

[3]) R. D. Kodis, S. Ruhman and W. D. Woo, I.R.E. Convention on Computors (1953) Paper No. 7.

[4]) D. Loev, W. Miehle, J. Paivinen and J. Wylen, Proc. I.R.E., Vol. **44**, No. 2 (1956) pp. 154–162.

[5]) G. H. Perry, G. R. Hoffman and E. W. Shallow, Proc. I.E.E., Part B Supplement B, Vol. **103**, No. 3 (1956) pp. 412–417.

[6]) R. P. Mayer, Engineering Note E-472, Digital Computor, Lab. Mass. Inst. Tech. (August, 1952).

[7]) M. Karnaugh, Proc. I.R.E., Vol. **43**, No. 5 (1955) pp. 570–584.

circuit can most conveniently be obtained from a transistor circuit and this influences the choice of scaling circuit. In general it is an advantage to use a circuit which only requires that the amplitude and duration of the current pulses be above a certain minimum value rather than that they be fixed between limits. Circuits have been described[5]) using one transistor for each magnetic core but these have been rejected due to the relatively high cost of transistors.

As a result of the non-power consuming nature of the information storage, it is difficult to obtain an indication of the state of the cores, and therefore of the number of pulses received, by the usual arrangement of indicator lamps. etc., without considerable complication of the electronic circuits. However an indicator has been developed in which the currents flowing in the scaling circuit magnetise thin strips of nickel-iron mounted around an astatic pair of compass needles, the needles being attracted by the one strip magnetised one way and repelled by the other nine magnetised oppositely.

2. Switching of Rectangular Hysteresis Loop Cores

Fig. 1 shows a typical rectangular hysteresis loop together with the waveforms that result on the application of both current and voltage pulses to a winding on a core with such a loop. A current pulse, as in fig. 1 (ii) of sufficient magnitude, results in the voltage waveform (a) if the core is taken from remanence in one direction to saturation in the other, i.e. $-B_r$ to $+B_s$ and a much smaller voltage waveform (b) if taken from remanence to saturation in the same direction. The area of the voltage to time waveform is given by the expression:

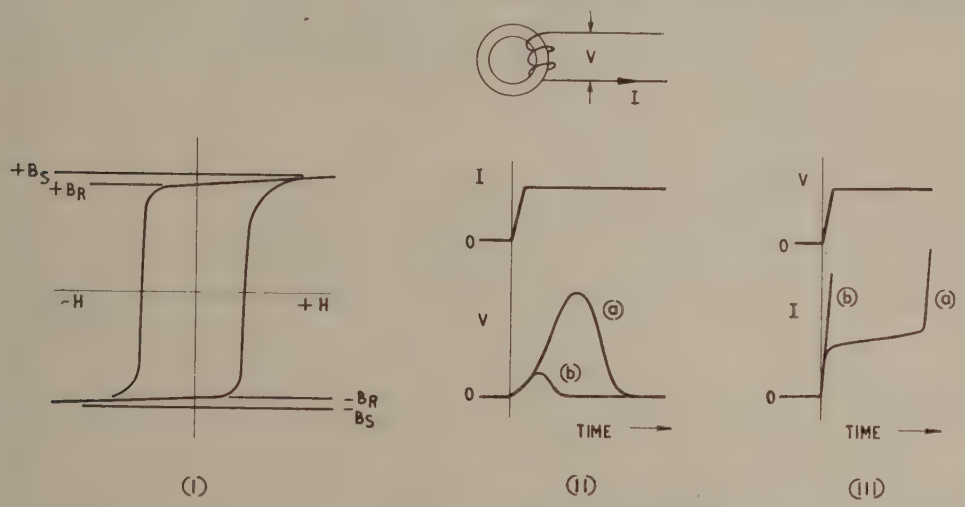

Fig. 1. Waveforms obtained with rectangular loop cores.

$$Vt = B\,N\,A\,10^{-8} \qquad (1)$$

where V = mean voltage
t = duration of switching time
B = change of flux density in gauss
A = area of core
N = number of turns.

In switching a given core from $-B_r$ to $+B_s$ or $+B_r$ to $-B_s$ (1) can be reduced to

$$\frac{Vt}{N} = k \qquad (2)$$

where k is a constant for the particular core.

If a voltage pulse is applied to the core and, as in fig. 1 (iii) (b), tends to magnetise the core in the direction in which it is already magnetised, then the current rapidly rises to a value limited only by the resistance of the winding. If,

on the other hand, the applied pulse drives the core in a direction opposite to that in which it is already magnetised, then waveform (a) results. Here the current is limited to the value fixed by the rate at which the core is being switched until the product of applied voltage and elapsed time reaches a value corresponding to the flux change necessary to saturate the core. The current then rises to a value limited by the circuit resistance.

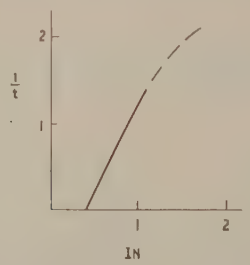

Fig. 2. Magnetisation reversal time as a function of applied ampere turns.

The D.C. magnetising force required to change the flux level of the core from remanence in one direction to saturation in the other direction corresponds approximately to the coercive force of the material. Under pulse conditions the magnetising force required is larger and is related to the switching time. If the ampere turns (IN) required to switch a particular core from remanence in one direction to saturation in the other are plotted against the reciprocal of the switching time ($1/t$), then a graph as in fig. 2 results.

Below a certain value of ampere turns (slightly larger than that corresponding to the coercive force of the material) no switching action takes place and above this value the switching speed is proportional to the increase of IN, except at very high values. This proportionality extends, in the case of the 2 mm ferrite core type FX1508, at least up to the value of IN necessary to switch the core in 0.5 microseconds, and, therefore, over the whole range in which the core would be used normally. Thus, we have

$$\frac{1}{t} = (IN - a)b \qquad (3)$$

where a and b are constants for a particular core.

(2) and (3) may be combined to give the following relationship between the mean voltage and current, independent of switching time.

$$V = (IN - a)Nbk\,. \qquad (4)$$

In using these expressions it must be remembered that the voltage waveform can be as in fig. 1 (ii) with a peak value as high as twice the mean value (V).

Measurements made on the 2 mm ferrite core type FX 1508, which is used in the circuits to be described, gave the following values for the constants when t was in microseconds.

$$a = 0.4$$
$$b = 2$$
$$k = 0.09\,.$$

3. Circuit Symbols for Magnetic Circuits

The representations of magnetic circuits of this type can be made easier by using a convention proposed by Mayer[6]) and Karnaugh[7]). Fig. 3 shows an example.

The vertical line represents the magnetic core and the horizontal lines the winding leads. The 45° mirror symbols represent the windings and the directions of their slope shows the phasing

Fig. 3. Example of magnetic circuit notation.

of these windings. By reflecting the current in the mirror symbol, the direction of the field is obtained, and reversing the field and reflecting again in the mirror symbol, gives the induced voltage. The example shows a current I, passing through a 50 turn winding on core 1 and thereby inducing a voltage of the same polarity in a 30 turn winding and of opposite polarity in a 20 turn winding.

4. Choice of Scaling Circuit

There are two main types of magnetic shift register suitable for use as a scaling circuit. In

the first type, the cores are arranged in cascade, and are driven from one current pulse source, the stored information being transferred from the cores to an equal number of capacitors during the drive pulse, and fed back to the cores one step forward at the end of the drive pulse. In the second type of circuit the cores are connected in two lines and the stored information is moved alternately from one set of cores to the other, always in a diagonally forward direction, by applying the drive pulses alternately to each line of cores.

1 (ii) (b)). At the end of the drive pulse, C_0 discharges through R_0 and the winding of core 1, and, in so doing, switches core 1 so that it is magnetised in a direction opposite to that produced by the drive pulse, i.e. it is put into the set condition. The position of the oppositely magnetised core thus progresses one step round the ring of cores for every drive pulse. On reaching core 9, a transformer is required to allow the discharge current of C_0 to set core 0.

This circuit is relatively simple and has the advantage of requiring only a single winding on

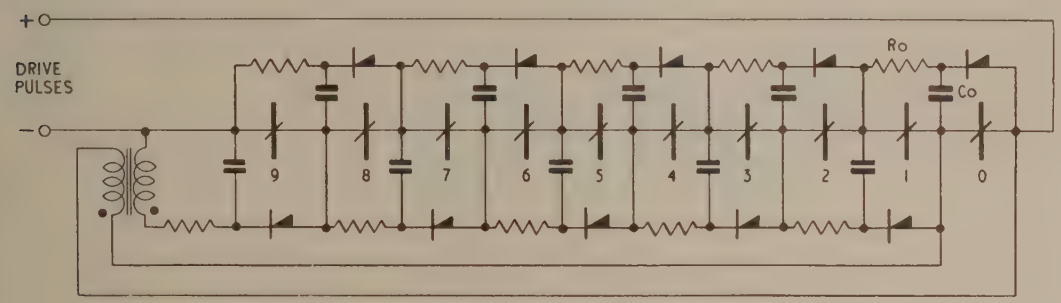

Fig. 4. Magnetic scaling circuit with intermediate condenser storage.

Fig. 4 shows a circuit of the first type in which the cores are wound with only a single winding thus permitting a large gauge of wire to be used and reducing the cost of winding.

In order to simplify descriptions of circuit operation the convention will be adopted of describing the two remanent states of a core as the "set condition" and "unset conditon". The "unset condition" will describe the direction of magnetisation brought about by a drive pulse, while the "set condition" will describe the opposite direction of magnetisation.

Initially cores 1–9 are in the unset condition and core 0 is in the set condition. This is brought about by a switching arrangment not shown in the diagram. The first current pulse to be counted switches core 0 from remanence in one direction to saturation in the other and, in so doing, develops a voltage pulse across the winding which charges the capacitor C_0. The voltage pulses developed across the windings on the other cores are very much smaller (as in fig.

each core. It is, however, inefficient, in that considerably more energy must be supplied during each pulse than is required to switch two cores. This is mainly due to the losses in the resistors, the value of which is arrived at by a compromise. Too low a value causes excessive losses during the charging period, while too high a value causes excessive losses during the discharge period. Also, the rectifiers of this circuit must have low forward resistance and therefore must be of a relatively expensive germanium type.

However, the main disadvantage of this circuit, is that the duration of the drive pulses, which are generally produced by a transistor circuit must be fixed within fairly close limits. Too short a pulse results in the capacitor not receiving its full charge, while if the pulse width is too great, the capacitor is allowed to discharge before it can switch the next core. For a fixed value of pulse current, the pulse width must be maintained to within about $\pm$ 15%. Let us assume that all the input energy goes in charging

the capacitor, i.e. that the proportion used in switching the first core and that lost in the resistor is small. Let us assume that the voltage drop in the diode can be ignored and that the voltage across the core and capacitor rises linearly. Then,

$$\frac{I V_{\max} t}{2} = \frac{C V^2_{\max}}{2}.$$

Substituting $V_{\max} = 2kN/t$ from (2) then

$$t = \sqrt{\frac{2CkN}{I}}.$$

This is only an approximate result, but it shows that the required pulse width (t) is not a constant for a particular circuit, but is related to the magnitude of the current. It is difficult to provide such a current pulse from a transistor circuit, to the accuracy required, without considerable circuit complication or the use of preset controls.

Circuits of the second type, using two sets of cores pulsed alternately, have the advantage that the duration of the current pulses is only required to exceed a certain minimum value, there being no upper limit apart from that set by the mean current rating of the circuit components.

In these two-phase circuits the scaling circuit itself employs only the same total number of cores as the first type, and only one core has the opposite polarity of magnetisation at any one time. However, the drive pulses have to be applied alternately to half the cores, and this necessitates a preceding scale-of-two circuit. Fortunately a combined drive circuit and scale-of-two can be made with only two rectangular loop magnetic cores and two transistors, as shown in fig. 5.

The collector and base windings on each core are so connected as to provide positive feedback from collector to base. If one of the cores is initially magnetised in a direction opposite to that which would result from a flow of collector current, i.e. it is in the set condition, then the application of a trigger pulse, large enough to exceed the constant a of eq. (3) and produce a voltage across the base winding greater than the bias voltage on the emitter, causes collector current to flow. Positive feedback via the core produces a rapid rise of collector current and the transistor bottoms. After the trigger pulse has initiated the action, the transistor remains conducting until the core saturates. Actually, due to hole storage, the transistor remains conducting for slightly longer than the switching time of the core. If the core is not initially magnetised in the right direction, then the trigger

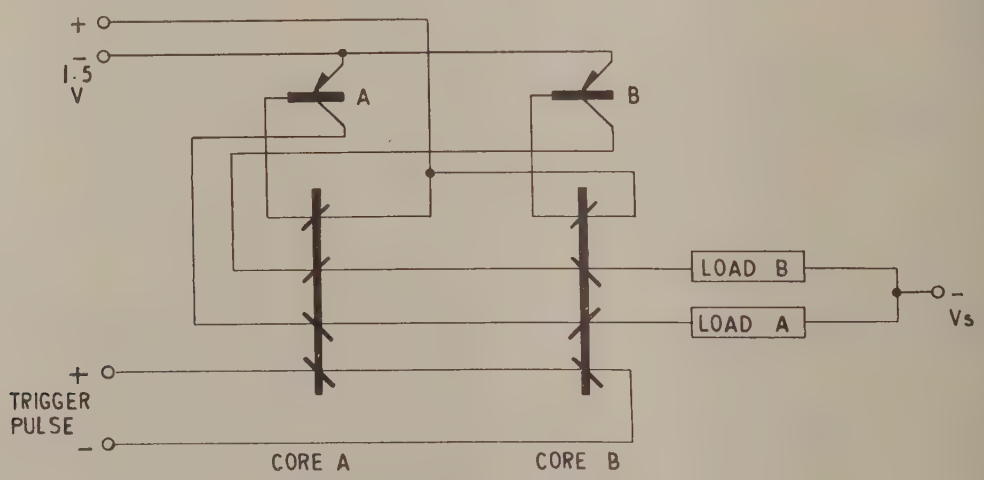

Fig. 5. Combined scale-of-two and drive circuit.

pulse is unable to produce a voltage across the base winding and there is no flow of collector current.

The operation of the circuit therefore commences with say core A magnetised in the direction which allows it to be triggered and with core B magnetised in the opposite direction. (This situation is brought about by a switching arrangement not shown in the diagram.) The first trigger pulse turns on transistor A and a current pulse is passed through load A, which can be a set of cores in a scaling circuit. This current pulse also passes through a winding on core B, such as to reset it into such a state that it can be triggered on by the second trigger pulse. The circuit thus produces alternate drive pulses through loads A and B.

Leaving the detailed design of this drive circuit to be dealt with later, consideration is now given to the type of scaling circuit with which it can be used. The most simple circuit of this type is shown in fig. 6 as a scale of ten.

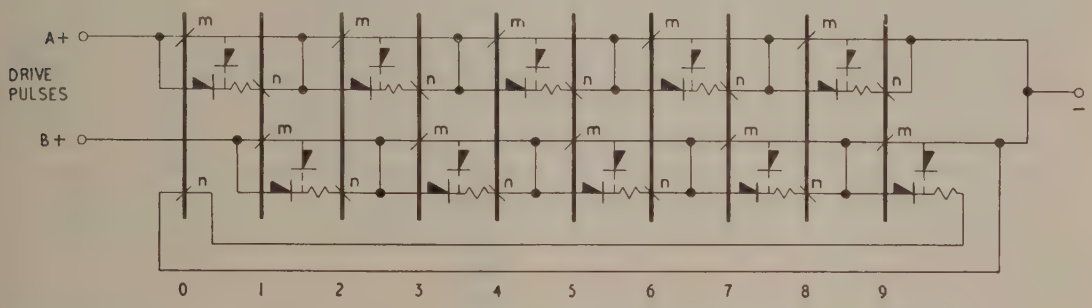

Fig. 6. Magnetic scaling circuit of the two-phase type.

Initially cores 1–9 are in the unset condition, and core 0 is in the set condition. The first drive pulse is applied to the A line and switches core 0. This core is however shunted by a diode, a resistor and a winding on core 1 in series. With suitable values for the components and for the windings, it can be arranged that core 1 is switched to the set condition during the time core 0 is switched to the unset condition. The next drive pulse appears on the B line and so core 2 becomes the oppositely magnetised core. This state of opposite magnetisation therefore progresses around the ring of cores.

The purpose of the series diode is to prevent the core which is being switched to the set condition from being short circuited by the circuit coupling it to the next core, e.g. to prevent current flowing in the circuit between core 1 and 2 when cores 0 and 1 are being switched.

The value of the resistor is made such that the correct proportion of the pulse current passes through the winding n. If the number of turns on the two windings are N_m and N_n and the currents passing through them I_m and I_n, then for the two cores to switch in the same time,

$$I_m N_m = I_n N_n \, .$$

From expression (3), the values of I_m and I_n required to give the desired switching time can be calculated. Then, from eq. (4), the voltages across the m and n windings are, respectively,

$$\begin{aligned} V_m &= (I_m N_m - a)\, N_m bk \\ V_n &= (I_n N_n - a)\, N_n bk \, . \end{aligned} \tag{5}$$

Thus, if R is the total resistance in series with the n winding,

$$I_n R + (I_n N_n - a)\, N_n bk = (I_m N_m - a)\, N_m bk$$

$$\text{or} \qquad R = \frac{\{(I_m N_m - a)\, N_m - (I_n N_n - a)\}\, bk}{I_n} \, . \tag{6}$$

To ensure a margin of safety, R should be made smaller than this value, and thus allow the core which is being driven on its n winding always to complete its switching operation before

the core which is being driven on its m winding does so.

A weakness of this type of circuit is, that when switching say cores 0 and 1, there is a tendency partially to set core 9. It will be noted that the disturbing current which does this flows through the diode in the forward direction. If this is allowed to happen, then the partial set builds up on succeeding drive pulses, until all five cores are set. This can be prevented by making the n winding two-five times smaller than the m winding, thus reducing the voltage applied to the previous m winding through the diode and series resistor and thereby using the non-linearity of the diode's forward characteritsic to greater advantage. There is a threshold voltage below which no set action takes place; this being the voltage across the diode and resistor for the value of current necessary to make the ampere turns on the m winding equal to a in eq: (3). It follows, therefore, that it becomes more difficult to prevent some setting of the previous core when the switching speed is high and the voltages large. Where it is necessary to operate with a switching time smaller than 2 microseconds, in order to secure a resolving time for the counting circuit of this order, it becomes necessary to use the additional parallel diodes, shown with dotted connections in fig. 6, which reduce the fed-back current by about half.

For operation at lower speeds use of the series diode alone is satisfactory and the diode and resistor can then be replaced by a cheaper higher resistance diode — in fact for operation at 3 microseconds or so a type of midget selenium rectifier can be used. This is a rectifier with a forward resistance of about 20 ohms at 100 milliamps and a reverse capacitance of about 0.001 micro-farad at 2 volts.

This circuit does however only operate over a limited range of core switching speeds. The lower limit is fixed by the fact that the value of R required to satisfy eq. (6) becomes less than the lowest value achievable in practice. The upper limit is fixed by the tendency of the circuit to reset the previous core.

If the circuit is driven by the arrangement shown in fig. 5, then the switching speed is controlled by the supply voltage. To secure reliable operation of the scale of ten it becomes necessary to keep the supply voltage to within $\pm$ 10% of a fixed value.

This circuit has a further disadvantage when used with an indicator of the type described below, in that the inclusion of the indicator tends to increase the feed-back difficulties.

There is a further type of scaling circuit[7]), using, as before, alternate drive pulses on two sets of cores, in which any tendency of the driven cores to set the previous one is completely prevented by an arrangement of diodes. This circuit requires three windings on each core and an increase in the total number of turns, but the increased freedom to operate over a wider range of switching speeds and hence supply voltages, together with a simplification of the problems associated with the operation of an indicator, justifies the extra cost in winding the cores.

A scale of ten of this type, together with the drive circuit, is shown in fig. 7. Before counting commences, the reset switch is closed for an instant to bring the circuit to zero. In this condition, cores 1 to 9 are in the unset condition and core 0 in the set condition, while core B is set and core A unset. The first trigger pulse thus turns on transistor B which passes a pulse of current through the l winding of core 0, switching the core into the same state as the others. During switching, a voltage is developed across the m winding of core 0 which applies a forward bias to D_{12} and tends to oppose the forward bias on D_2 provided by the drive circuit. Consequently, the pulse current, after passing through the l windings of the even-numbered cores, returns to the negative line not through D_2, but through the n winding of core 1, the m winding of core 0 and D_{12}. In so doing it sets core 1, so that this core now becomes the one magnetised in the opposite direction to the others. While this is happening, current is prevented from flowing in the circuit coupling cores 1 and 2 by the diode D_3, and in the circuit coupling cores 9 and 0 by D_1. The design of this type of scaling circuit,

together with the drive circuit, will now be considered in further detail.

Consider a single stage of the scaling circuit as shown in fig. 8. R represents the forward

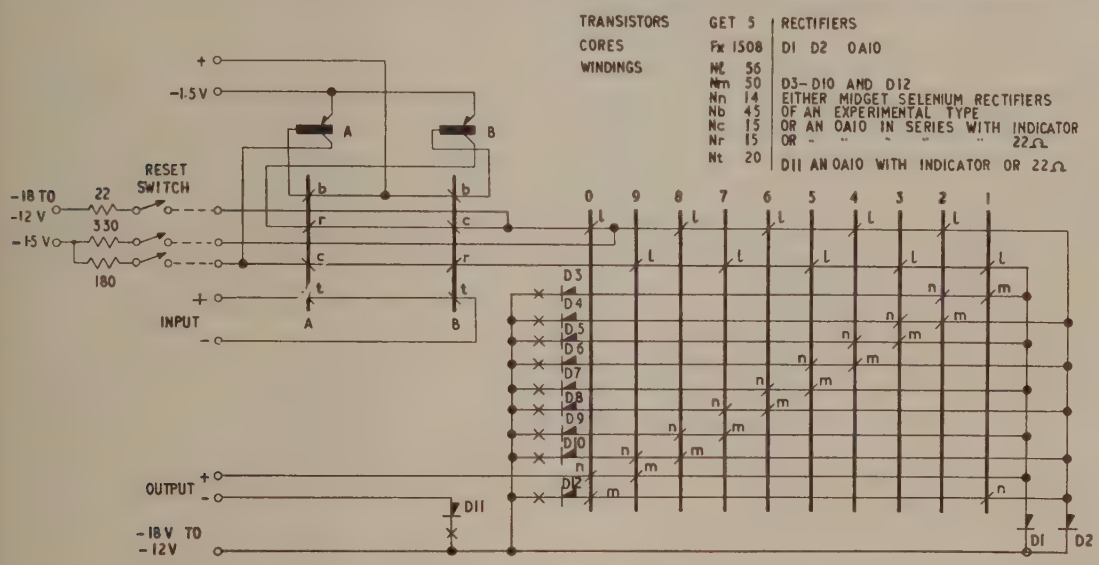

Fig. 7. Improved two-phase circuit.

resistance of the diode plus any additional load, as for example an indicator winding. It is desirable that the loss in D_2, either of current or voltage, be at a minimum and the design is therefore based on the assumption that during the switching operation, I_2 will be equal to I_1 and that the voltage across D_2 will be zero.

The design can commence by fixing the value of N_n in relation to the desired pulse current (I_1), and switching time (t_n) from eq. (3).

$$\frac{1}{t_n} = (I_1 N_n - a)\, b$$

then from eq. (2)

$$V_n = \frac{kN_n}{t_n}$$

and

$$V_m = \frac{kN_m}{t_m}.$$

If $t_n = t_m = t$ then

$$V_m = \frac{kN_m}{t} = \frac{kN_n}{t} + I_1 R\,.$$

Thus

$$N_m = N_n + \frac{I_1 R t}{k}. \qquad (7)$$

This value of N_m can reasonably be increased by a further 50% as a factor of safety to ensure that core 1 always switches before core 0.

The value of N_1 is fixed by consideration of the total ampere turns on core 0 to switch it in time t. As I_2 is assumed to be equal to I_1, the effective ampere turns are equal to I_1 $(N_l - N_m)$.

$$\frac{1}{t} = (I_1 (N_l - N_m) - a)\, b$$

and

$$N_l = N_m + \frac{a}{I_1} + \frac{1}{bt\, I_1}. \qquad (8)$$

It will be seen that if N_l is larger than this, core 0 will be switched faster, by reason of the greater ampere turns, the voltage across m will

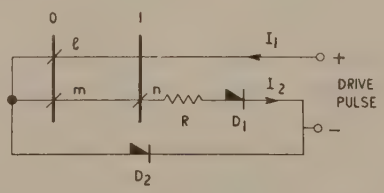

Fig. 8. Single stage of the improved two-phase circuit.

be greater than that across n and R, and the difference will appear as a reverse voltage across D_2. On the other hand, if N_l is too small, I_2

becomes smaller than I_1, the difference passing through D_2, such that the effective ampere turns on core 0 correspond to the same switching time as fixed by the voltage across m, which is the voltage across n and R, less the small voltage across D_2.

The operation of a single stage of the whole circuit, as in fig. 9, is now considered. The scale of ten circuit having been designed for operation at a given speed with a current pulse of magnitude I_1, it follows that the reset windings on cores

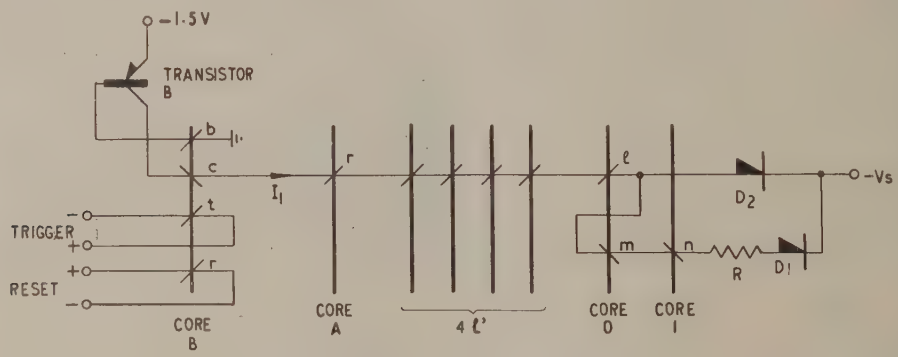

Fig. 9. One phase of a complete decade circuit.

A and B (N_r) should be such that these cores are set in the same time, and thus N_r should be approximately the same value as N_n. $4\,l'$ represents the four cores (Nos. 2, 4 ,6 and 8 in the present example) which are already magnetised in the right direction.

The transistor in this circuit can be regarded as a switch which is normally open, but which, on the application of a trigger pulse, closes to allow a current I_1 to flow and which stays closed for a longer time than is required for the scale of ten circuit to operate. The first requirement of the transistor circuit is thus that it can be triggered into the "on" condition and remain "on" after the trigger pulse has ceased. This means that the voltage across the base winding, V_b, during the time core B is being switched, must produce at least sufficient base current for a collector current equal to I_1 to flow. Since the base is driven very heavily, nearly the whole of the drive voltage is dropped across the extrinsic base resistance, and we therefore have, to a fair degree of accuracy,

$$V_b - 1.5 \geqslant \frac{I_1 r_b}{\alpha'} . \qquad (9)$$

Some allowance must be made, in this value of α', for the fact that the collector current does not rise to its full value immediately. A transistor with a cut-off frequency of about 2 Mc/s is, in any case, necessary to ensure rapid turn on and turn off times, particularly if a short resolving time is required.

Making V_b larger than that given by expression (9), ensures that the base current will be more than enough, and that the transistor will therefore "bottom" with a very small voltage between collector and emitter. This also ensures that there is a sharp triggering action, and the trigger level is then fairly accurately fixed, being just above the value of ampere turns which equals the constant "a" for the particular core.

It is now necessary to make the number of turns on the base winding, b, such that the transistor will remain conducting for the required time. Thus from the eq. (2):

$$N_b = \frac{V_b t_0}{k} .$$

The collector winding c, can then be determined by a consideration of the total ampere turns on core B to switch it in time t_0, i.e.

$$\frac{1}{t_0} = (I_1 N_c - I_b N_b - a)\, b$$

$$N_c = \frac{(1/t_0 b) + I_b N_b + a}{I_1} .$$

The supply voltage required to operate the circuit is the sum of the voltages required to switch l, r and c. If the same switching time is assumed then,

$$V_s = \frac{k\,(N_l + N_r + N_c)}{t}\,.$$

In practice the voltage required is slightly greater, due to the nature of the voltage waveforms, the resistance in the circuit and the voltage lost across cores 2, 4 and 6 and 8 (in the present example) at the start of the pulse.

Consider now the sequence of switching in the circuit. The trigger pulse develops a voltage across b, which causes the transistor to conduct and thereafter to be held in the bottomed state by core B. The supply voltage is then shared between N_l, N_r and N_c and the voltage across each determines its switching time. The circuit having been designed so that for the same current, the switching time of the core of c is greater than that for the cores of l or r, it follows that, initially, the collector current is determined mainly by the switching rate of the cores of l and r. After the latter cores have switched, a much larger voltage is available to c, and the collector current rises to a larger value, completing the switching of the core of c very quickly.

Due to hole storage in the transistor, the collector current continues for slightly longer than the switching time of core B. Another effect which must be considered, is that when the collector current does fall to zero, the flux level in the other transistor core which has just been set (core A in the present example), falls from saturation to the remanence level, and in so doing develops a voltage across its base winding which tends to turn on transistor A. The emitter bias voltage must therefore be greater than this voltage and it becomes necessary in fixing the value of V_b, to compromise between the desired sharpness of the trigger action and the tendency to retrigger after setting.

In some designs, particularly when using fast transistors, it may be necessary to reduce the rate of fall of the collector current to prevent the other transistor from triggering. If the base circuit contains only the winding b, then, when the core saturates, the base current reverses and assists in clearing the holes from the base, thus bringing the collector current to zero fairly quickly. If the base current is prevented from reversing by a series diode, then the collector current falls off at a much slower rate. The rate at which the collector current falls off can be set by a parallel resistor across the diode. With transistors type GET 5 in the circuit of fig. 7 this arrangement is not necessary.

It is of interest to consider the range of supply voltage over which this circuit will operate satisfactorily. If the voltage is reduced, the operating speed is reduced and a lower limit is set to this by the fact that in expression (7), I_1R remains approximately the same (due to I_1 tending towards the constant fixed by a in expression (3)), while V_m decreases, so that eventually a state is reached when there is insufficient voltage available for setting to occur via the n winding. On the other hand, if the supply voltage is increased, the increase of I_1 resulting from the increase in operating speed, is slightly less than the increase in V_m and there is no limit from this point of view to the supply voltage at which the circuit will work. The upper limit is normally set by the voltage rating of the transistor.

In a complete scaling equipment the scales of ten, as in fig. 7, are coupled together by connecting the output of the first one to the input of the next. The trigger windings are such that the input ampere turns are about four times the constant "a" for the core. This ensures an adequate margin of safety in triggering and the disturbance passed back to the previous circuit, when the next circuit turns on, is quite small. The trigger pulse must be shorter in duration than the "on" time of the circuit it is triggering in order that the collector current may reset the other core (A or B) in that circuit. This condition is fulfilled in operating one circuit from the previous one, but for the first circuit, it is necessary to provide a trigger pulse of the correct amplitude and duration. An additional magnetic core circuit can be employed for this purpose.

The power required to operate a complete scaling equipment is little more than the power required for the first scale of ten. For the circuit of fig. 7, the standing current due to the I_{co} of the transistors can be ignored and the power required is therefore proportional to the count rate. This is of the order of 3 milli-watts for a count rate of 1000 per second.

The resolving time of this circuit is 3 microseconds and the maximum mean count rate, fixed by the collector current rating of the transistor, is 250 000 counts per second.

It is the transistor which limits the resolving time and the highest mean count rate at which the circuit can work. With faster transistors (cut off frequency 6 Mc/s) a faster turn on action can be obtained and, although the turn off speed has to be limited due to the tendency of the circuit to re-trigger, a resolving time of less than 1.5 microseconds can be obtained. Such transistors do however have low collector voltage and mean current ratings, which seriously limits the mean count rate which they can handle.

Faster transistors have been considered for applications when a high mean count rate is not encountered and tests have been made to determine whether operation with a high pulse current had any adverse effect. Several 0C45 transistors with a peak collector current rathing of 10 mA, have been running on a life test for over 5 months producing 2 microsecond wide collector current pulses of between 300 and 600 mA, at the rate of 500 per second. There has been no change in their characteristics and it does appear that they can safely be used in this way provided that the mean current and power ratings are not exceeded.

5. Magnetic Indicator

For some applications of these counting circuits, a visual indication of the number counted is not required. It may, for instance, be sufficient for the circuit to stop some timing device on reaching a given number of counts. Alternatively, the number counted may be read out electrically into another store, or printing device, for example by counting the pulses required to bring each scale of ten individually to zero. However, it is frequently necessary to provide a visual indication of the number counted. This calls for a simple method of showing which core in the ring has the reversed polarity of magnetisation.

The mechanical arrangement of the method adopted is shown in fig. 10. A balanced pair of compass needles, rigidly connected with like

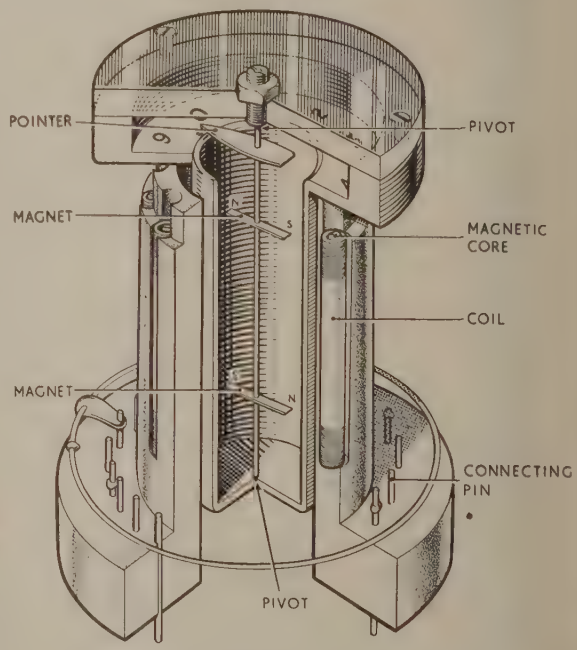

Fig. 10. Arrangement of magnetic indicator.

poles pointing in opposite directions, is pivoted at the centre of a circle of ten thin strips of nickel iron, each of which is wound with three windings. The compass needles are balanced to nullify the effect of the earth's magnetic field. By making the nickel-iron strips long and thin, it is possible to obtain a high remanence using magnetic material with a reasonably low coercive force. These strips can be magnetised by the pulse currents in the scaling circuit, so that one strip is magnetised in the opposite direction to the other nine in correspondence with the polarities of magnetisation of the cores of the scaling circuit. One end of the compass needles

is then attracted to the oppositely magnetised strip and repelled by the others. As counts are registered, the position of opposite magnetisation moves round the ring as in the scaling circuit and, with a suitable pointer and dial, the number of counts can be read. Such an indicator will not follow a fast count rate, but this is not important, as the reading takes place after counting has ceased and the fact that the circuits are counting would be shown by the indicators in the later stages.

The circuit can be arranged so that more than one strip is magnetised in the reverse direction

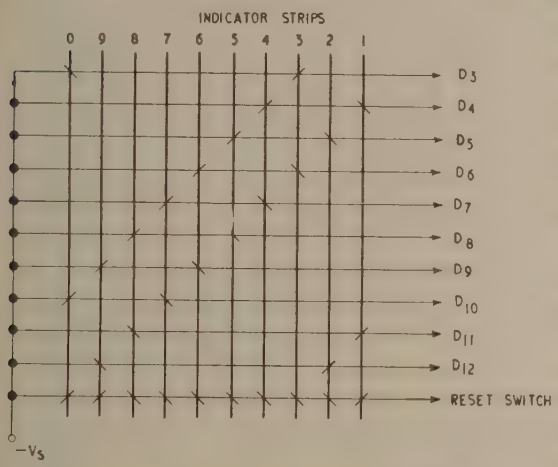

Fig. 11. Connections of the coils of the indicator.

to the others and this has the advantage of increasing the torque acting on the compass needles and spreading the field pattern. The diagram of fig. 11 shows the circuit arrangement for a pattern of three strips magnetised one way and seven the other.

Two of the windings on each strip are connected between the diodes D_3–D_{12} of fig. 7 and the negative supply lead, and the third winding is used to reset the indicator at the start of a new count. The circuit arrangement is such that the action of resetting magnetises strips 9, 0 and 1 to attract the pointer end of the compass system and magnetises strips 2, 3, 4, 5, 6, 7 and 8 in the opposite direction. The pointer therefore points to strip 0. The first pulse to be registered by the counting circuit causes a current to flow through D_{12}, and thus magnetises strip 2 positively and strip 9 negatively, with the result that strips 0, 1 and 2 attract and the pointer moves to strip 1. The field pattern thus progresses one step round the ring for each pulse counted.

The energy available from the counting circuit is small and the indicator must be designed to make the most of the available energy. The indicator strips must therefore be made from a rectangular hysteresis loop magnetic material to secure a high ratio of remanence to saturation flux and, as the time available for magnetisation is only of the order of one microsecond, the material used must be capable of switching at this speed without requiring an excessive magnetising force. A material which fulfils these requirements has been produced by the Post Office Research Station[8]) with a composition of 80 Ni, Mo, 8 Fe, and in a thickness of 0.0005″.

The coercive force of the material must be large enough to withstand the magnetic field of the compass system and also such that the self demagnetising effect of the strip is small for a strip of adequate dimensions. With normal annealing to about 1050° C the 80/12/8 alloy has a coercive force of only about 0.03 oersted, but a much higher coercive force can be obtained, without serious detriment to the other magnetic properties, by annealing at much lower temperatures. A suitable value of coercive force was found to be about 1.5 oersteds, which was obtainable by annealing at a temperature of 430° C. The magnetising force to switch it in 1 microsecond was then about 2.2 oersteds.

The behaviour of this metal has not been fully investigated but, on annealing at higher temperatures, the tendency is for the D.C. coercive force to decrease to a much greater extent than does the magnetising force to switch in 1 microsecond. Thus while it is desirable, from the circuit point of view, to make the required magnetising force as small as possible, this can only be achieved at the expense of a

[8]) U. K. Provisional Patent No. 477/1957, Post Office Research Station.

much greater tendency of the strips towards self demagnetisation.

The demagnetising field (H_D) which the strip exerts upon itself is given by,

$$H_D = \frac{N}{4\pi} B_R$$

where B_R is the flux density at remanence and $N/4\pi$ is a factor related to the dimensions of the strip.

The value of B_R for the metal used is approximately 1200 gauss and taking the maximum value of H_D as 0.75 oersteds (half the coercive force) this gives the maximum value of $N/4\pi$ as 6.75×10^{-4}. The relationship of $N/4\pi$ to the dimensions has been measured for cylindrical shapes[9]) and a value of $N/4\pi = 6.75 \times 10^{-4}$ corresponds to a diameter to length ratio of 1/90.

The length of the indicator strips must be such that the two ends of the strips do not interact appreciably when attracting the magnet system from the furthest distance and also such as to permit a resonable cross-sectional area of metal to be used. In the present design, this dimension has been fixed at 1 inch. The number of turns required on the indicator coils is thus determined by the required magnetising force of 3 oersteds, the length of 1 inch and the current I_1 in the circuit. Allowing a factor of safety, a 50 turn winding has been used.

The cross sectional area of the indicator strips can now be determined by consideration of the maximum voltage which can be developed across the indicator coils without disturbing the operation of the counting circuit, provided the ratio of mean diameter to the length of the strip does not exceed 1/90. Satisfactory operation of the indicator and the counting circuit has been achieved using strips $1/8'' \times 0.0005'' \times 1''$.

The magnets used to form the moving system were $1/2'' \times 1/8''$, pointed at the ends to reduce the moment of inertia of the moving system and were made from 0.002" thick Cunife.

[9]) R. M. Bozorth, Ferromagnetism, Bell Laboratories (Series, Van Nostrand, 1955).

The indicator can be affected by the presence of strong external magnetic fields and, in a complete scaling equipment, the indicators would be housed in a magnetically screened compartment.

The development of this indicator for use with a counting circuit employing ferrite ring cores has led to the use of thin strips of rectangular hysteresis loop magnetic material. These strips in themselves have the right sort of characteristics for use as memory elements in the counting circuit, and it might be possible with further development therefore to eliminate the need for the separate ferrite cores. In addition to this economy a further probable saving in cost would arise from the fact that it would almost certainly be possible to use low-cost selenium rectifiers in positions D_3 to D_{12}. The elimination of the ferrite cores would probably also allow a reduction in the resolution time of the circuit.

6. Conclusion

The circuits which have been described have many advantages over those at present being used in scaling equipment. Principally they make possible the design of scaling equipment which is small, light, cool running, of low power consumption, and very reliable. As compared with scaling circuits using only transistors, these magnetic circuits should prove appreciably cheaper, even when employing an indicator.

The circuits themselves are mechanically extremely rugged. The indicator, having a moving system supported on pivots, is more subject to damage by mechanical shock, but should be at least as robust as the 0–50 microamperemeter, which has been used extensively in portable radiation monitoring equipment subject to rough handling[11,12]).

[10]) J. A. Rajchman and H. P. Crane, I.R.E. Transactions on Electronic Computers.

[11]) E. Franklin and J. B. James, Proc. I.E.E., Vol. **103**, Pt. B, No. 10, pp. (1956) 497–504.

[12]) E. Franklin and J. Hardwick, Journ. Brit. I.R.E., Vol. II, No. 10 (1951) pp. 417–434.

NUCLEAR INSTRUMENTS 2 (1958) 361–362; NORTH-HOLLAND PUBLISHING CO. – AMSTERDAM

LETTER TO THE EDITOR

THIN CARBON FILMS FOR USE WITH ELECTROSTATIC ACCELERATORS

N. SARMA

Atomic Energy Establishment, Trombay, India

Received 20 December 1957

The study of the properties and uses of thin films has become increasingly important in recent years. Most precision experiments in nuclear physics use them either as targets or as target backings. Electron microscopy and electron diffraction experiments employ thin films either as specimen supports or as targets in replica work; for this purpose organic films such as formvar or collodion are generally employed but these films usually disintegrate when bombarded with high beam currents. Furthermore, the structural inhomogeneity of organic films shows up in high resolution electron microscopes. A support film must therefore be amorphous or have an easily recognisable structure.

Films of carbon are very stable under electron or nuclear bombardment. Their crystal structure seems to consist of randomly oriented graphite lamellae. Such films of carbon have been used by Bradley[1]) in support film and replica work and the average thickness of the films has been measured and correlated with their optical transmission by Cosslett[2]). Applications have also been found in nuclear physics for such films by Dearnaley in the Cavendish laboratory and by Holmgren *et al.* at Los Alamos.

This report describes the preparation of the very thin films of carbon used as targets in a nuclear physics experiment by Sarma *et al.*[3]).

[1]) D. E. Bradley, Brit. J. Appl. Phys. **5** (1954) 65.

[2]) A. Cosslett and V. E. Cosslett, Brit. J. Appl. Phys. **8** (1957) 374.

[3]) N. Sarma, M. Govindjee and H. R. Allan, Proc. Phys. Soc. A **70** (1957) 68.

Preparation of the films

The films were prepared by an evaporation technique. The vacuum system used for the evaporation was of conventional design. A pyrex glass work chamber of diameter 12 inches was evacuated by a oil diffusion pump backed by a rotary pump. Four heavy current electrodes led into the vacuum in order that two filaments may be heated one after another by an external switching system. Suitable arrangements were made inside the vacuum to hold the microscope slides on to which the carbon was to be deposited. The carbon arc (fig. 1) was similar in design to that used by Bradley. The points of the carbon rods are pressed together by springs; brass current terminals were clamped on to the rods as shown. For evaporation targets, glass microscope slides were cleaned thoroughly and a thin layer of NaCl was evaporated on to them. It was found necessary to use single crystals of NaCl to prevent deposition of large particles on the slide. Without breaking the vacuum, carbon was evaporated on to the NaCl by passing a current of 100 A through the arc for periods of about 10 sec, separated by 30 sec intervals, till a deposit of the required thickness was obtained. The intermittent heating was necessary because heating of the carbon electrodes caused rapid outgassing with consequent rise in pressure in the work chamber.

The coated slide was then removed from the vacuum and was steadily lowered at an angle into a dish of water. The substrate of NaCl dissolved off leaving the carbon film floating on the surface.

Other salt substrates such as KI or LiCl were found unsuitable owing to the fact that they absorbed moisture through the film as soon as they were removed from the vacuum. The effect of a detergent substrate was also investigated. For this, the slide was coated with a liquid detergent and dried. Carbon was evaporated on to the detergent and floated off as before in warm water. These films were not as easy to strip off as those produced on a salt substrate and tended to have a matt surface.

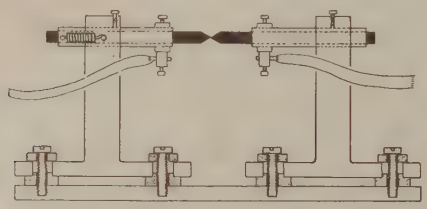

Fig. 1. The carbon arc.

The films of carbon were examined for structure under an electron microscope. It was found that the NaCl substrate films tended to be very non-uniform, due to shadow effects produced by particles of NaCl deposited on the slide during the evaporation. A little improvement was obtained by reducing the rate of evaporation and the distance between the slide and the NaCl boat. To get more uniform films, carbon was evaporated on to a liquid surface of glycerin. A shallow dish of glycerin was placed below the arc; the arc was flashed as before. As the low pressure and the heat from the arc induces boiling in the glycerin, the entire operation had to be carried out quickly. The film was floated off by carefully pouring the glycerin into a bath of water.

The film mount for the experiment, a metal foil with a hole punched in it, was brought up from under the film in a vertical plane at a steady rate. The film sticks to the mount by surface tension. Both single and double layers were satisfactorily mounted. The films once dried were extremely robust. Before use they were washed thoroughly with distilled water and again dried to get rid of traces of the substrate.

The stable NaCl and detergent substrate films varied in thickness from 50–100 μg cm^{-2}. The glycerin substrate films were much thinner being 10–20 μg cm^{-2}. They withstood beam currents of 5 μA of 1 MeV protons over a spot of diameter 0.1 cm. Higher intensities were not attempted. Because these carbon films are robust, thin and withstand nuclear beams, they should be useful as stripping foils in tandem accelerators. They may also be used as backing layers. NaCl, Li_2So_4, CaF_2, H_2Bo_3 and Be have been evaporated on to these films successfully and it should be possible to deposit other materials by evaporation or by electrolysis.

AUTHOR INDEX

Almén, O., G. Bruce and A. Lundén, Electromagnetic isotope separator in Gothenburg 249
Åström, B., Electronic instrumentation in nuclear pulse-height spectroscopy 117

Baldinger, E. and P. Santchi, High speed transistorized scale-of-two 128
Baldinger, E., Transistors in nuclear instruments 193
Bruce, G., *see* Almén
Bruijning, H. G., Some components used in the nanosecond field 81
Bujdosó, E. and L. Medveczky, Apparatus for processing nuclear emulsions 270

Cernigoi, C., G. Pauli and C. Poiani, On the pulse shape in a cylindrical ionization chamber . . . 261
Coleman, C. F., Gain-scanned single channel kicksorter using precision cascade attenuators . . . 44
Cottini, C. and E. Gatti, Improvement in the Vernier type nanosecond time delay analyzer 88
Cottini, C., E. Gatti and G. Giannelli, Transistor current generator for fast ferrite memory matrix 164

Dean, G., *see* Poole

Flinta, J., Pulsed high-intensity ion source 219
Flinta, J., *see* Pauli
Franklin, E. and J. B. James, Magnetic-memory scaling-system with magnetic count indication . 348
Fraser, J. S. and J. C. D. Milton, Automatic-recording apparatus for fission-fragment time-of-flight measurements 275

Gatti, E., Counting and storage systems 96
Gatti, E., *see* Cottini
Giannelli, G., *see* Cottini
Goldschmidt-Clermont, Y., G. von Dardel, L. Kowarski and C. Peyrou, Instruments for the analysis of track chamber photographs by digital computer 146
Goldschmidt-Clermont, *see* Von Dardel
Guillon, H., La standardisation des appareils électroniques au CEA 212

Hansen, P. G. and R. K. Sheline, Chemical techniques used in connection with β-spectroscopic work on rare earth elements 39
Heras, C. A., *see* Mayo
Howe, H., *see* Poole
Huq, M., Simple Čerenkov detector for the measurement of the energy of relativistic charged particles 342
Hutchinson, G. W., Some remarks about pulse-height analyser design 114

Iselin, F., *see* Von Dardel

James, J. B., *see* Franklin
Johansson, B., 25-channel time analyzer for the μs-range and a simple time to pulse-height converter 61

Kandiah, K., Recent developments in counting equipment 109
Kandiah, K., Unitised equipment at AERE . . . 216
King, N. M. and W. Walkinshaw, Spiral ridge cyclotron particle dynamics applied to conversion of the Harwell synchrocyclotron 287
Koch, J., Study of some characteristics of the GM-discharge 34
Kowarski, L., *see* Goldschmidt-Clermont

Lundén, A., *see* Almén

Maeder, D., Decimal memory systems 121
Maeder, D., Information handling systems for nuclear measurements 130
Maeder, D., A transistorised memory line 203
Maeder, D., Photographic recording methods in nuclear pulse spectrometry 299
Mayo, S., C. A. Heras and J. Rosenblatt, Regenerative beam extraction on the Buenos Aires synchrocyclotron 9
Medveczky, L., *see* Bujdosó
Meunier, R., Analyseur de temps de vol dans le domaine des nanosecondes; sommaire 90
Mey, J., Réalisation de circuits électroniques rapides dans le cadre du standard CEA 91
Milton, J. C. D., *see* Fraser
Moody, N. F., The present state of the transistor and its associated circuit art 182
Murray, R. B., Use of $Li^6I(Eu)$ as a scintillation detector and spectrometer for fast neutrons . . 237

Nielsen, K. O. and O. Skilbreid, The electromagnetic isotope separator in Copenhagen . . . 15

Orman, P. R., Recent work on nanosecond techniques at Harwell 95

Pauli, R. and J. Flinta, Pulsed high-intensity ion source 227
Pauli, G., *see* Cernigoi
Peyrou, C., *see* Goldschmidt-Clermont
Pizer, H. I., Standardization in the field of nucleonic instruments 207
Poiani, C., *see* Cernigoi
Pomerantz, M. A. and A. E. Smith, Automatic counting-rate recorder 49
Poole, M. J., G. Dean and W. Howe, Pulsed beam deflection system for a linear electron accelerator 282

Quercia, I. F., A general survey of electronics in the field of nuclear physics 210

Reaves, J. H., Speed of analogue electrostatic storage 136
Reaves, J. H., Fast logical binary adding network 139
Reaves, J. H. and J. F. Walton, Applications of isolated power supplies to instrumentation problems 178
Reaves, J. H. and J. F. Walton, Discussion . . . 181
Rosenblatt, J., *see* Mayo

Sagnell, B., System reliability 173
Santchi, P., *see* Baldinger
Sarma, N., Thin carbon films for use with electrostatic accelerators 361
Scarrott, G. G., Serial computer techniques 101
Sheline, R. K., *see* Hansen
Skilbreid, O., *see* Nielsen
Slätis, H., On a set of permanent magnet beta-ray spectrometers 332
Smith, A. E., *see* Pomerantz

Tanarro, A., Small gas compressor for accelerator ion sources 13
Tove, P. A., Automatic single-channel pulse-height analyser 1

Vervier, J. F., Correction de diffusion lors des mesures de sections efficaces totales pour neutrons rapides 53
Von Dardel, G., Y. Goldschmidt-Clermont and F. Iselin, The present state of the instrument for evaluation of photographs and future developments 154
Von Dardel, G. and F. Iselin, Printout of scaler position 169
Von Dardel, G., *see* Goldschmidt-Clermont

Waard, H. de, Some limitations and principles of nanosecond time measurement in nuclear physics 73
Walkinshaw, W., *see* King
Walton, J. F., *see* Reaves
Weller, R. I., Ionization chamber radioisotope comparator 5
Wells, F. H., Use of magnetic tapes and cores for nuclear data storage and computation 165

SUBJECT INDEX

Accelerators

Regenerative beam extraction on the Buenos Aires Synchrocyclotron, S. Mayo, C. A. Heras and J. Rosenblatt 9
Small gas compressor for accelerator ion sources, A. Tanarro 13
Pulsed beam deflection system for a linear electron accelerator, M. J. Poole, G. Dean and W. Howe 282
Spiral ridge cyclotron particle dynamics applied to conversion of the Harwell synchrocyclotron, N. M. King and W. Walkinshaw 287
Thin carbon films for use with electrostatic accelerators, N. Sarma 361

CERN MEETING

Counting and storage Systems

Counting and storage systems, E. Gatti 96
Serial computer techniques, G. G. Scarrott 101
Recent developments in counting equipment, K. Kandiah 109
Some remarks about pulse-height analyser design, G. W. Hutchinson 114
Electronic instrumentation in nuclear pulse-height spectroscopy, B. Åström 117
Decimal memory systems, D. Maeder 121
High speed transistorized scale-of-two, E. Baldinger and P. Santchi 128

Information handling Systems and other problems of big experiments

Information handling systems for nuclear measurements, D. Maeder 130
Speed of analogue electrostatic storage, J. H. Reaves 136
Fast logical binary adding network, J. H. Reaves 139
Instruments for the analysis of track chamber photographs by digital computer, Y. Goldschmidt-Clermont, G. von Dardel, L. Kowarski and C. Peyrou 146
The present state of the instrument for evaluation of photographs and future developments, G. von Dardel, Y. Goldschmidt-Clermont and F. Iselin 154
Transistor current generator for fast ferrite memory matrix, C. Cottini, E. Gatti and G. Giannelli 164
Use of magnetic tapes and cores for nuclear data storage and computation, F. H. Wells 165
Printout of scaler position, G. von Dardel and F. Iselin 169
System reliability, B. Sagnell 173
Applications of isolated power supplies to instrumentation problems, J. H. Reaves and J. F. Walton 178

Nanosecond Techniques

Some limitations and principles of nanosecond time measurement in nuclear physics, H. de Waard 73
Some components used in the nanosecond field, H. G. Bruijning 81
Improvement in the Vernier type nanosecond time delay analyzer, C. Cottini and E Gatti 88
Analyseur de temps de vol dans le domaine des nanosecondes; sommaire, R. Meunier 90
Réalisation de circuits électroniques rapides dans le cadre du standard CEA, J. Mey 91
Recent work on nanosecond techniques at Harwell, P. R. Orman 95

Standardisation of Nuclear Equipment

Standardization in the field of nucleonic instruments, I. PIZER 207
A general survey of electronics in the field of nuclear physics, I. F. QUERCIA 210
La standardisation des appareils électroniques au CEA, H. GUILLON 212
Unitised equipment at AERE, K. KANDIAH. 216

Transistor Circuits

The present state of the transistor and its associated circuit art, N. F. MOODY 182
Transistors in nuclear instruments, E. BALDINGER 193
A transistorised memory line, D. MAEDER 203

Chemical Techniques

Chemical techniques used in connection with β-spectroscopic work on rare earth elements, P. G. HANSEN and R. K. SHELINE 39

Counters, Chambers and Detectors

Ionization chamber radioisotope comparator, R. I. WELLER 5
Study of some characteristics of the GM-discharge, J. KOCH 34
Automatic counting-rate recorder, M. A. POMERANTZ and A. E. SMITH 49
Correction de diffusion lors des mesures de sections efficaces totales pour neutrons rapides, J. F. VERVIER 53
Use of $Li^6I(Eu)$ as a scintillation detector and spectrometer for fast neutrons, R. B. MURRAY 237
On the pulse shape in a cylindrical ionization chamber, C. CERNIGOI, G. PAULI and C. POIANI. 261
Apparatus for processing nuclear emulsions, E. BUJDOSÓ and L. MEDVECZKY 270
Photographic recording methods in nuclear pulse spectrometry, D. MAEDER 299
Simple Čerenkov detector for the measurement of the energy of relativistic charged particles, M. HUQ 342

Electronic Equipment

Automatic single-channel pulse-height analyser, P. A. TOVE 1
Gain-scanned single channel kicksorter using precision cascade attenuators, C. F. COLEMAN 44
25-channel time analyzer for the mμs-range and a simple time to pulse-height converter, B. JOHANSSON 61

Instruments for Nuclear Spectroscopy

Automatic-recording apparatus for fission-fragment time-of-flight measurements, J. S. FRASER and J. C. D. MILTON 275
Magnetic-memory scaling-system with magnetic count indication, E. FRANKLIN and J. B. JAMES 348

Ion Sources

Pulsed high-intensity ion source, J. FLINTA 219
Pulsed high-intensity ion source, R. PAULI and J. FLINTA 227

Isotope Separators

The electromagnetic isotope separator in Copenhagen, K. O. NIELSEN and O. SKILBREID 15
Electromagnetic isotope separator in Gothenburg, O. ALMÉN, G. BRUCE and A. LUNDÉN 249

Spectrometers (*see also* Instruments for Nuclear Spectroscopy)

On a set of permanent magnet beta-ray spectrometers, H. SLÄTIS 332